

A STUDY OF BEAM-COLUMN JOINTS UNDER SEISMIC LOADS:
COMPONENT TESTS VERSUS BUILDING RESPONSE

APPROVED:

To my parents,
Alex and Patricia Murray

A STUDY OF BEAM-COLUMN JOINTS UNDER SEISMIC LOADS:
COMPONENT TESTS VERSUS BUILDING RESPONSE

BY

PAUL ALEX MURRAY, B.S.C.E.

THESIS

Presented to the Faculty of the Graduate School of

The University of Texas at Austin

in Partial Fulfillment

of the Requirements

for the Degree of

MASTER OF SCIENCE IN ENGINEERING

THE UNIVERSITY OF TEXAS AT AUSTIN

August 1982

A C K N O W L E D G M E N T S

The author wishes to express his gratitude to all those who had a part in the completion of this thesis: to Dr. James O. Jirsa for his assistance and supervision of the author's research work and graduate studies, and to Dr. Ned H. Burns, who served on the author's thesis committee and also assisted with the preparation of this report.

The author would like to extend his personal thanks to Milind Joglekar for his invaluable assistance throughout the project. The assistance, support, and friendship provided by the author's fellow graduate students, Neil Cichy, Jefferson Reeder, Mark Moore, Roberto Leon, and Julio Ramirez is greatly appreciated. The author would like to express his sincere thanks to the Ferguson Structural Engineering Laboratory staff including George Moden, Gorham Hinckley, Dick Marshall, Maxine DeButts, Laurie Golding, and Deanna Thomas.

The financial support of the National Science Foundation for this project is gratefully acknowledged.

Finally, the author would like to express his sincere love and gratitude to Lezlie, soon to be his wife, for her love, encouragement and understanding.

P.A.M.
May 1982

T A B L E O F C O N T E N T S

Chapter		Page
1	INTRODUCTION	1
	1.1 Background	1
	1.2 Cooperative Research Program	2
	1.2.1 Research and Objectives	2
	1.2.2 Full-Scale Tests	4
	1.3 Proposed Study	8
	1.3.1 Test Program	8
	1.3.2 Scope and Objective	12
2	SPECIMEN DESIGN AND GEOMETRY	13
	2.1 General	13
	2.2 Specimen Geometry	13
	2.3 Details and Member Strengths	19
	2.3.1 Reinforcing Details	19
	2.3.2 Member Strengths	21
3	DESCRIPTION OF EXPERIMENTAL PROGRAM	26
	3.1 Specimen Fabrication	26
	3.1.1 General	26
	3.1.2 Formwork	26
	3.1.3 Casting Preparation	26
	3.1.4 Reference Inserts	28
	3.1.5 Casting and Curing Procedure	28
	3.2 Material Properties	32
	3.2.1 Concrete	32
	3.2.2 Steel Reinforcement	35
	3.3 Instrumentation	35
	3.3.1 Reinforcing Bars	35
	3.3.2 Beam Rotations	37
	3.3.3 Beam Deflections	44
	3.3.4 Beam Loads	44
	3.3.5 Joint Shear strain	44
	3.3.6 Additional Instrumentation	44

Chapter	Page
3	DESCRIPTION OF EXPERIMENTAL PROGRAM (Cont.)
3.4	Testing Apparatus 48
3.4.1	Loading Frame 48
3.4.2	Pin Connections 48
3.4.3	Hydraulic System 52
3.5	Test Procedure 54
3.6	Data Acquisition and Reduction 54
4	PRESENTATION OF TEST RESULTS 55
4.1	Introduction 55
4.2	Test Descriptions 56
4.2.1	General 56
4.2.2	Test 2 57
4.2.3	Test 3 64
4.2.4	Test 4 71
4.2.5	Test 5 79
4.3	Test Results 84
4.3.1	General Behavior and Observations 84
4.3.2	Drift-Angle Index (R) 89
4.3.3	Bar and Hoop Strains 90
4.3.4	Longitudinal Beam Rotations 101
4.3.5	Joint Shear Strain 105
5	COMPARISONS OF TEST RESULTS 107
5.1	Introduction 107
5.2	Comparisons with Half-Scale Tests 107
5.2.1	Description of Tests 107
5.2.2	Cracking Patterns 110
5.2.3	Hysteresis Relationships 113
5.3	Comparisons with the Full-Scale Seven-Story Structure 118
5.3.1	Introduction 118
5.3.2	Cracking Patterns 119
5.3.3	Reinforcement Strains 121
5.3.4	Longitudinal Beam Rotations 125
5.4	Suggestions for Future Testing 127

Chapter		Page
6	SUMMARY AND CONCLUSIONS	132
	6.1 Summary	132
	6.2 Conclusions from Full-Scale Joint Tests	134
	6.3 Conclusions from Test Comparisons	134
	BIBLIOGRAPHY	137

L I S T O F T A B L E S

Table		Page
3.1	Concrete Batch Proportions	32
4.1	Measured and Calculated Beam Loads	87

L I S T O F F I G U R E S

Figure	Page
1.1 Full-scale seven-story structure	3
1.2 Plan view of full-scale structure.	5
1.3 Elevation view of full-scale structure	6
1.4 Actuators between wall and specimen	7
1.5 Interior beam-column joint assembly	9
1.6 Exterior beam-column joint assembly	10
2.1 Plan view of interior joint specimen	14
2.2 Elevation view of interior joint specimen	15
2.3 Member dimensions	17
2.4 Member dimensions	18
2.5 Column cage	20
2.6 Beam cage	20
2.7 Slab reinforcement detail	22
2.8 Column interaction curve	23
2.9 Longitudinal beam moment-curvature relationships	24
3.1 Typical column forms	27
3.2 Formwork on casting platform	27
3.3 Lower pipe sleeve secured	29
3.4 Beam and column cages in place	29
3.5 All cages and formwork in place	30
3.6 Slab reinforcement placed	30
3.7 Joint core reference inserts	31
3.8 PVC tube inserts	31
3.9 Upper column cage	33
3.10 Upper column forms secured	34
3.11 Stress-strain relationships for reinforcement	36
3.12 Mounted strain gages	38

Figure	Page
3.13 Beam and column bar gage locations	39
3.14 Slab gage locations	40
3.15 Gage locations for joint and beam hoops	41
3.16 Beam rotation instrumentation	42
3.17 Beam rotation geometry	43
3.18 Beam deflection instrumentation	45
3.19 Joint shear strain instrumentation	46
3.20 Joint shear strain calculation	47
3.21 Testing apparatus	49
3.22 Floor fixture	50
3.23 Lower column pin connection	51
3.24 Hydraulic loading system	53
4.1 Slip correction	58
4.2 Load history, Test 2	59
4.3 Load versus deflection behavior, Test 2	61
4.4 Slip correction for load-deflection behavior, Test 2	62
4.5 Initial flexural cracks in west beam	63
4.6 Load history, Test 3	65
4.7 Load versus deflection behavior, Test 3	66
4.8 Stiffness deterioration, Test 3	68
4.9 Flexural cracking in east beam	69
4.10 Flexural cracking in the slab	69
4.11 First torsional cracks in transverse beam	70
4.12 Crack propagating diagonally in slab	70
4.13 Load history, Test 4	72
4.14 Load versus deflection behavior, west beam (Test 4)	73
4.15 Load versus deflection behavior, east beam (Test 4)	74
4.16 Comparison of west and east beam stiffness, Test 4	75
4.17 Diagonal cracks in west beam, Test 4	77

Figure	Page
4.18 Cracking in slab near loading points	77
4.19 Crack patterns at load stage 509	78
4.20 Deterioration in hinging zones, west beam	78
4.21 Load history, Test 5	80
4.22 Load versus deflection behavior, west beam (Test 5)	81
4.23 Load versus deflection behavior, east beam (Test 5)	82
4.24 Stiffness degradation with cyclic loading, west beam	83
4.25 Cracking near NE corner of joint, Test 5	85
4.26 Vertical cracks in north beam	85
4.27 SE quadrant after testing	86
4.28 Deterioration of NW joint region	86
4.29 Drift-angle calculation	90
4.30 Strain versus drift angle, west beam bars (Test 2)	92
4.31 Strain versus drift angle, longitudinal beam bars (Test 3)	93
4.32 Strain versus drift angle, west beam bars (Tests 2 through 4)	95
4.33 Strain versus drift angle, longitudinal slab bar (5CB), Test 4	97
4.34 Strain versus drift angle, longitudinal slab bar (5DT) Test 4	98
4.35 Strain distribution of bottom slab bars (Test 4)	99
4.36 Strain distribution of top slab bars (Test 4)	100
4.37 Strain versus drift angle, east column face bar	102
4.38 Beam rotation versus drift angle, Test 2	103
4.39 Beam rotation-drift angle relationships, Tests 3 through 5	104
4.40 Joint shear strain-drift angle relationships, Tests 3 through 5	106
5.1 Drift-angle index, full-scale structure	108
5.2 Cracking patterns for half-scale and full-scale joint specimens	111

Figure	Page
5.3 Cracking patterns for half-scale and full-scale joint specimens	112
5.4 Story shear versus story displacement relationship (Specimen I-1)	114
5.5 Story shear versus story displacement relationship (Specimen I-2)	115
5.6 Nondimensionalized hysteresis relationships	116
5.7 Cracking patterns of the full-scale structure	120
5.8 Strain gage locations for joint in full-scale structure	122
5.9 Strain versus drift-angle relationships, top beam bars .	123
5.10 Strain versus drift-angle relationships, bottom beam bars	124
5.11 Strain versus drift-angle relationships, upper column bars	126
5.12 Beam rotation versus drift-angle relationships	128
5.13 Schematic of suggested instrumentation	130

C H A P T E R 1

INTRODUCTION

1.1 Background

In recent years, much experimental work has been initiated to investigate the response of reinforced concrete structures under simulated earthquake conditions. In general, the lack of available scientific knowledge in the field of earthquake engineering and the need for improved design recommendations and practices has prompted these research programs. Furthermore, the poor performance exhibited by many reinforced concrete structures in relatively recent earthquakes, such as the Tokachi-Oki earthquake,¹ Japan, 1968 and the San Fernando earthquake, 1971, heightened this interest in research. Several of these reinforced concrete buildings which suffered extensive damage were of modern design. Obviously, many serious questions were raised by investigators, researchers, and government agencies concerned with the adequacy of design provisions and recommendations used at that time.

Following each of the earthquakes mentioned, joint seminars sponsored by the U.S.-Japan Cooperative Science Program were held to review the damage structures sustained as well as the current design provisions, and to define areas of needed research. In response, primarily, to the meetings held in Japan after the Tokachi-Oki earthquake, where a number of reinforced-concrete school buildings were severely damaged, the U.S.-Japan Cooperative Research Program on Earthquake Engineering with Emphasis on the Safety of School Buildings was established in 1973. Near the end of this program in 1975 Japanese and U.S. investigators drafted and signed a set of Recommendations for U.S.-Japan Cooperation in the Field of Earthquake

Engineering. Included among these recommendations was the organization and implementation of a Cooperative Research Program involving large-scale testing. Finally, in 1977, funds were granted to proceed with the planning of a joint research program entitled U.S.-Japan Cooperative Research Program Utilizing Large-Scale Testing Facilities.²

1.2 Cooperative Research Program

1.2.1 Research and Objectives. The general objective of the U.S.-Japan Cooperative Earthquake Research Program is to improve the scientific knowledge and engineering practices prevalent in the design of seismic-resistant structures. Previous research programs with similar intentions have included analytical studies, small-scale tests, and shake-table tests. However, such experimental work provides very little test data or information to correlate with the behavior of actual structures. Design concepts and recommendations, up to this point, have been based on theory and observations of earthquake damage, to a great extent. Therefore, a second objective of the Cooperative Research Program is to correlate test results from component tests, shake-table tests, and small-to-medium scale tests with the behavior of a prototype, full-scale structure subjected to seismic-type forces. If the merits and limitations of component testing used to predict prototype response can be established from such correlation studies, improvements in seismic-resistant design practices can be achieved.

The research program included the design, construction, and testing of a full-scale seven-story reinforced concrete building structure. A series of tests conducted on this structure were done in the Large-Size Structures Laboratory, Building Research Institute, Tsukuba New Town for Research and Education, Japan (see Fig. 1.1). Supporting tests, performed in both the U.S. and Japan, included component, beam-column joint assemblies, scale models of the

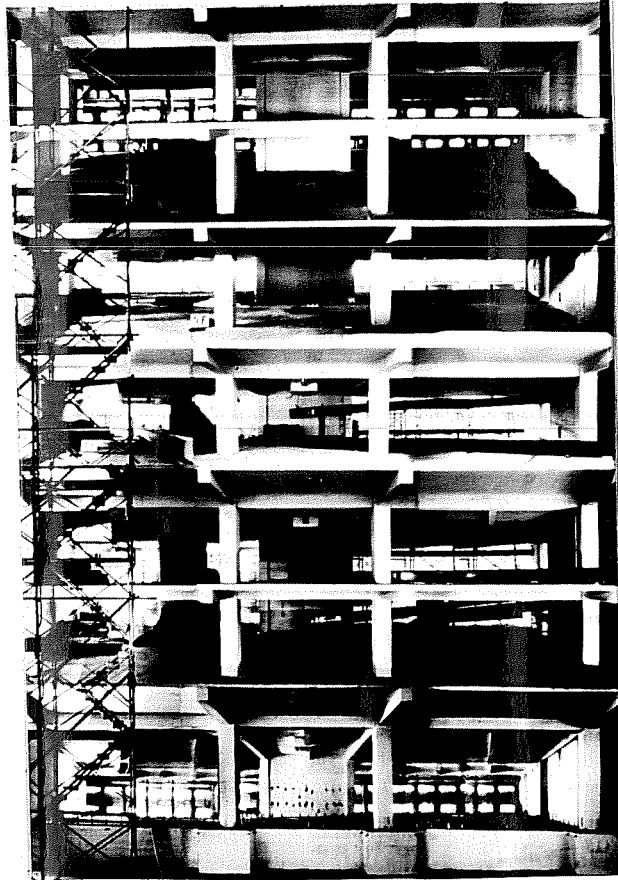


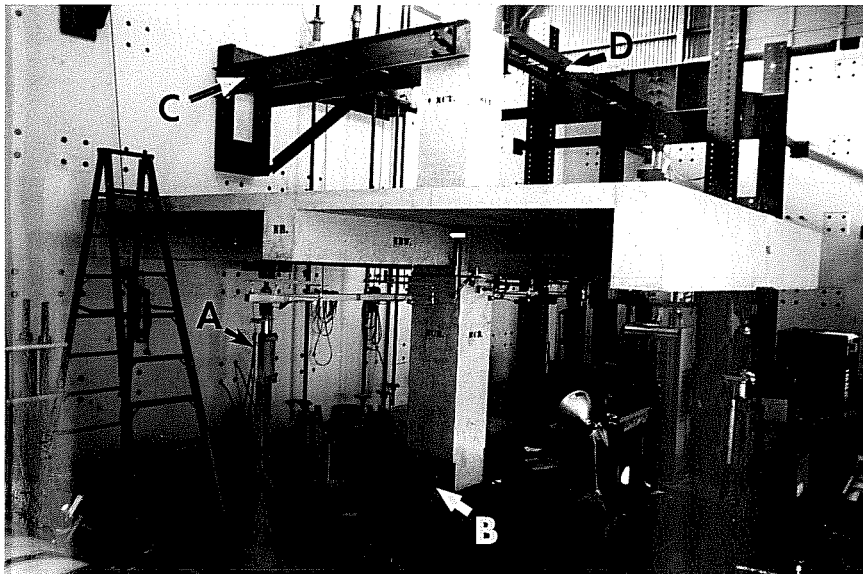
Fig. 1.1 Full-scale seven-story structure

full-scale structure, and shake-table models. These coordinated experiments provide important test data such as force-deformation relationships, energy dissipation characteristics, and damage and failure modes. In addition, the supporting work in both countries was necessary to achieve several specific goals of the research program which include the following:

- (1) Test component assemblies and scale models with boundary and loading constraints representative of the conditions in real building systems and structures.
- (2) Assess the practicality of full-scale testing versus the adequacy of component and model testing.
- (3) Fabricate and test specimens which represent typical design practices in both the U.S. and Japan.
- (4) Use the test results and comparisons as a basis to review and improve current design procedures for seismic-resistant structures.

1.2.2 Full-Scale Tests. In general, the design of the full-scale test structure, which represented a portion of a building in plan dimensions, was typical of earthquake engineering practices in both the U.S. and Japan. The lateral load resistance of the structure was provided by the interaction of the frame-shear wall structural system. The frame elements, column and beam members, were rather large sections lightly reinforced, characteristic of Japanese seismic design. Some of the reinforcing details differed from standard U.S. practice as well (see Chapter 2). The plan and elevation views of the prototype building are shown in Figs. 1.2 and 1.3, respectively.²

The test program consisted of a series of tests on the bare frame structure with increasing levels of drift. The lateral displacements were applied parallel to the plane of the shear wall with eight actuators fixed to the reaction wall. One actuator was located at each floor level and two at the roof level (see Fig. 1.4). To simulate dynamic excitations, a self-determined or



A--beam ram
B--floor fixture
C--channel strut
D--angle strut

Fig. 1 Beam-column joint test,

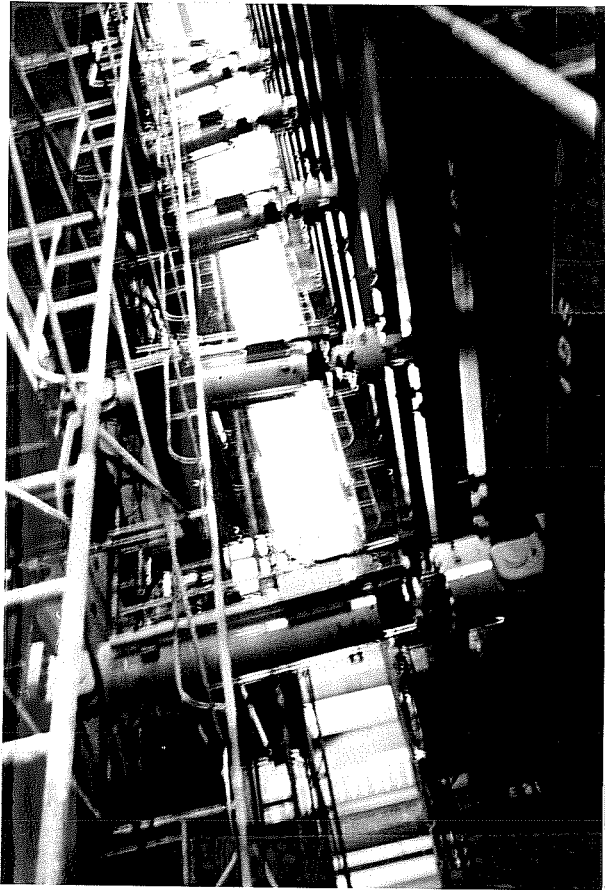


Fig. 1.4 Actuators between wall and specimen

pseudo-dynamic test procedure was originally suggested which utilized a selected ground motion. However, due to the complexity of such a system and the anticipated difficulty of precisely controlling the actuators, an alternative loading method was chosen. The compromise loading scheme incorporated the pseudo-dynamic procedure but with an earthquake record modified so that primarily a first mode response of the test structure would be obtained. The ground motion, representing an equivalent single degree of freedom system, was input for displacement control of the actuators at the roof level. At the second through seventh levels, the actuators were operated by load control to obtain an inverted triangular load distribution on the structure. The simplified loading procedure reduced the difficulty of the loading sequence, and facilitated the interpretation of test data and the correlation of test results with the supporting tests.

A second series of tests, similar to the initial tests, was conducted following the repair of the structure and addition of nonstructural elements. The primary purpose of these tests was to investigate repair techniques used on damaged structures. However, the results obtained from the second test series were not relevant to this experimental study.

1.3 Proposed Study

1.3.1 Test Program. The experimental work conducted at the University of Texas, Austin in the Ferguson Structural Engineering Laboratory involves the fabrication and testing of full-scale reinforced concrete beam-column joint specimens. The proposed test program includes plans for two interior and two exterior joint assemblies with geometries identical to the beam-column joints at the second level in the prototype structure. The locations of typical interior and exterior joints in the full-scale building are indicated in Fig. 1.2. Typical interior and exterior joint specimens are shown in Figs. 1.5 and 1.6, respectively.² For

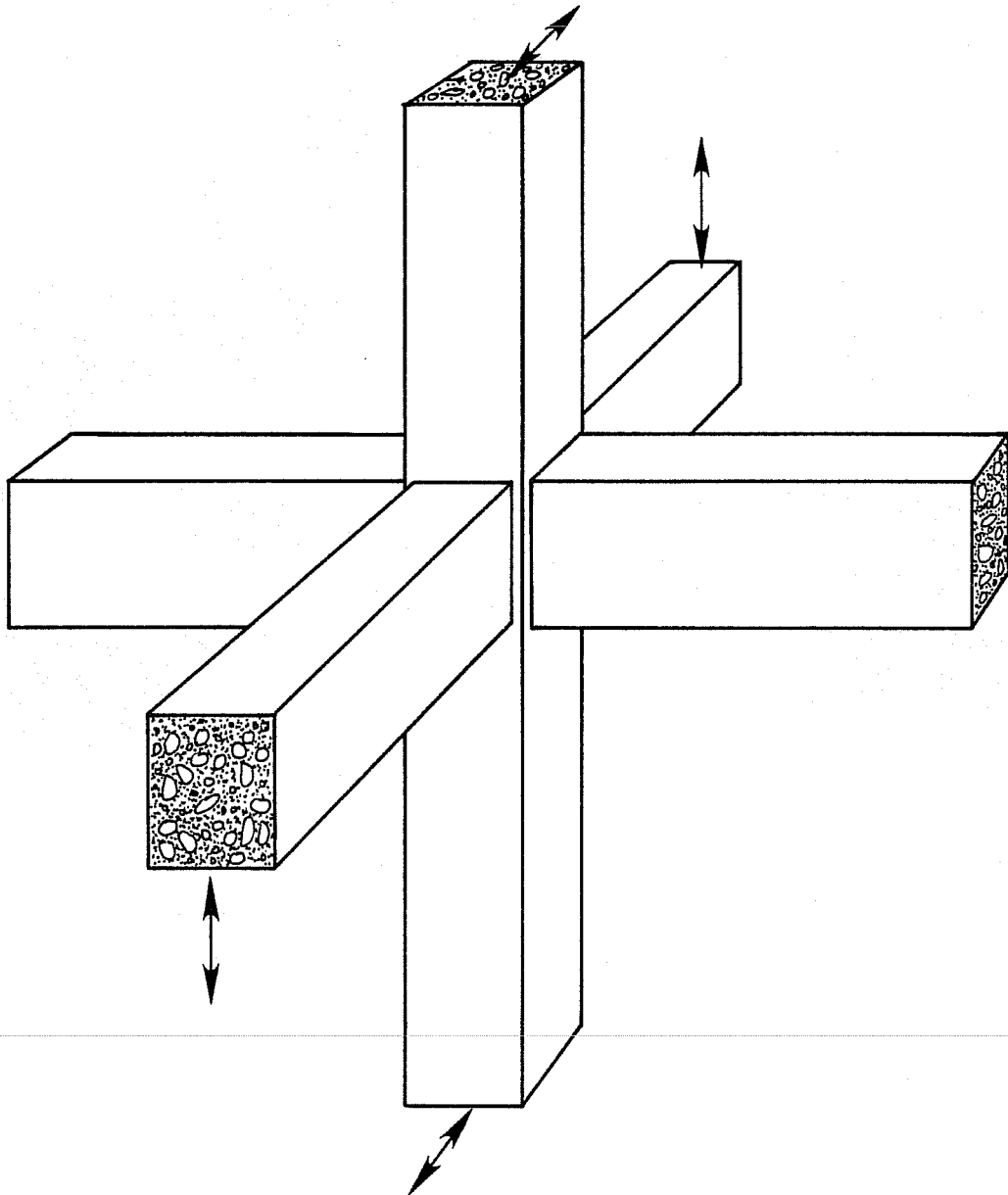


Fig. 1.5 Interior beam-column joint assembly

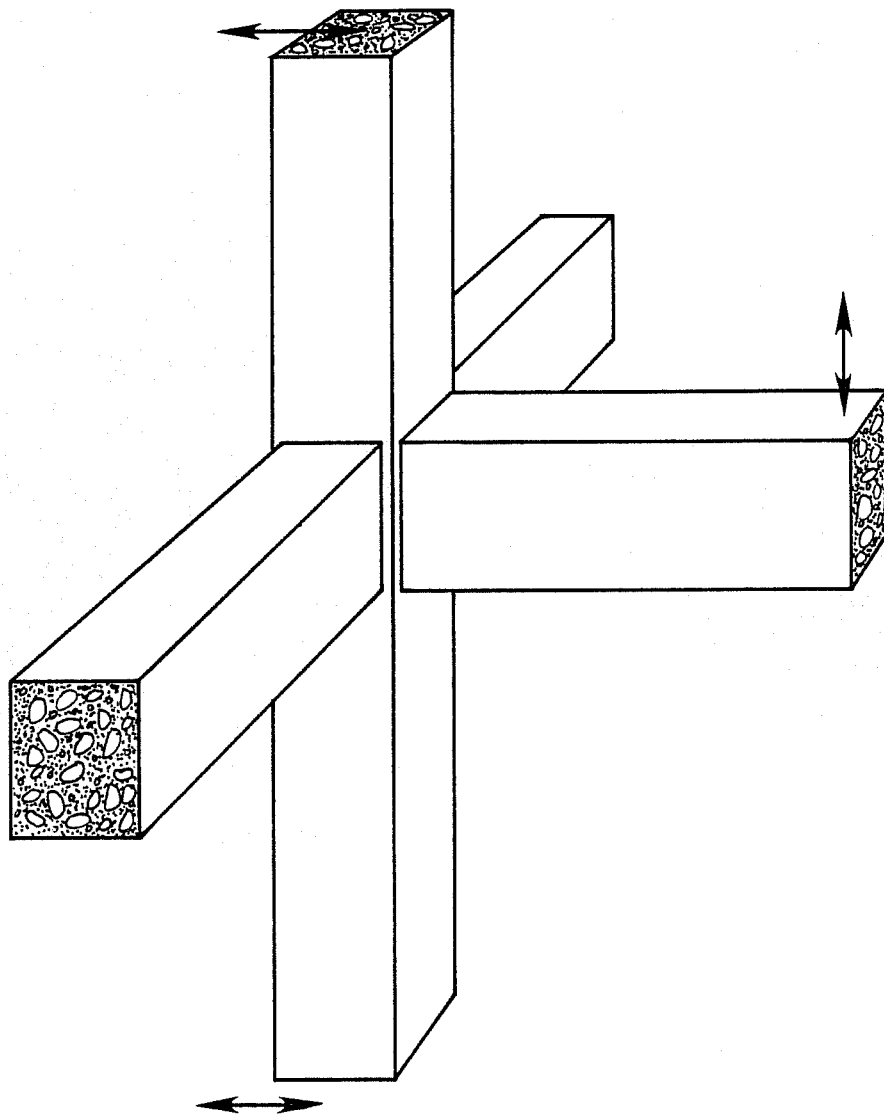


Fig. 1.6 Exterior beam-column joint assembly

clarity, the floor slabs are not shown, but were included as part of the test assembly.

It should be mentioned that the proposed research program represents the first opportunity to correlate test results and observations from full-scale joints with the response of a full-scale structure subjected to simulated earthquake loads. In the past, experimental work has generally failed to define the relationships between component tests and real structures, particularly concerning geometric restraints and the loadings applied to test assemblies. This test program will, however, provide information through the correlation studies necessary to begin establishing these relationships. Furthermore, with a better understanding of the relationships between component assemblies and real structures, effective reviews of current design recommendations for reinforced concrete joints will be possible.

The four test specimens will be tested under reversed, cyclic loading patterns with increasing levels of displacement. The displacements will be applied at the beam ends along the longitudinal axis of the specimen (see Figs. 1.5 and 1.6), and will be similar to the magnitudes of drift imposed on the full-scale structure. Originally, an axial load on the column was proposed to simulate gravity loads. However, due to difficulties expected with fabrication and testing, no column axial loads will be applied during testing. This could be justified since the gravity axial load would be less than the balanced axial load for the column. Therefore, with no axial load the moment capacity of the column would be less and represent a worse condition in the column. The first two specimens, interior and exterior joints, will have reinforcement details identical to those in the full-scale structure. Specimens 3 and 4, also interior and exterior joints, will have modified reinforcing details.

1.3.2 Scope and Objective. The subject of this experimental study will be the test results from the first specimen, USJ-1, an interior beam-column joint, and the subsequent comparisons with the half-scale component test results and the full-scale structure test results. As mentioned earlier, the geometry and reinforcing details of the joint specimen were identical to the interior beam-column joints in the prototype structure. A series of five tests with increasing levels of beam displacement were conducted on the interior joint assembly. The selected peak beam displacements represented interstory displacements imposed at the second level of the full-scale building. Therefore, a common parameter, drift level or more accurately, drift rotation index (see Chapter 4) was used to correlate test results. The test comparisons considered load-deflection characteristics, cracking patterns, reinforcement strains near the joint region, longitudinal beam rotations, and damage and failure characteristics. The correlation study, which included test results from the prototype structure, half-scale component tests completed in Japan and the full-scale component tests here at Texas, was the fundamental objective of the research program.

C H A P T E R 2

SPECIMEN DESIGN AND GEOMETRY

2.1 General

The test specimen, USJ-1, was built using dimensions and details of an interior joint at the second level of the full-scale structure. Therefore, no detailed design calculations were required. Since the full-scale building was designed and built in Japan, using metric dimensions, certain conversions and approximations for specimen and member dimensions as well as for material properties were necessary. Furthermore, fabrication and testing constraints had to be considered before selecting the final geometry of the interior joint assembly. Finally, some attention had to be given to crane restrictions when handling the specimen and removing it from the laboratory when testing was completed.

2.2 Specimen Geometry

The as-built dimensions of the test specimen are shown in plan and elevation views of the interior joint assembly, Figs. 2.1 and 2.2, respectively. The longitudinal beam refers to the single beam in the long direction of the specimen intersecting the joint region. Since racking loads were applied only at either end of this beam, the beam is parallel with the direction of loading for the specimen. The beam which intersects the joint region in the orthogonal direction is called the transverse beam. The two beams parallel to the transverse beam, at opposite edges of the specimen, are referred to as end beams. The orientation (north, east, etc.) of the joint assembly, as positioned in the test set-up is shown in Fig. 2.1. These directions were utilized during testing to

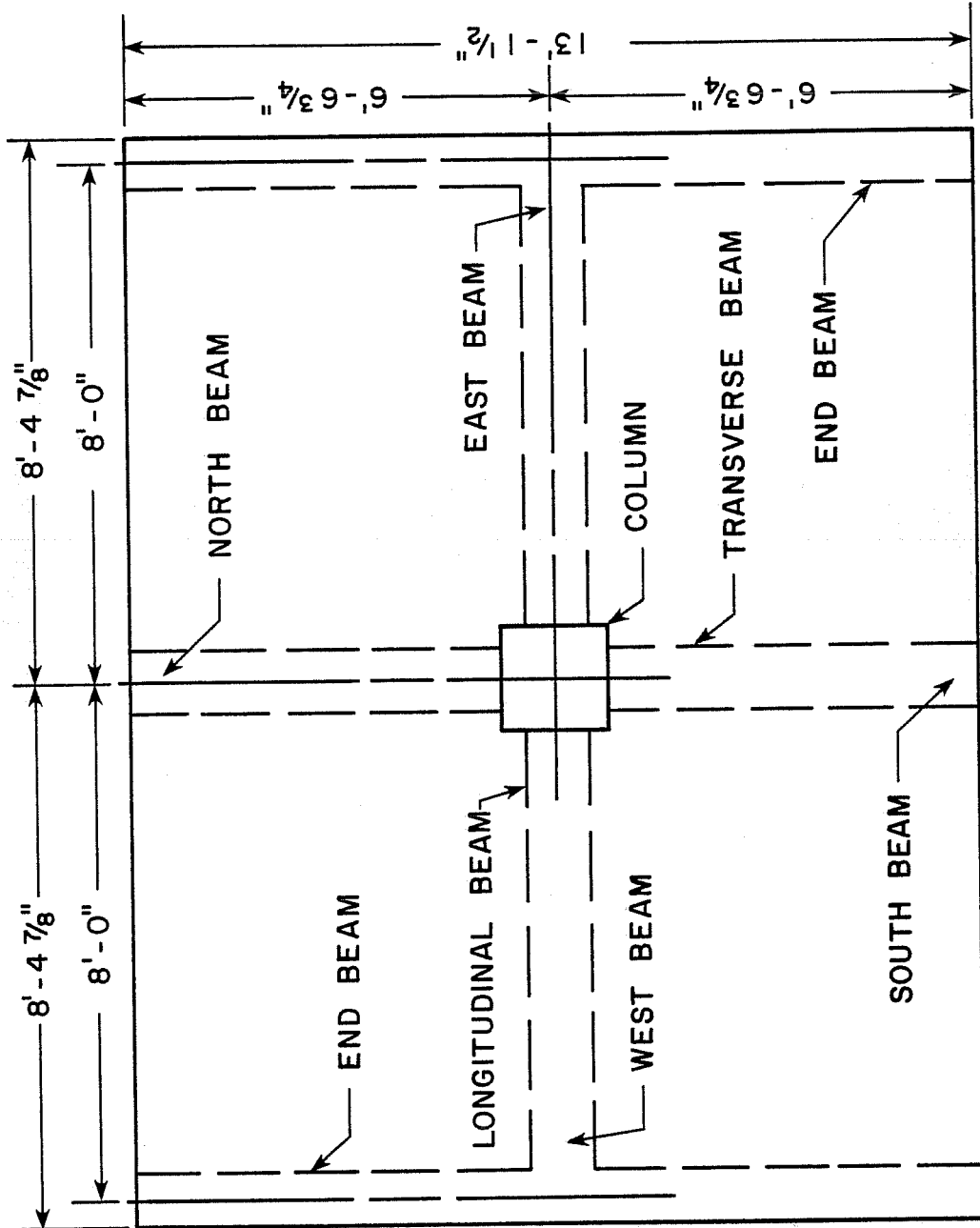


Fig. 2.1 Plan view of interior joint specimen

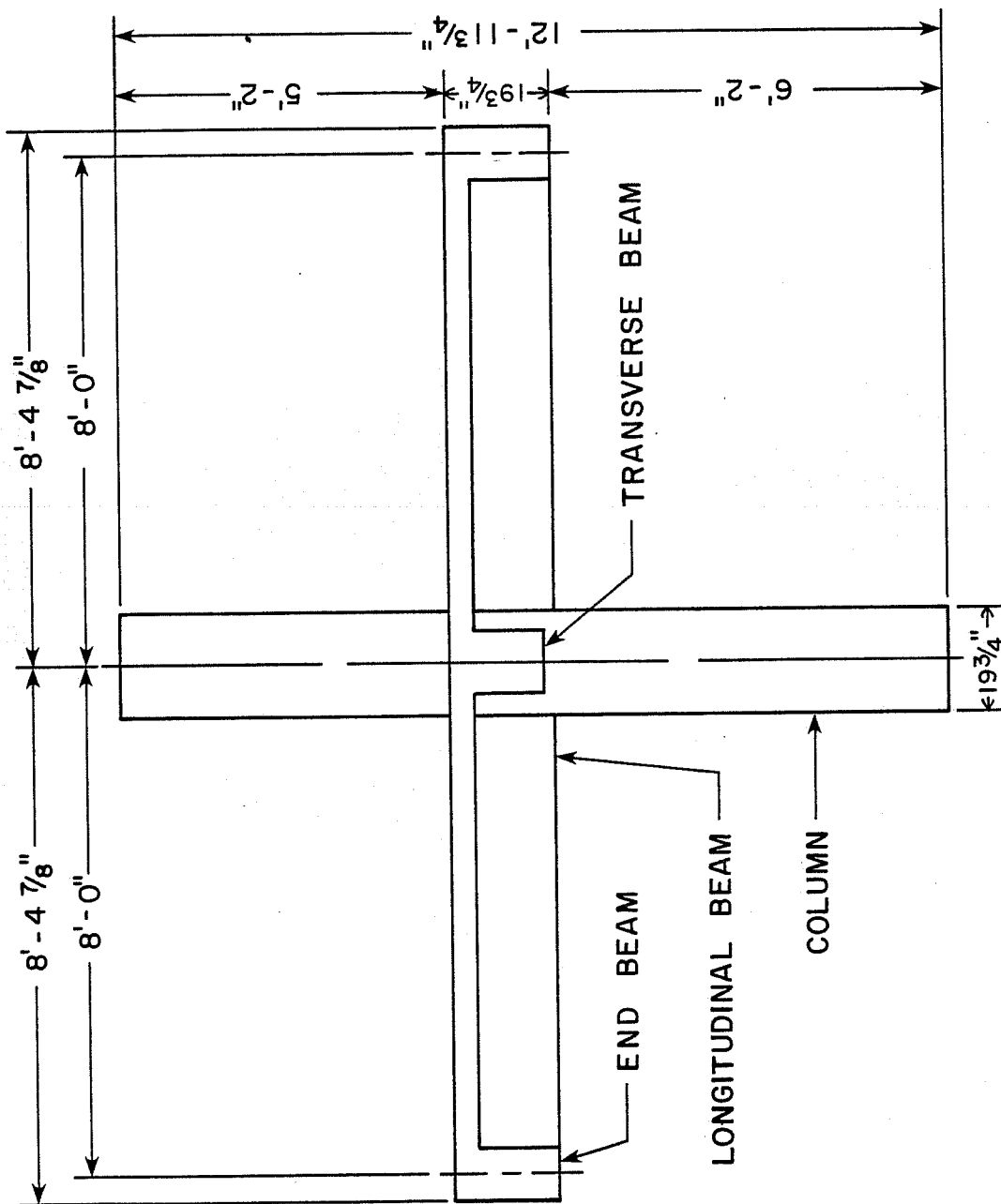


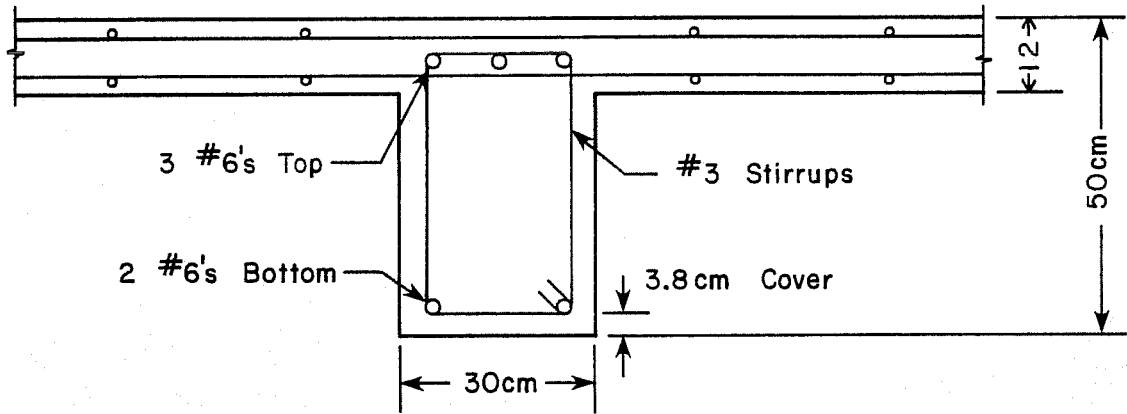
Fig. 2.2 Elevation view of interior joint specimen

locate instrumentation and to identify crack patterns and damage to the specimen.

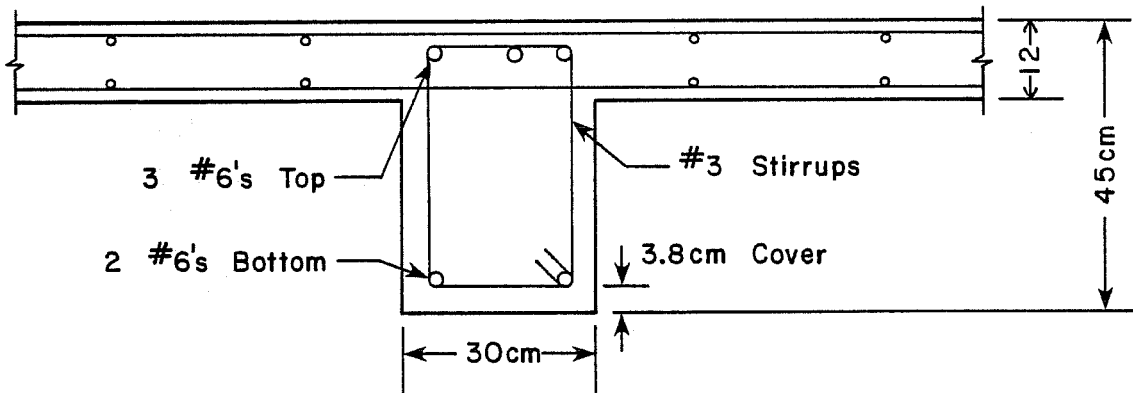
The length of the longitudinal beam, measured on either side of the column centerline, represents approximately half the span length of the middle bay in the full-scale structure (see Fig. 1.1). A half-span length of 8 ft. was convenient with regard to the layout of the structural floor in the laboratory where bolt groups are centered at 4 ft. intervals. The transverse dimension of the specimen, 4 meters, was chosen to duplicate the transverse span length shown in the prototype structure (see Fig. 1.1). The 2 meter dimension of the beam stubs at either end of the frames in the transverse direction was doubled to obtain an appropriate specimen width. The end beams were included as part of the test assembly and represented secondary transverse beams at the midspan of all the bays in the full-scale structure.

Ideally, the column height of the test specimen should be equal to the story height from mid-story to mid-story assuming zero-moment conditions at those points. Figure 2.2 shows, however, that the lower column was 12 in. longer than the upper column. Two considerations led to the column geometry. First, the existing casting bed and the loading actuator height in the planned test set-up imposed restrictions on the dimensions. Secondly, the first story height in the full-scale structure was 3.75 meters compared to a 3 meter height for the remaining six stories. Therefore, although the upper and lower column dimensions were different, they reflected the geometry of the prototype structure.

The cross-sectional dimensions of the longitudinal and transverse beams, drawn as T-sections, the column, and the end beams are given in Figs. 2.3 and 2.4. The metric dimensions were used for fabrication of the test specimen. English units were used for dimensions which had to be compatible with similar dimensions in the test set-up.

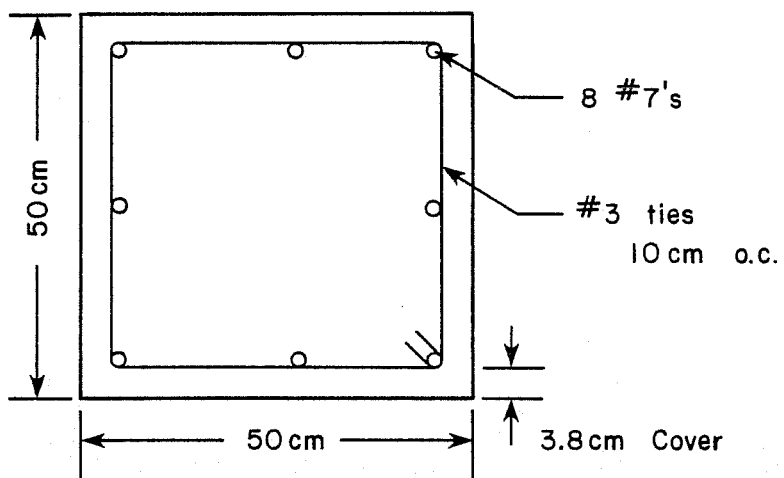


(a) Longitudinal beam

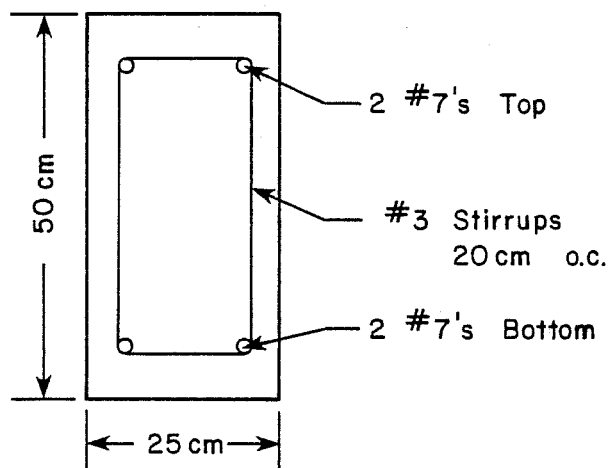


(b) Transverse beam

Fig. 2.3 Member dimensions



(a) Column



(b) End beam

Fig. 2.4 Member dimensions

2.3 Details and Member Strengths

2.3.1 Reinforcing Details. The design reinforcement ratios for each of the individual members in the full-scale structure are quite low, particularly by U.S. standards where they approach the minimum recommended values given by ACI 318-77.³ However, as indicated in Chapter 1, large, lightly reinforced sections are typical of Japanese seismic design practice. Duplicating the steel percentages and arrangements in the test specimen was facilitated because of the equivalence of the metric bars used with standard U.S. bar sizes and grades.

The column reinforcement consisted of eight #7 bars, three in each face (see Fig. 2.5), which corresponded to a reinforcement ratio of 1.23 percent. The transverse reinforcement, #3 hoops, were placed at 10 cm. spacings along the height of the column, including the joint region, with a 3.8 cm (1-1/2 in.) cover. The hook detail for these hoops, as well as the beam hoops, differed slightly from standard U.S. practice. In Japan, it is common practice to use $6d_b$ hook extensions for transverse reinforcement compared to the $10d_b$ hook extension required by Appendix A of ACI 318-77.³ The $6d_b$ hook extension detail was used in the test specimen to remain consistent with the full-scale structure.

The longitudinal and transverse beams were reinforced with three #6 bars top and two #6 bars bottom. These bars were continuous through the joint and anchored at the end of each of the beams with standard 90° hooks. Transverse reinforcement was provided by #3 hoops spaced at 10 cm for the first meter from the column face, and 20 cm spacings thereafter. In Fig. 3.6, note the position of the top steel in the longitudinal beam which crosses under the top steel in the transverse beam. Again, this was identical to the detailing of the interior joints in the prototype structure.

The end beams were detailed with two #7 bars top and bottom, and #3 stirrups spaced uniformly at 20 cm along the beams.

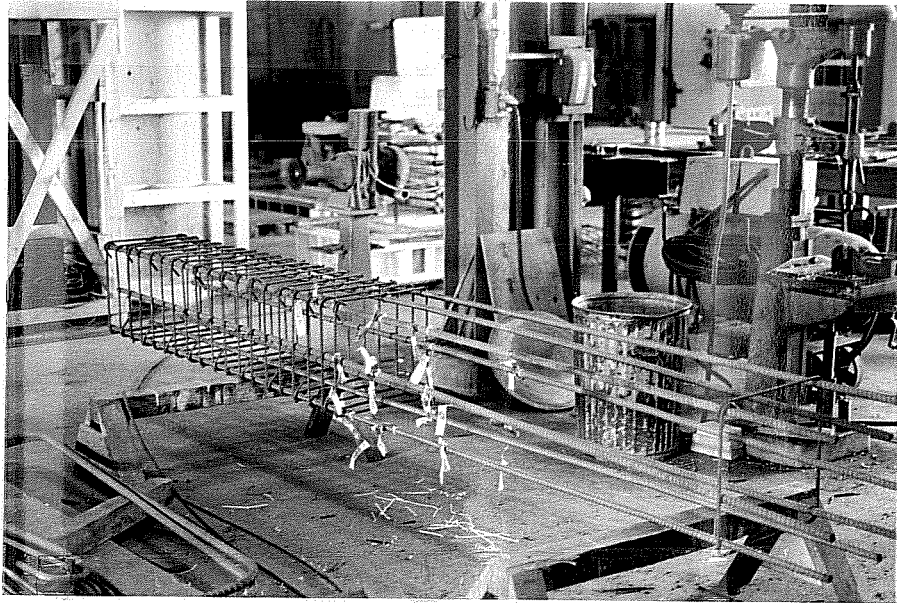


Fig. 2.5 Column cage

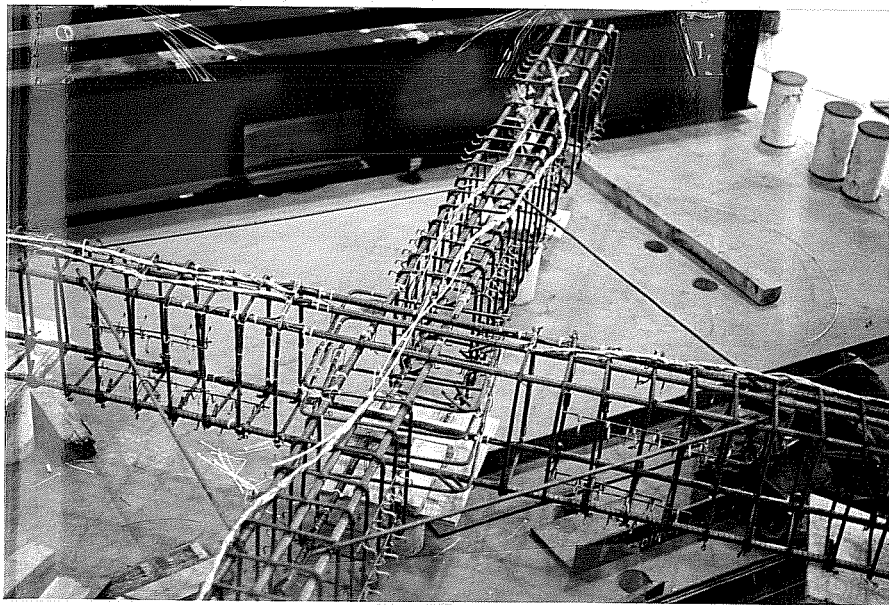


Fig. 2.6 Beam cage

The slab reinforcement consisted of two mats of steel, #3 bars with a 2 cm (3/4 in.) cover (see Fig. 2.7). Detailing of this steel varied somewhat in either direction. The longitudinal reinforcement was placed at 30 cm spacings for the first 90 cm, and then decreased to 20 cm spacings, measured from the beam centerline. Note, that the bottom layer of the longitudinal slab steel was continuous across the transverse beam, a detail not normally used in U.S. practice. A uniform spacing of 30 cm was used in the transverse direction. In addition, standard 180° hooks were specified for the longitudinal slab steel, but not for the transverse steel.

2.3.2 Member Strengths. The column interaction curve and the longitudinal beam moment-curvature relationships for both positive and negative bending are shown in Figs. 2.8 and 2.9, respectively. With no axial load on the column, the design moment capacity was approximately 3200 kip-in. The design positive and negative yield moments for the longitudinal beam were nearly 1000 kip-in. and 2150 kip-in., respectively. To determine these moments, a T-section was analyzed with an effective slab width of 59 in. (150 cm), in compliance with ACI 318-77 (Sec. 8.10.2).³ The effective slab width assumed had very little effect on the moment capacity for the case of positive bending, bottom steel in tension. However, the negative moment capacity depended on the effective slab width assumed and varied substantially as indicated by the range of moment capacities given in Fig. 2.9. A maximum negative moment of 4250 kip-in., nearly twice the design moment, was obtained using the entire slab width. The actual negative yield moments for the west and east beams will likely be higher than the design moment of 2150 kip-in., presuming ACI procedures to be conservative.

The ratio of column-to-beam yield moments ($6400/3150 = 2.03$) was considerably larger than the value of 1.4 recommended by ACI-ASCE Committee 352.⁴ A moment ratio of this magnitude indicated that failure of the test specimen would occur primarily by longitudinal

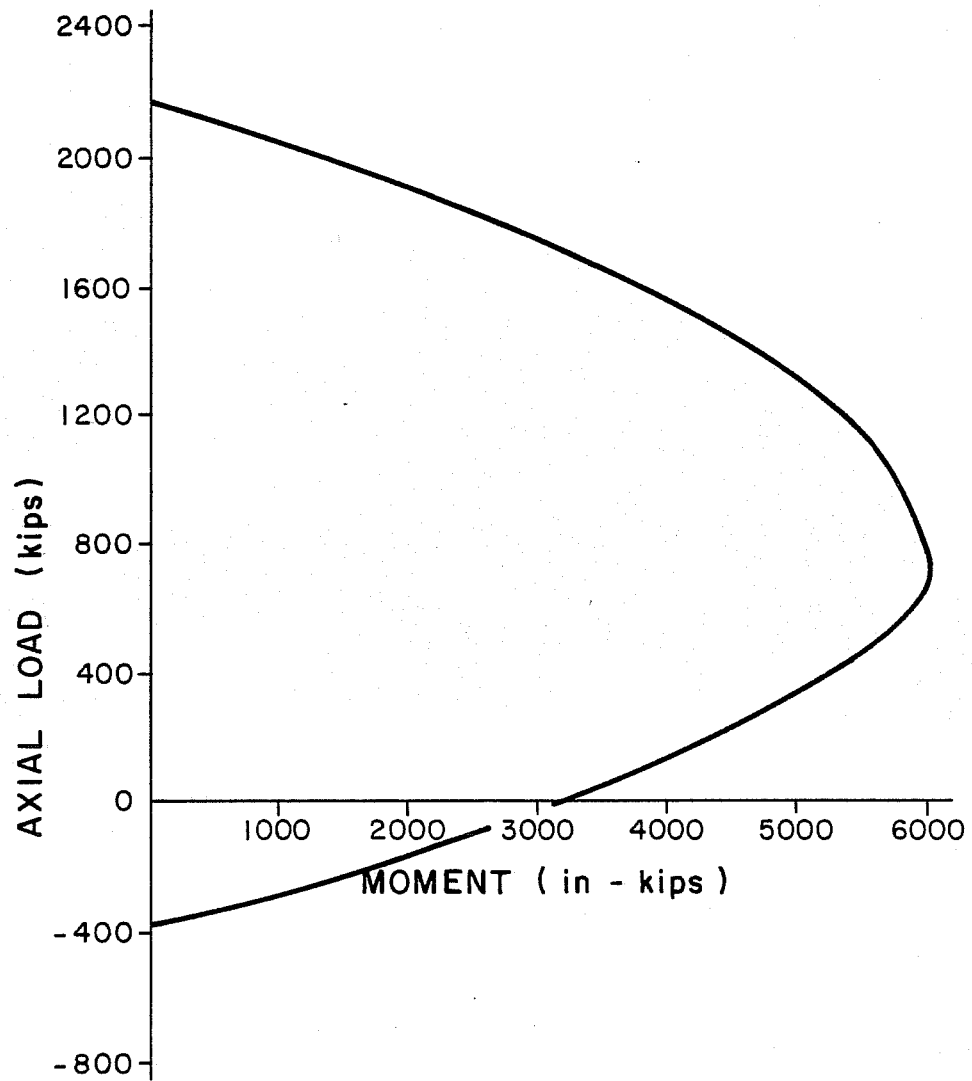


Fig. 2.8 Column interaction curve

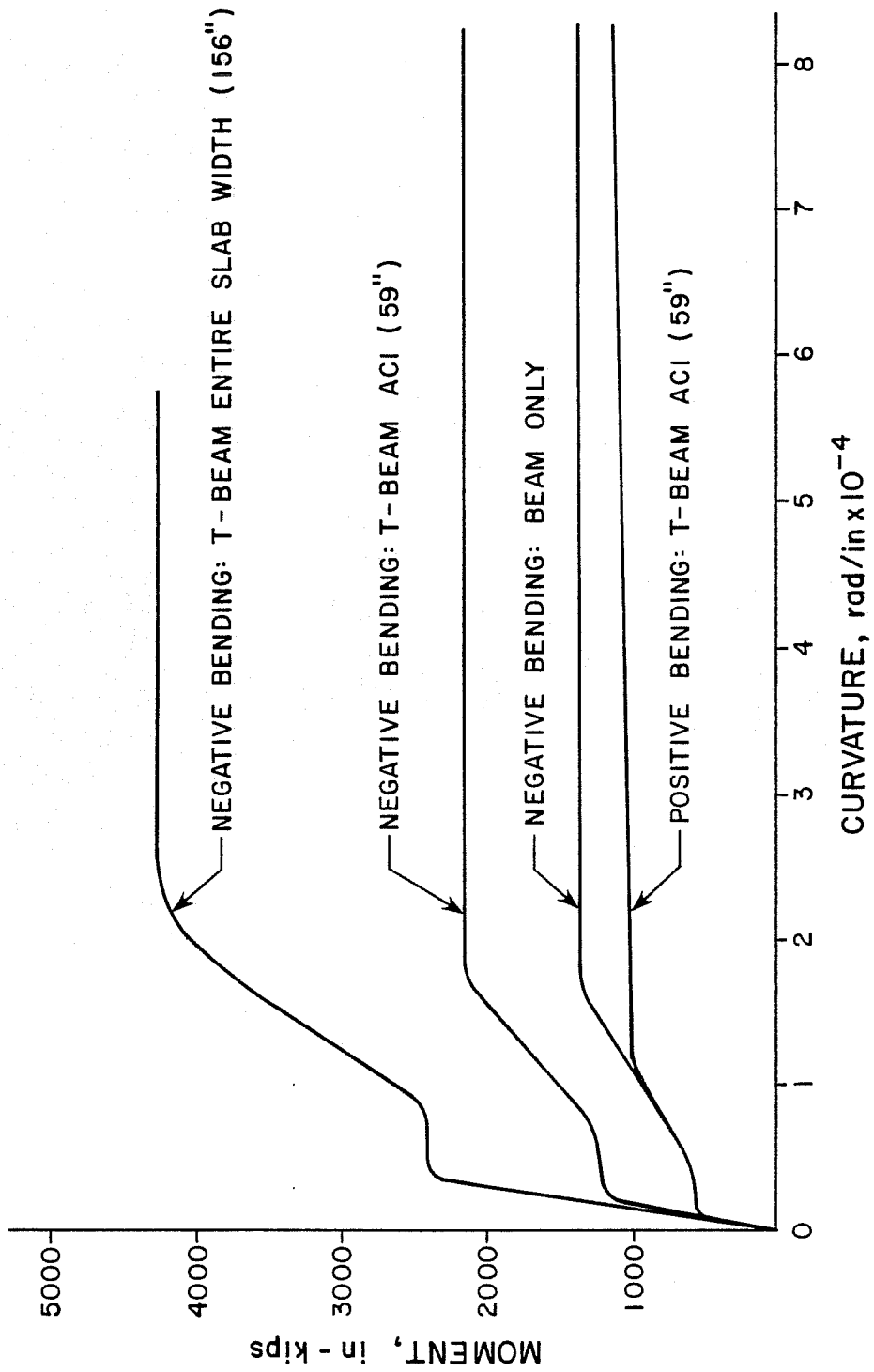


Fig. 2.9 Longitudinal beam moment-curvature relationships

beam hinging near the column face. In seismic-resistant structures such behavior is ideal where energy dissipation is provided by beam hinging, and the formation of hinges in critical column elements is prevented. Note, however, that as the contribution of the slab steel increases and the negative beam moment becomes larger, the moment ratio, calculated above, decreases. The design moment ratio may in fact be unconservative, less than 1.4, if the negative moment capacity approaches the maximum value in Fig. 2.9.

C H A P T E R 3

DESCRIPTION OF EXPERIMENTAL PROGRAM

3.1 Specimen Fabrication

3.1.1 General. The fabrication sequence of USJ-1 consisted of the following steps; design and construction of the formwork, attachment of strain gages to the reinforcement, tying the beam and column cages, placing the cages in the formwork, securing various reference inserts for instrumentation, casting the concrete, and curing the specimen for several days. However, before fabrication could proceed an existing casting bed for large joint specimens had to be extended into a 22 ft. by 16 ft. rectangular platform to accommodate the size of the test specimen.

3.1.2 Formwork. The formwork included typical lower and upper column forms (see Fig. 3.1) and four rectangular pans with side forms used to mold the four beams and the slab (see Fig. 3.2). To prevent the possibility of the pan forms binding between the transverse and end beams, due to swelling of the wood during casting and curing, each of the pans were built as two individual units separated by a narrow opening. Before casting the openings were filled with strips of styrofoam and then caulked to inhibit water loss between the pans. The formwork was lacquered several times to provide a protective coating as well as a smooth, glossy finish.

3.1.3 Casting Preparation. To prepare for casting, the eight pan forms were first positioned and attached to the platform with lag bolts. The column cage with only the lower column hoops tied in place was lowered into the casting platform. A thick-walled pipe, 19-3/4 in. (50 cm) long, was carefully aligned and tied in

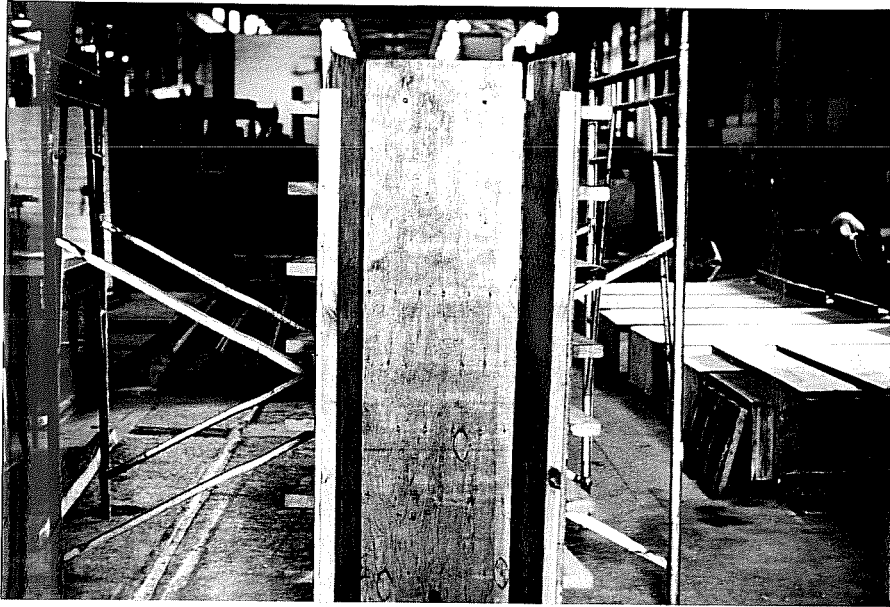


Fig. 3.1 Typical column forms

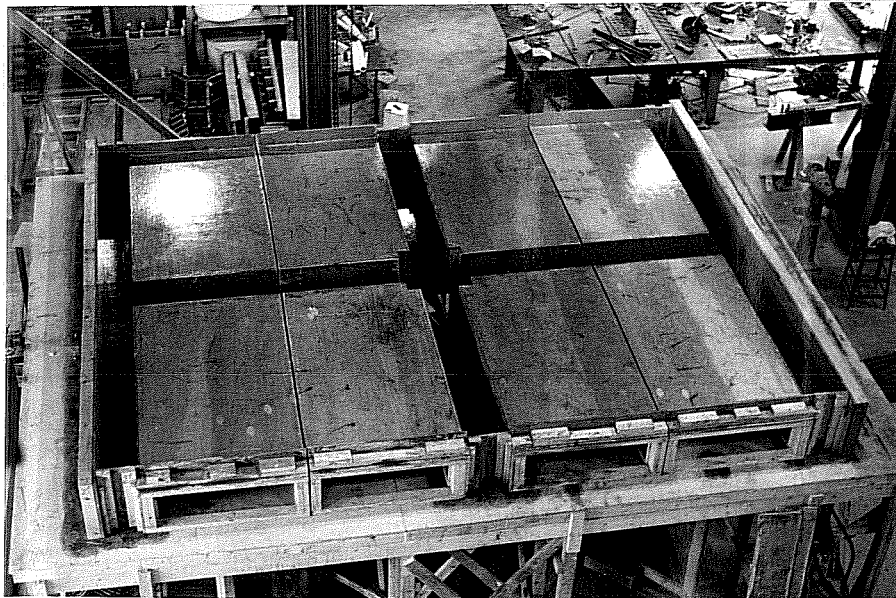


Fig. 3.2 Formwork on casting platform

place near the bottom of the column to serve as a sleeve through which a high-strength bolt would be inserted to provide a pin connection at the base of the specimen. Figure 3.3 illustrates the added precautions taken to confine the concrete around the pipe with extra column hoops and crossties as well as a spiral around the pipe to prevent a pull-out failure. Once the pipe was secured, the lower column forms were oiled and bolted in position to restrain any further movement of the column cage. The longitudinal and transverse beam cages and four transverse joint core ties were simultaneously threaded through the upper column bars and lowered into place (see Fig. 3.4). The partially fabricated end beam cages were placed and the remaining forms were oiled and bolted to the platform (see Fig. 3.5). Finally, the two slab steel mats were placed (see Fig. 3.6), and the strain gage lead wires were bundled and tied to the upper column bars.

3.1.4 Reference Inserts. Inserts were secured in selected positions in and near the joint core to serve as reference points for various types of instrumentation such as beam and joint rotations. As a precaution against inaccurate readings due to spalling concrete, the inserts were isolated from the cover concrete with foam rubber and tape (see Fig. 3.7). Two straight rods (1/2 in. diameter steel stock) were embedded in the longitudinal beam, on either side of the column, at 6 in. and 24 in. from the column face to provide reference points for beam rotations. At the longitudinal beam-end beam joints, four PVC tubes were placed to correspond with the four holes in the loading plates used to attach the rams to the specimen (see Fig. 3.8). To remove the specimen from the casting bed, four 1-in. lifting inserts were symmetrically arranged in the longitudinal and transverse beams.

3.1.5 Casting and Curing Procedure. The specimen was cast in two stages with the lower column, joint region, beams, and slab cast in the first operation. Following a four-day curing period,

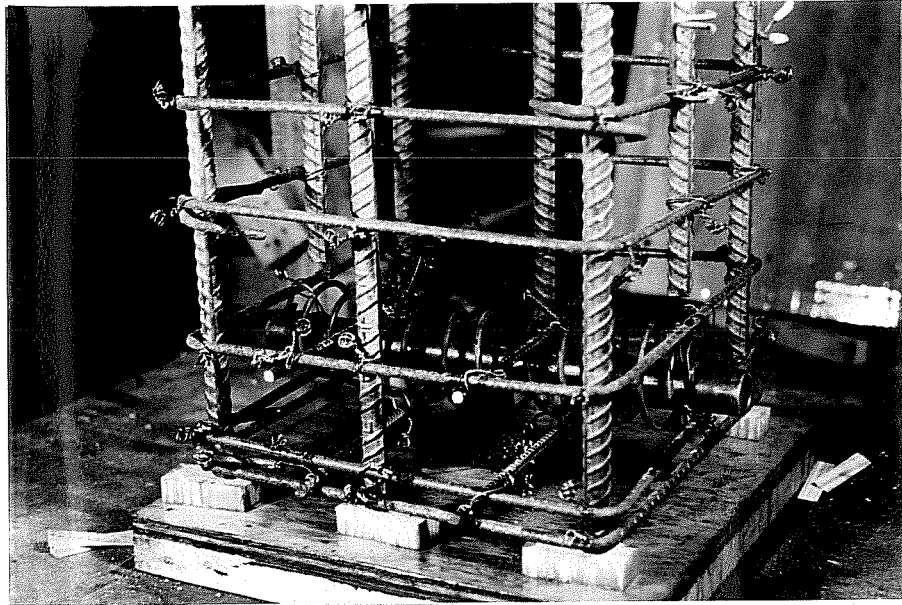


Fig. 3.3 Lower pipe sleeve secured

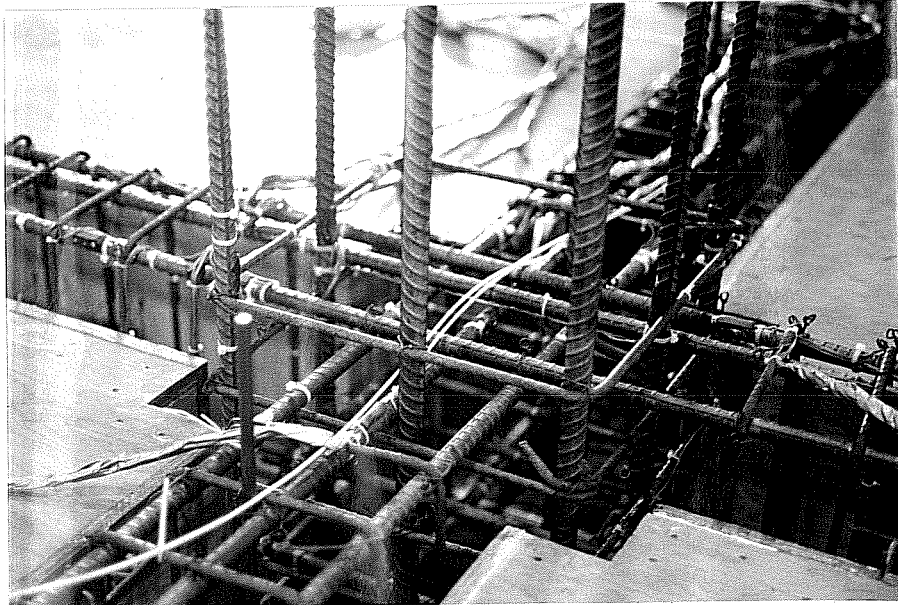


Fig. 3.4 Beam and column cages in place

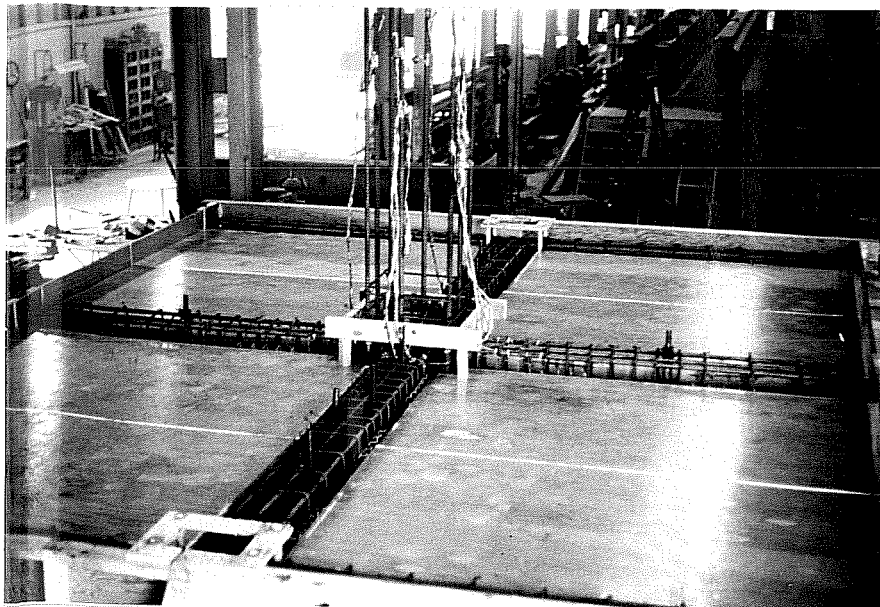


Fig. 3.5 All cages and formwork in place

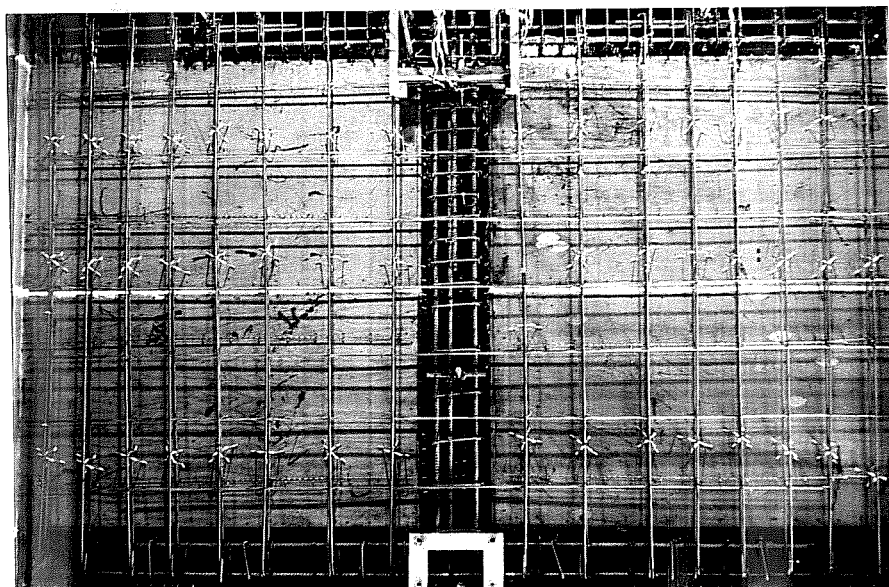


Fig. 3.6 Slab reinforcement placed

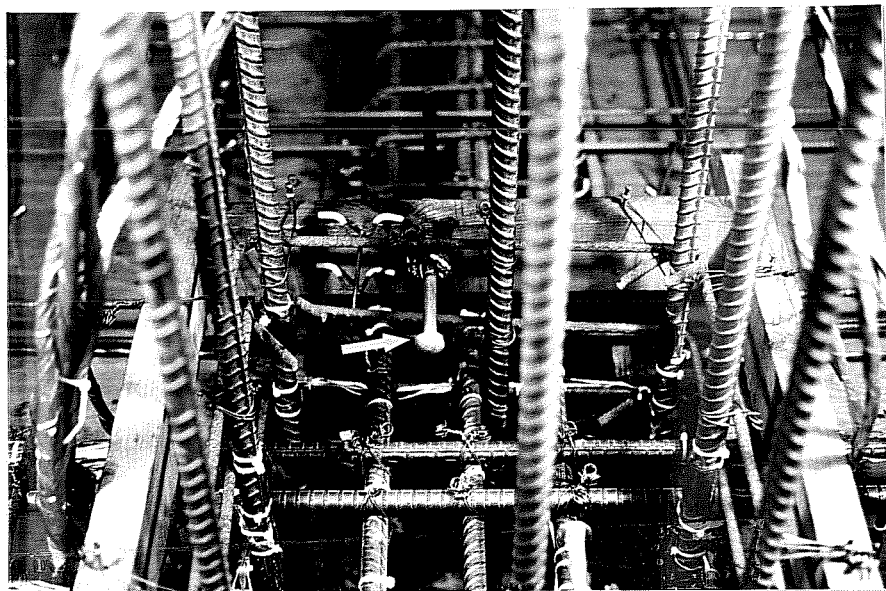


Fig. 3.7 Joint core reference inserts

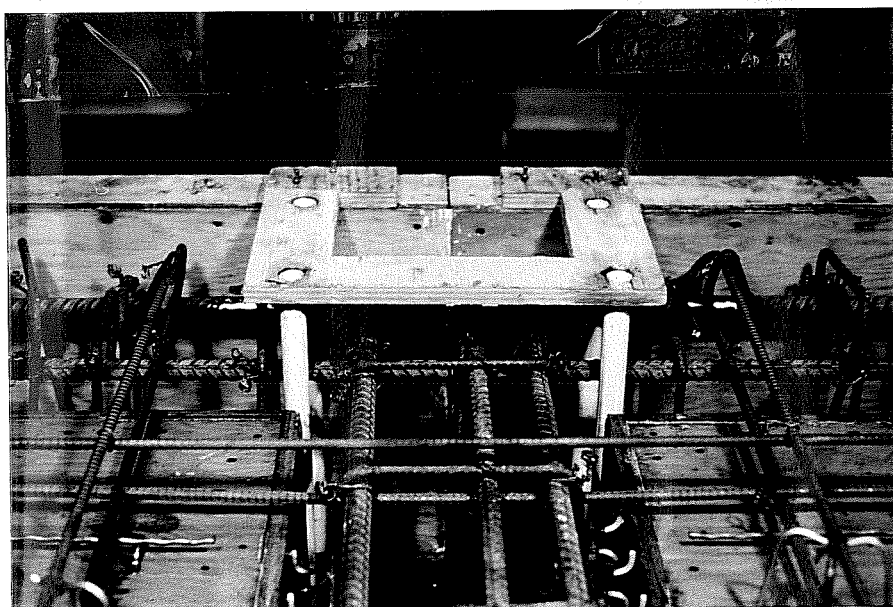


Fig. 3.8 PVC tube inserts

the forms were stripped and the specimen lifted from the platform and moved to a steel frame where the upper column was prepared for casting. Figure 3.9 shows the upper column pipe, pin connection, in place and two 3/4-in. bolts situated vertically in the column cage to be used for lifting and positioning the assembly in the test set-up. The upper column forms were carefully aligned with the help of a small stub cast in the first lift (see Fig. 3.10) and the remaining part of the column was then cast and allowed to cure for several days.

3.2 Material Properties

3.2.1 Concrete. The concrete mix design was proportioned according to standard ACI procedures with an adjustment made for the high strength characteristic of Texas cements. The design strength was 4000 psi and a 1-in. maximum aggregate size was specified, similar to the full-scale structure. Table 3.1 gives the concrete batch proportions, by weight, for the specimen.

During each casting operation, concrete cylinders were cast in standard 6 in. x 12 in. molds and cured for several days as was the test specimen. Concrete strengths were evaluated for various cylinder ages up to twenty-eight days and then again at the time of testing. The average cylinder strengths for USJ-1 at time of testing were 4850 psi and 3450 psi for the first and second casts,

TABLE 3.1 CONCRETE BATCH PROPORTIONS

Cement	545 lbs./yd ³
Coarse Aggregate	1880 lbs./yd ³
Sand	1230 lbs./yd ³
Water*	34 gal./yd ³

*The design slump was 6 in.

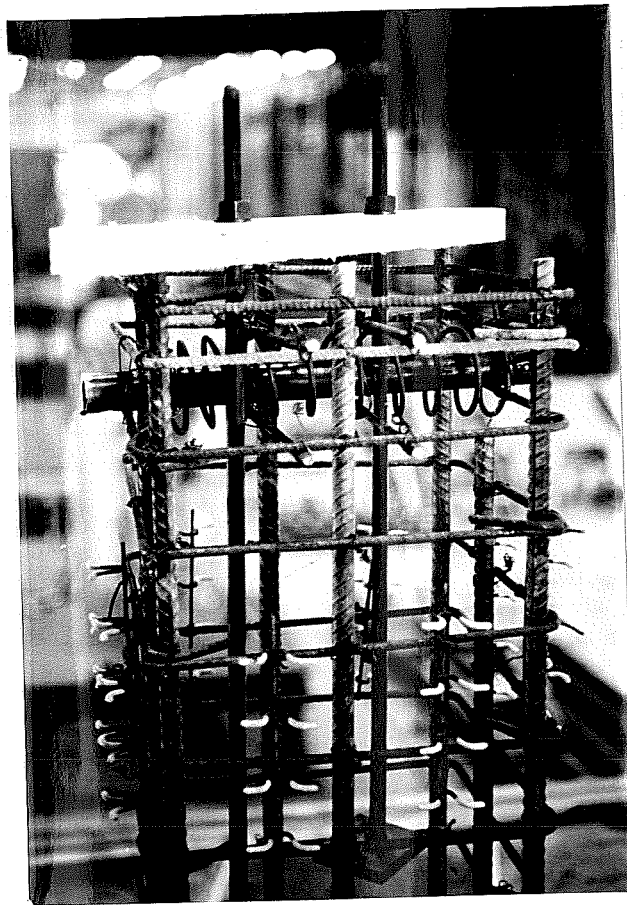


Fig. 3.9 Upper column cage

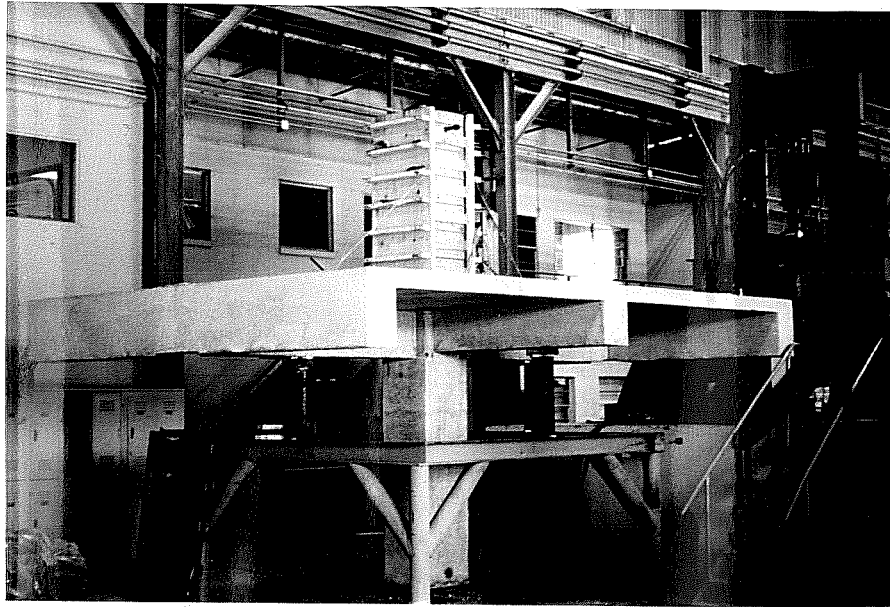


Fig. 3.10 Upper column forms secured

respectively. This significant difference in concrete strengths was not considered a problem, however, because all of the instrumentation was located within regions of higher strength concrete, and relatively small forces were expected on the upper column.

3.2.2 Steel Reinforcement. The steel reinforcement used in the test specimen included #3 beam and column ties, #3 slab bars, #6 longitudinal and transverse beam bars, and #7 column and end beam bars. Coupons representative of each bar size were tested. Two paper-backed strain gages were attached to each coupon to permit stress-strain relationships to be electronically recorded and plotted with an x-y plotter (see Fig. 3.11). It should be mentioned that it was not possible to obtain the complete strain hardening curves to ultimate strain or load levels.

The high yield stress, 78 ksi, of the #7 bars increased the column moment capacity approximately 25 percent, but was not considered a problem for the component tests. Since the loads were applied through the beams, relatively small forces were transferred to the column. Therefore, yielding in the column was not expected at deflection levels corresponding to measured drifts in the full-scale structure whether the column was reinforced with 60-ksi or higher strength steel. However, the use of higher strength reinforcement in beams of frame structures can lead to potential problems such as higher shears transferred to the joint, larger development lengths required for beam bars, and less ductility.

3.3 Instrumentation

3.3.1 Reinforcing Bars. Electrical resistance strain gages were mounted on the beam, column, and slab bars as well as the beam and column transverse reinforcement. The procedure for instrumenting the bars required grinding off the bar deformations, sanding and cleaning the surface, attaching the gage with epoxy, soldering a lead wire to the gage, coating the gage and solder connection with

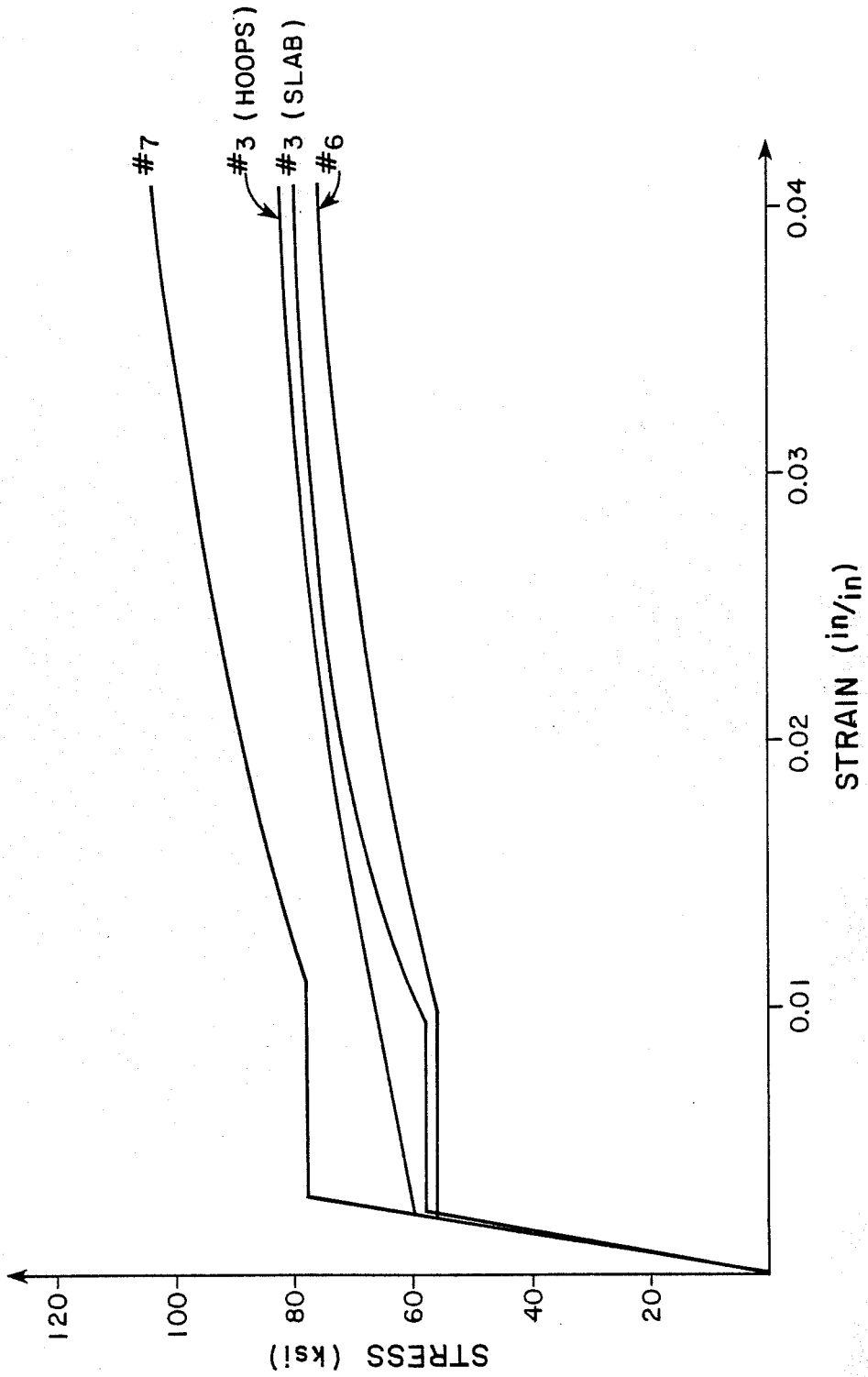


Fig. 3.11 Stress-strain relationships for reinforcement

a moisture barrier, and then covering it with an adhesive rubber compound. The strain gages on the larger bars, #6 and #7, had a 0.64-in. gage length and the gages on the smaller, #3 bars, had a 0.32-in. gage length. Figure 3.12 shows a typical reinforcing bar for USJ-1 with mounted strain gages.

The principal strain gage locations in the test specimen were identical to those in the prototype structure which included gages on the beam and column bars near the critical sections at the beam-column interfaces (see Fig. 3.13), and longitudinal slab bars at the transverse beam-slab interfaces. Additional gages were located in the slab (see Fig. 3.14), in the joint core on the column hoops, and in the transverse beam on the beam ties (see Fig. 3.15). The number of strain gages were reduced to a minimum by taking advantage of the specimen symmetry to instrument the south-west quadrant rather heavily and place only a few gages in the remaining three quadrants as checks. Comparisons of strain magnitudes with the full-scale test results, in Chapter 5, will deal primarily with longitudinal beam and column bar strains.

3.3.2 Beam Rotations. The longitudinal beam rotations near the east and west column faces were measured relative to the column with potentiometers mounted on the embedded rods above and below the longitudinal beam (see Fig. 3.16). Aluminum plates were bolted to the inserts embedded in the column above and below the joint to provide smooth reference surfaces for the plungers of the potentiometers. The potentiometers measured horizontal displacements over a known gage length as the beam rotated (see Fig. 3.17). The difference in the two readings was used to determine the angle of beam rotation between the column and the rod embedded in the beam 6 in. from the column face. The calculated rotations included the effects of both elastic and inelastic beam deformations as well as slip of the beam bars through the joint. Similar instrumentation was used to measure rotations in the prototype structure, but over an 8 to 9 in. length from the column face.

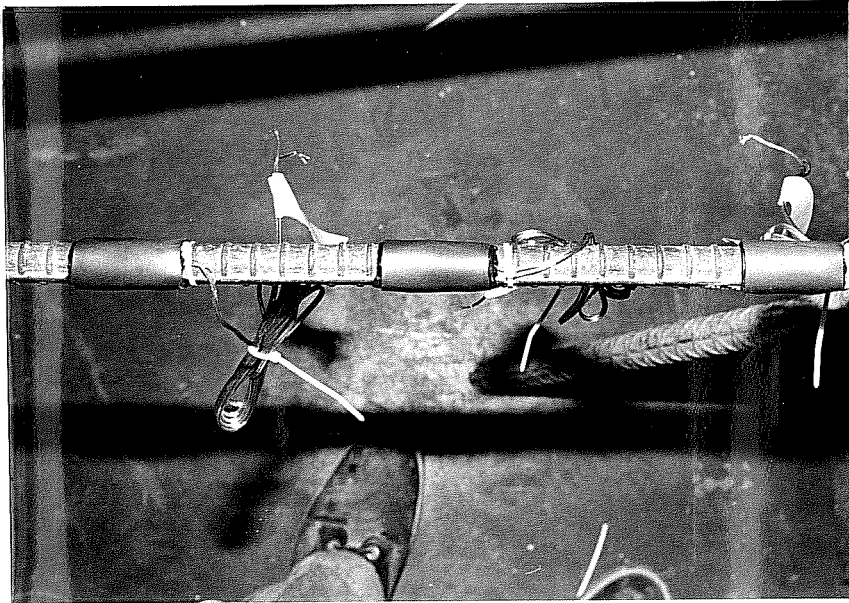


Fig. 3.12 Mounted strain gages

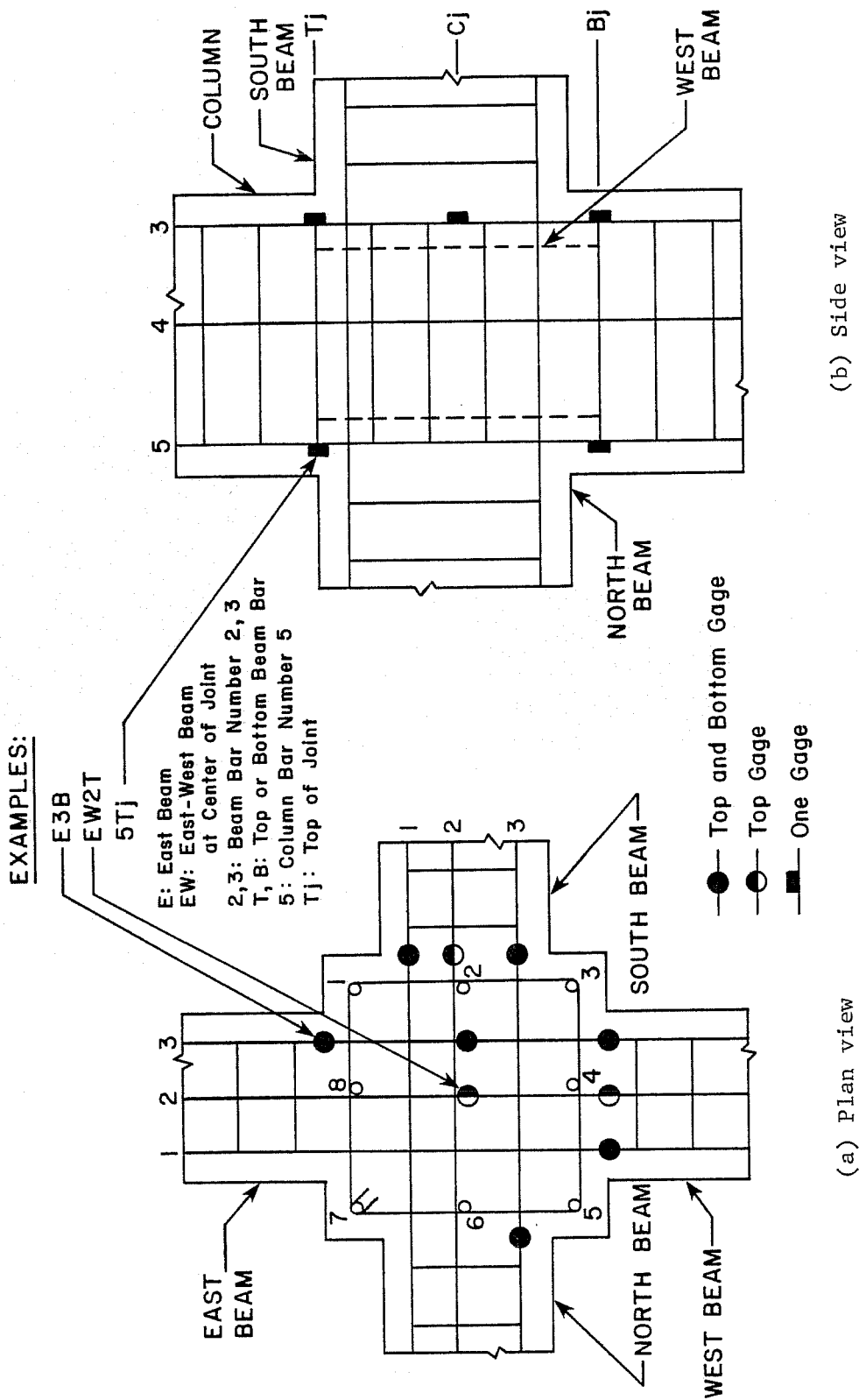


Fig. 3.13 Beam and column bar gage locations

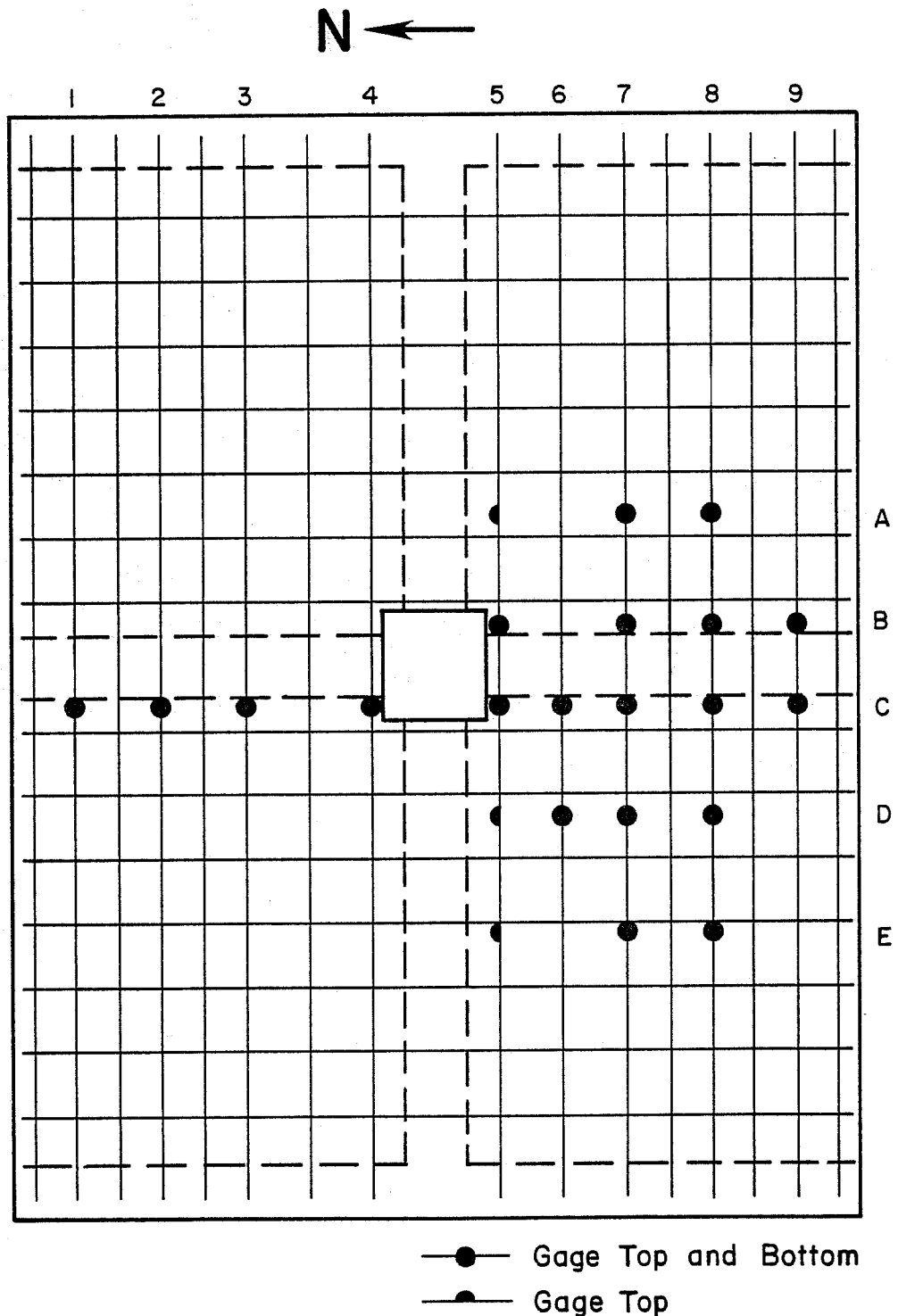


Fig. 3.14 Slab gage locations

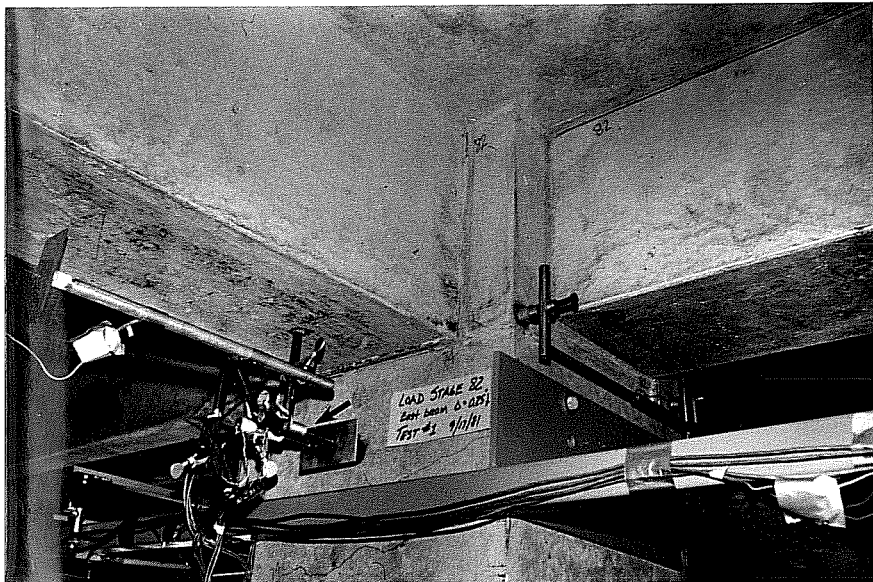
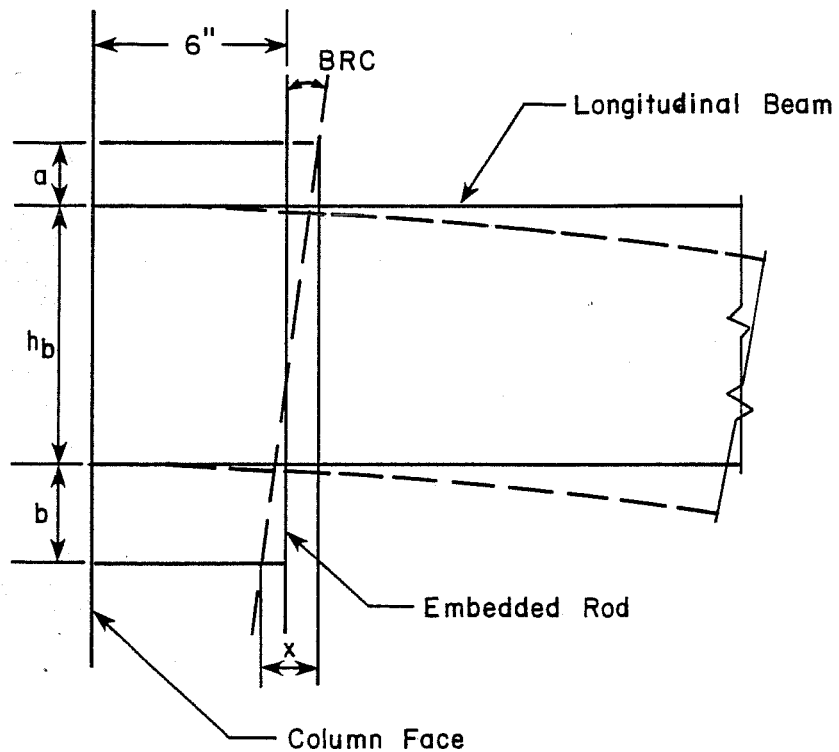


Fig. 3.16 Beam rotation instrumentation



BRC = beam rotation relative to column, rad.

h_b = beam height, in.

a = distance of potentiometer above beam, in.

b = distance of potentiometer below beam, in.

x = difference in potentiometer readings, in.

By geometry,

$$\text{BRC} = \frac{x}{h_b + a + b}$$

For this geometry; $h_b = 19.75$ in., $a = 2.75$ in., $b = 5.5$ in.,

$$\text{BRC} = 0.0357x$$

Fig. 3.17 Beam rotation geometry

The following calculations for beam rotations, relative to the column, are based on the approximate geometry and beam deformations shown in Fig. 3.17. Observe that the calculated rotations do not represent the actual beam rotations since no corrections have been made for joint rotations or elastic flexural rotations of the column. However, the rotations were determined in an identical manner for the test specimen, the half-scale component tests, and the full-scale tests.

3.3.3 Beam Deflections. The beam deflections were measured with 12-in. potentiometers attached to the rams as illustrated in Fig. 3.18. The sliding arm of the potentiometer was connected to an aluminum reference plate situated at the top of the ram piston so that the arm displacement of the potentiometer corresponded to the piston displacement.

3.3.4 Beam Loads. The east and west beam loads were measured electronically with load cells attached to the hydraulic rams.

3.3.5 Joint Shear Strain. The joint shear strain was measured with the stainless-steel assembly shown in Fig. 3.19. Two sliding arms were attached to three reference inserts embedded in the joint core and located on the north column face below the slab. A potentiometer was mounted between the two sliding arms, which extended past a pivot point, to form a triangle (see Fig. 3.20(a)). As shear strains were imposed on the joint core and the arms moved relative to each other, the potentiometer measured changes in the length of the third side of the triangle between the arms. The joint shear strain could then be obtained using the law of cosines as illustrated by the calculations in Fig. 3.20.⁵

3.3.6 Additional Instrumentation. Additional instrumentation on the test specimen was used to measure joint rotations, longitudinal beam rotations 24 in. from the column face, slip of the longitudinal

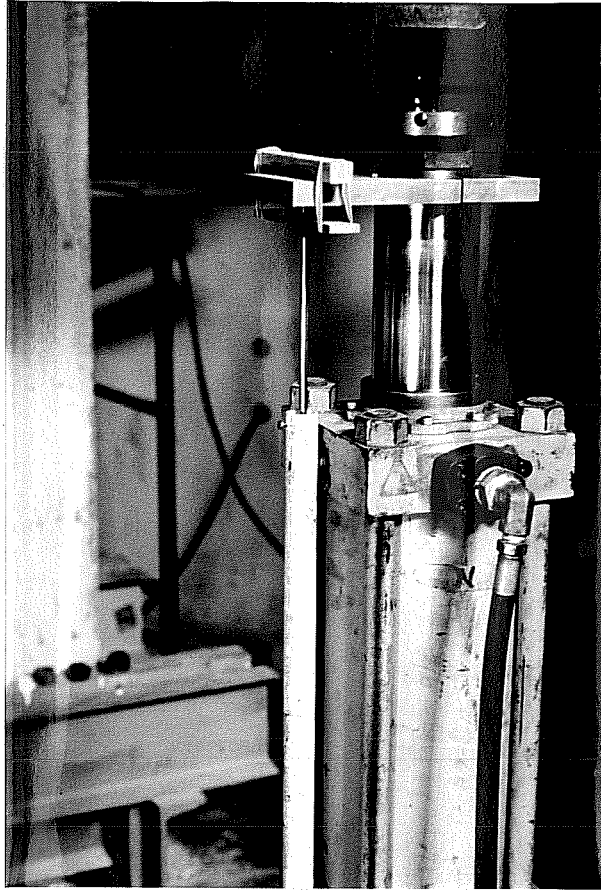


Fig. 3.18 Beam deflection instrumentation

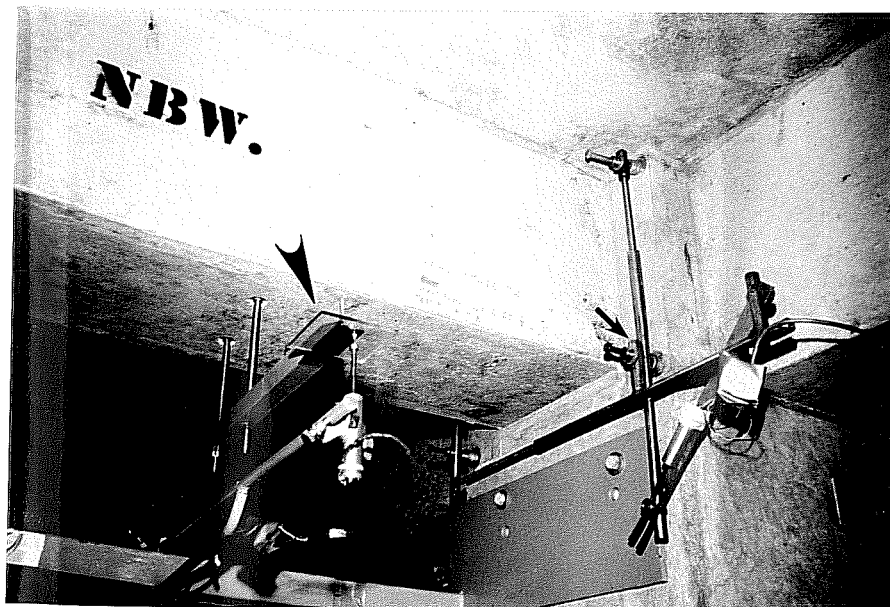
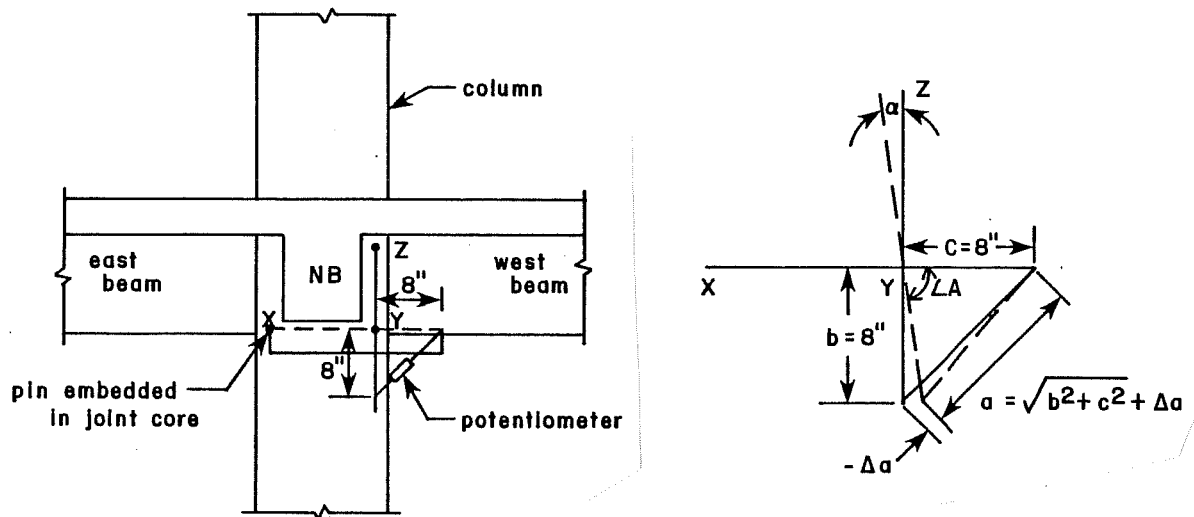


Fig. 3.19 Joint shear strain instrumentation



(a) Location of shear strain assembly

(b) shear strain geometry

α = joint shear strain, rad.

Δa = potentiometer measurement, in.

Law of cosines:

$$a^2 = b^2 + c^2 - 2bc \cos \angle A$$

$$\angle A = \cos^{-1} \left(\frac{-a^2 + b^2 + c^2}{2bc} \right)$$

$$= \cos^{-1} \left(\frac{b^2 + c^2 - (\sqrt{b^2 + c^2 + \Delta a^2})^2}{2bc} \right)$$

$$= \cos^{-1} \left(\frac{128 - (11.31 + \Delta a)^2}{128} \right)$$

$$\alpha = \angle A - \frac{\pi}{2}$$

Fig. 3.20 Joint shear strain calculation

beam bars, and twist of the transverse beam. However, no further consideration of these measurements will be given in this study since similar instrumentation was not used in the prototype structure or the half-scale component tests.

3.4 Testing Apparatus

3.4.1 Loading Frame. The testing apparatus, illustrated in Fig. 3.21 with the specimen in place, included a floor fixture, a wall bracket fixture, two channel struts extending from the reaction wall, two angle braces extending from an adjacent testing frame, and the reaction wall and floor. Pin connections, using 1-1/4 in. high-strength bolts, were provided to simulate zero-moment conditions at the top and bottom of the specimen, as mentioned in Chapter 2. The lower column was pinned to the floor fixture, bolted to the reaction floor, and in a similar manner the upper column was pinned to the channel struts, bolted to the wall bracket. The angle members, attached to the south channel strut, supplied lateral bracing to the specimen.

3.4.2 Pin Connections. The pin connections at the top and bottom of the column were very similar in design and detail so only the lower assembly will be discussed further. The floor fixture, shown in Fig. 3.22, was fabricated with two 18-in. deep channel sections and a large rectangular 1-1/4 in. floor plate. To facilitate positioning the specimen in the testing frame, only one of the channels was welded to the floor plate and the other bolted after the specimen was in place. Two clamping plates, one between the column face and the channel and the second on the outside of the channel, were firmly bolted to each channel after the pin was inserted through the entire assembly, including the column, to secure the specimen (see Fig. 3.23). Oversized holes, for the pin and the four clamping bolts were drilled in each channel section to offset any alignment problems due to fabrication errors.



Fig. 3.22 Floor fixture

A minor problem with the pin connections did arise during testing. Slip of the top and bottom pins in the oversized holes was detected as the specimen was loaded up to a particular deflection level, at which point the pins became seated. A gradual increase in slip did continue at higher load levels which was attributed to bending of the pin. In Chapter 4, a correction calculated from the measured displacements, or slip of the lower and upper columns in the pin connections, was used to adjust the beam deflections.

3.4.3 Hydraulic System. The procedure for applying the racking loads to the west and east beams is illustrated in Fig. 3.24. Two double-rod hydraulic rams, each with a capacity of 100 kips, were used to apply the loads at either end of the longitudinal beam. The sequence of loading the two beams was reversed, displacing one beam downward and the other upward. For the west beam, hydraulic oil was pumped through the right manifold of pump #1 and into the bottom of the west ram to displace the beam downward. The oil displaced from the top of the west ram returned to the pump through valve 1. To load in the opposite direction, for either ram, valve 2 was opened to release the pressure and the flow of oil was reversed.

Two hydraulic systems were used in Tests 4 and 5 which were independent of each other (see Fig. 3.24). However, for the first three tests, a single hydraulic system was used to apply the west and east beam-end deflections. Ideally, the volume of oil in such a system remains constant. But due to an error in the hydraulic line connections, the specimen was tested under a load control rather than deflection control system, and the west and east beam displacements differed. This problem was corrected for the subsequent tests.

3.5 Test Procedure

The specimen was subjected to predetermined displacement levels typical of the inter-story drift levels imposed on the prototype structure. A series of five tests, with increasing magnitudes of beam deflection, were conducted and a complete description of each of the applied load histories will be given in Chapter 4.

To begin testing a zero-load reading, used as a reference base for all succeeding readings, was taken for the 125 channels of data. The three valves on the hydraulic pump consoles were used to control the applied racking loads according to the particular loading history. Following each increment of displacement, a data reading was taken. The east and west beam deflections and corresponding beam loads were continuously monitored with x-y recorders. Also, certain data channels were periodically checked to verify observed and predicted behavior of the specimen throughout the test.

3.6 Data Acquisition and Reduction

The test data were recorded on magnetic tape with a digital data acquisition system. A hard copy of the voltage readings was obtained on a printer near the test set-up. The magnetic tape was mounted on a mini-computer tape drive to store the data on a computer disc for future processing. The mini-computer along with an available data reduction program converted the voltage readings into engineering units. With the aid of other selected software packages, the converted data could be assembled into plot files according to channel numbers and plots could be produced on a digital plotter.

C H A P T E R 4

PRESENTATION OF TEST RESULTS

4.1 Introduction

Test results and observations from the series of tests performed on the interior joint specimen are presented and discussed in this chapter. Specifically, load histories, beam load versus beam-end deflection plots, cracking patterns, and test measurements; strains, rotations, etc., are given for Tests 2 through 5. Test 1 was not included since it was used essentially to check the hydraulic and electronic systems and to establish suitable test procedure. The load versus deflection behavior and the cracking patterns were reviewed at various load stages in each test to evaluate the observed response of the specimen to simulated seismic excitations. Measurements of longitudinal beam, column, and slab bar strains, joint hoop strains, longitudinal beam rotations, and joint shear strains were used to assess the overall performance of the interior joint specimen.

The beam-column joint assembly was subjected to uniaxial, reversed cyclic loads throughout the test series. The chosen load histories, deflections applied at the longitudinal beam ends, represented inter-story drifts measured at the second level of the full-scale structure. The beam displacements in Tests 1, 2, 3, and initially in Test 4 and the lateral drift levels were similar in magnitude; however, it was not feasible to duplicate the loading sequence used in the prototype tests. The load histories for the seven-story structure were based on recorded earthquake motions modified to excite primarily a first-mode response of the structure. A displacement record based on ground motion would be difficult to

reproduce in the component tests. Therefore, selected peak deflection levels which increased as testing continued were used to correlate test results between the full-scale structure and the component tests.

4.2 Test Descriptions

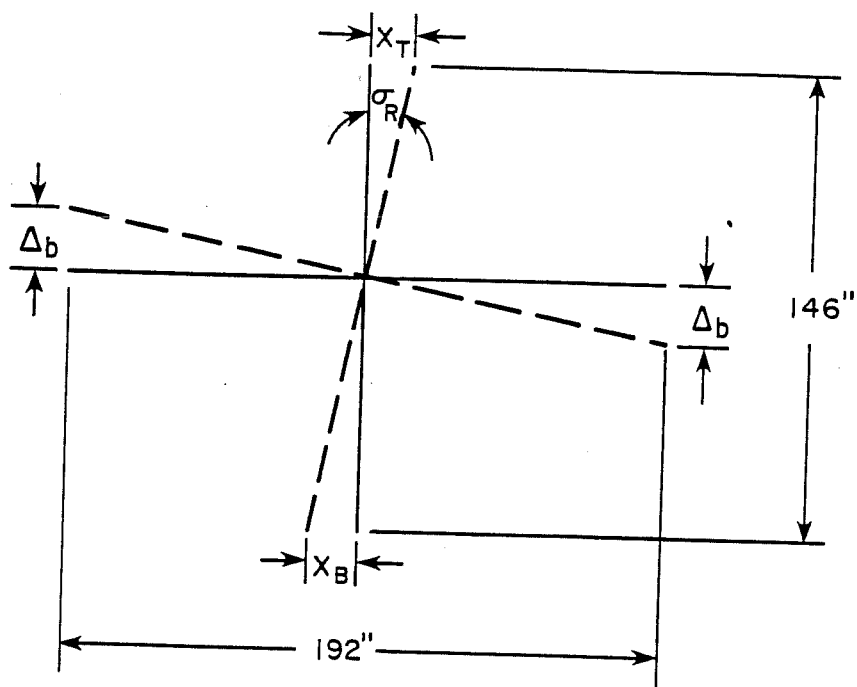
4.2.1 General. The applied west and east beam-end deflections were controlled in the hydraulic loading system used for testing USJ-1 (refer to Sec. 3.4.3). The advantage of such a system was its capability of imposing consistent beam displacements, particularly once the behavior became inelastic where a load-control system would not be suitable. However, as mentioned in Chapter 3, an improper connection in the hydraulic lines resulted in a load-control rather than deflection-control system for Tests 2 and 3. For Test 2, this error in the loading system was insignificant due to the relatively small displacement levels. In Test 3, however, a large beam displacement was inadvertently applied to the east beam. An upward deflection, defined as negative, of nearly 2.5 in. was recorded for the east beam. Since the beam was bending in the flexurally weak direction some permanent deformation was produced. The damage appeared to be minimal and was confined primarily to the tension zone near the bottom of the east beam at the column face. The strain in the lower beam bars was considerably higher than yield, but below strain hardening, and yielding of these bars had spread into the joint. Test data obtained prior to the last load cycle in Test 3 were acceptable since the applied beam displacements, although not equal, were small. Furthermore, useful information such as yield loads and deflections for positive bending, and stiffness characteristics were acquired as the negative deflections of the east beam increased. Finally, the damage to the specimen was not extensive and was not considered to significantly affect further test results.

A second problem which developed during testing, also mentioned in Chapter 3, concerned the slip or horizontal displacement of the lower and upper column pin connections. Attempts to eliminate the slip, attributed to the oversized holes in the channel sections and bending of the pin, were unsuccessful. Therefore, potentiometers were used to measure the horizontal displacements of the lower and upper columns at the pin levels so a correction could be calculated for the beam-end deflections. The potentiometers were secured to the loading frame and measured lateral deflections, at pin level, on the east face of the lower column and the west face of the upper column.

The correction used to adjust the beam deflections, or slip correction, was calculated from the potentiometer readings, assuming rigid body rotation of the specimen (see Fig. 4.1). The relative magnitude of the slip correction varied depending on the intensity of the load history. At small deformation levels, i.e., Tests 2 and 3, the slip accounted for 15 to 25 percent of the beam deflection. However, in Tests 4 and 5, the slip accounted for 7 percent or less of the beam deflection. In Sec. 4.2.2.2 load versus deflection plots for Test 2 with and without the adjustment for slip are compared.

4.2.2 Test 2

4.2.2.1 Load History. The load history for Test 2 is shown in Fig. 4.2. Note, a downward beam displacement is defined as a positive deflection. The initial beam displacement of 0.05 in. was estimated to be the deflection corresponding to torsional cracking of the transverse beam; however, this was not the case. Subsequent peak deflections were selected by simply doubling the previous peak displacements to a maximum of 0.4 in., calculated as the yield deflection for the bottom longitudinal beam steel. The smaller deflection cycles were repeated prior to each new displacement peak so comparisons of load-deflection behavior, at various



X_T = measured slip at top, in.

X_B = measured slip at bottom, in.

σ_R = angle of rigid body rotation, rad.

Δ_b = correction for beam deflection, in.

$$\sigma_R = \frac{X_T + X_B}{146}$$

$$\Delta_b = \frac{X_T + X_B}{146} (96) = 0.658(X_T + X_B)$$

Fig. 4.1 Slip correction

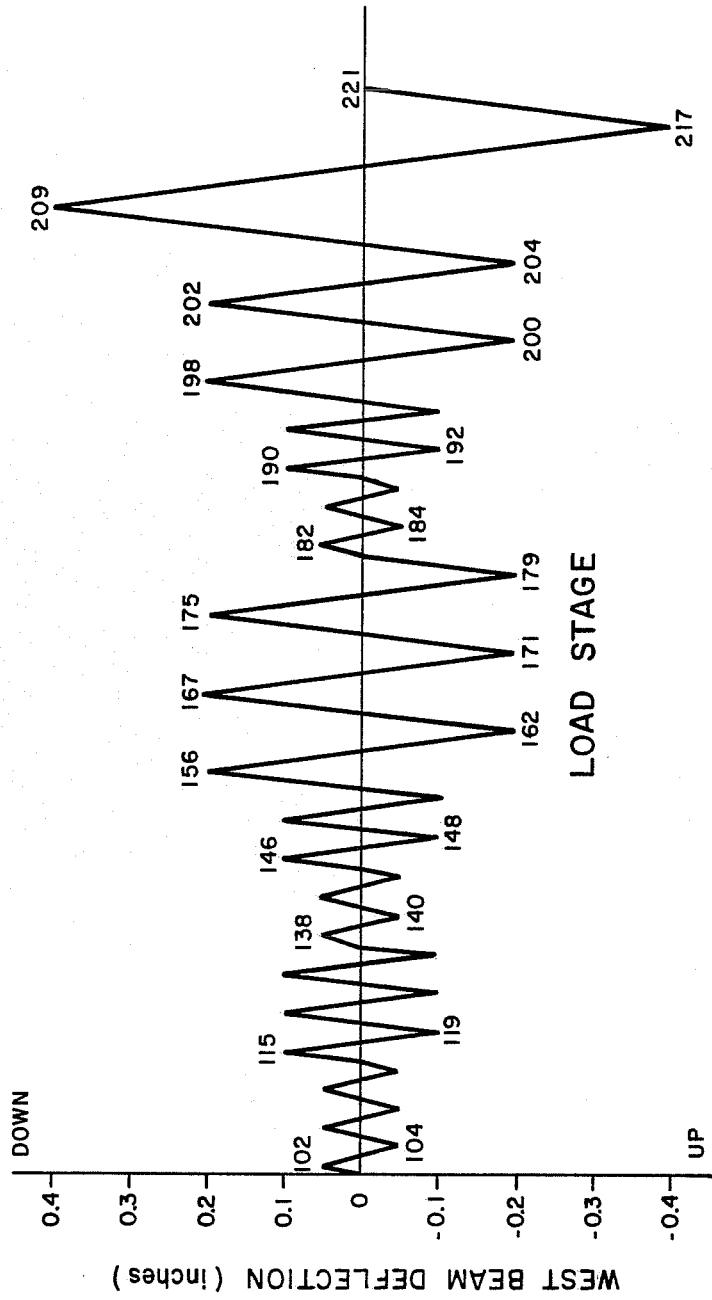


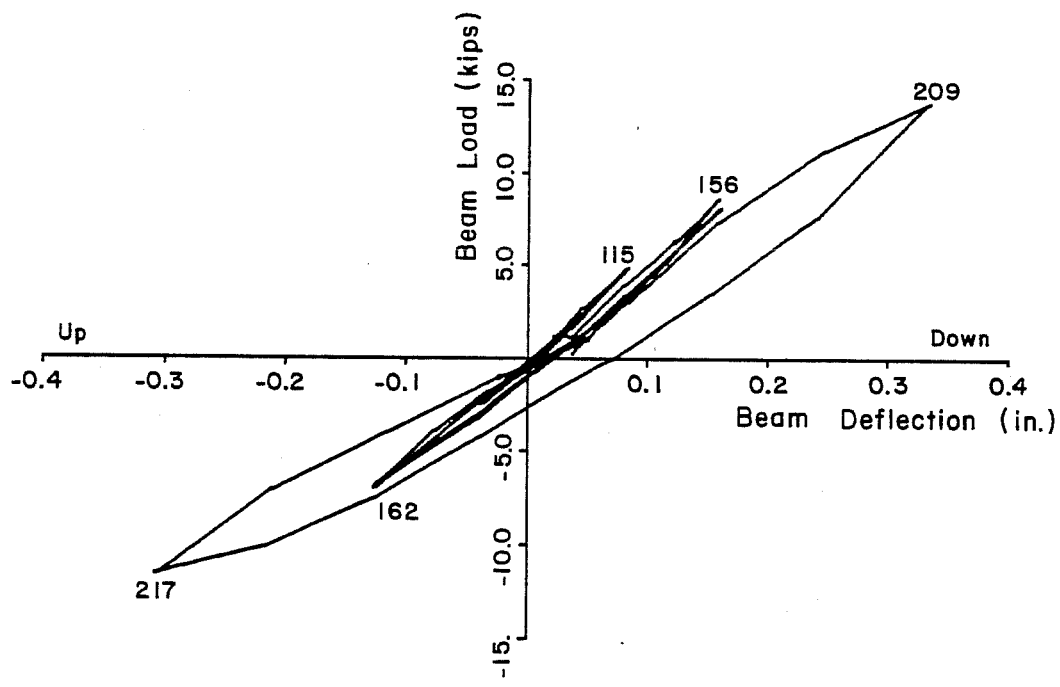
Fig. 4.2 Load history, Test 2

stages in the testing, could be made. Test 2 was stopped following completion of the first deflection cycle at 0.4 in. to determine if the slip of the pin connections could be reduced or eliminated.

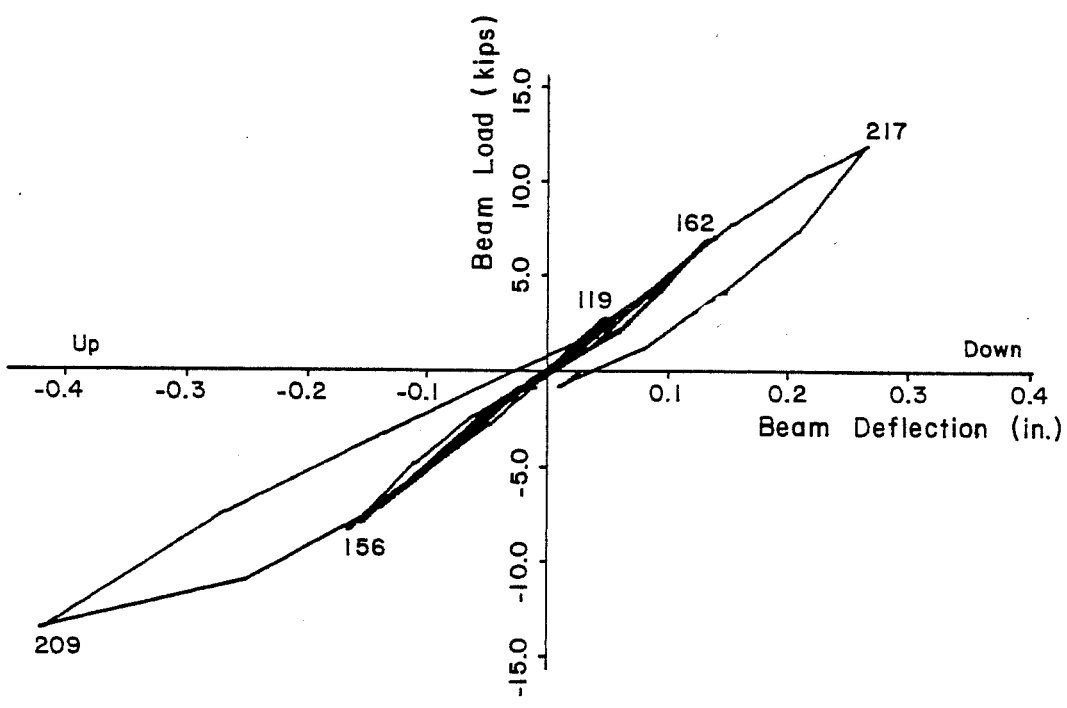
4.2.2.2 Load-Deflection Behavior. The beam load versus beam-end deflection plots, shown in Fig. 4.3, indicate that the behavior of the specimen, prior to the last deflection cycle, was relatively elastic during Test 2. As the displacement levels were increased, the stiffness deteriorated slightly, primarily due to the initial flexural cracking in the beams and slab. At the peak beam displacement, a small hysteresis loop was observed (see Fig. 4.3). The west and east beam deflections varied somewhat, particularly during the last displacement cycle, because the loading system was inadvertently operated by load control. The positive and negative deflections of the west beam were nearly identical since the displacement of the west ram was monitored during testing.

The adjustments made to the load versus deflection plots using the calculated slip corrections are illustrated in Fig. 4.4. The misleading increase in beam stiffness which was characteristic of crack closure with load reversal was no longer evident once the slip was removed.

4.2.2.3 Cracking Patterns. Flexural cracking in the column and longitudinal beams, and at the transverse beam and slab interface, first appeared during the last stages of Test 1 at a beam deflection of approximately 0.20 in. Separation cracks at the longitudinal beam and slab interface, which extended along the length of the beam, were visible in Test 1. In general, the amount of cracking observed in Test 2 was minimal. The flexural cracks extended slightly (see Fig. 4.5), as did the separation cracks, during the last deflection cycle of Test 2, at load stages 209 and 217; however, no new cracks appeared.



(a) West beam



(b) East beam

Fig. 4.3 Load versus deflection behavior, Test 2

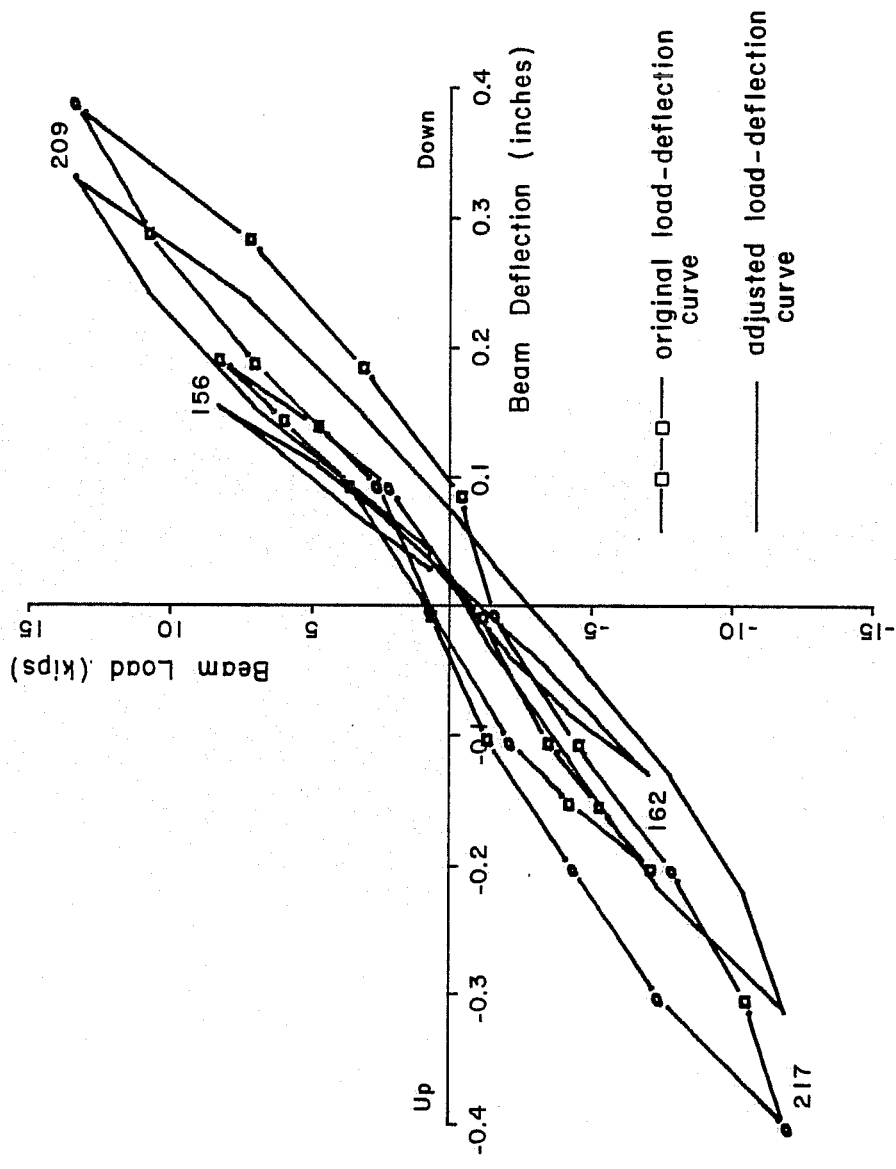


Fig. 4.4 Slip correction for load-deflection behavior, Test 2

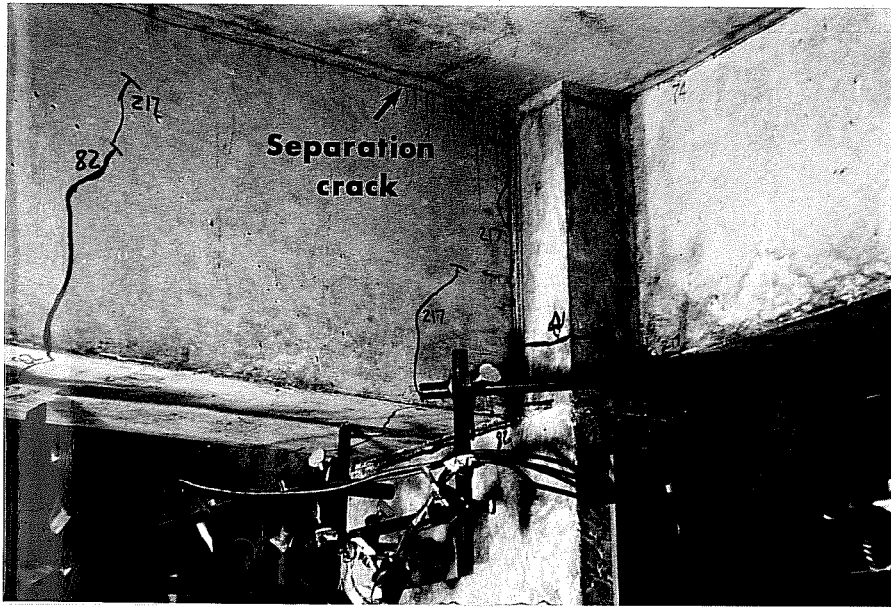


Fig. 4.5 Initial flexural cracks in west beam

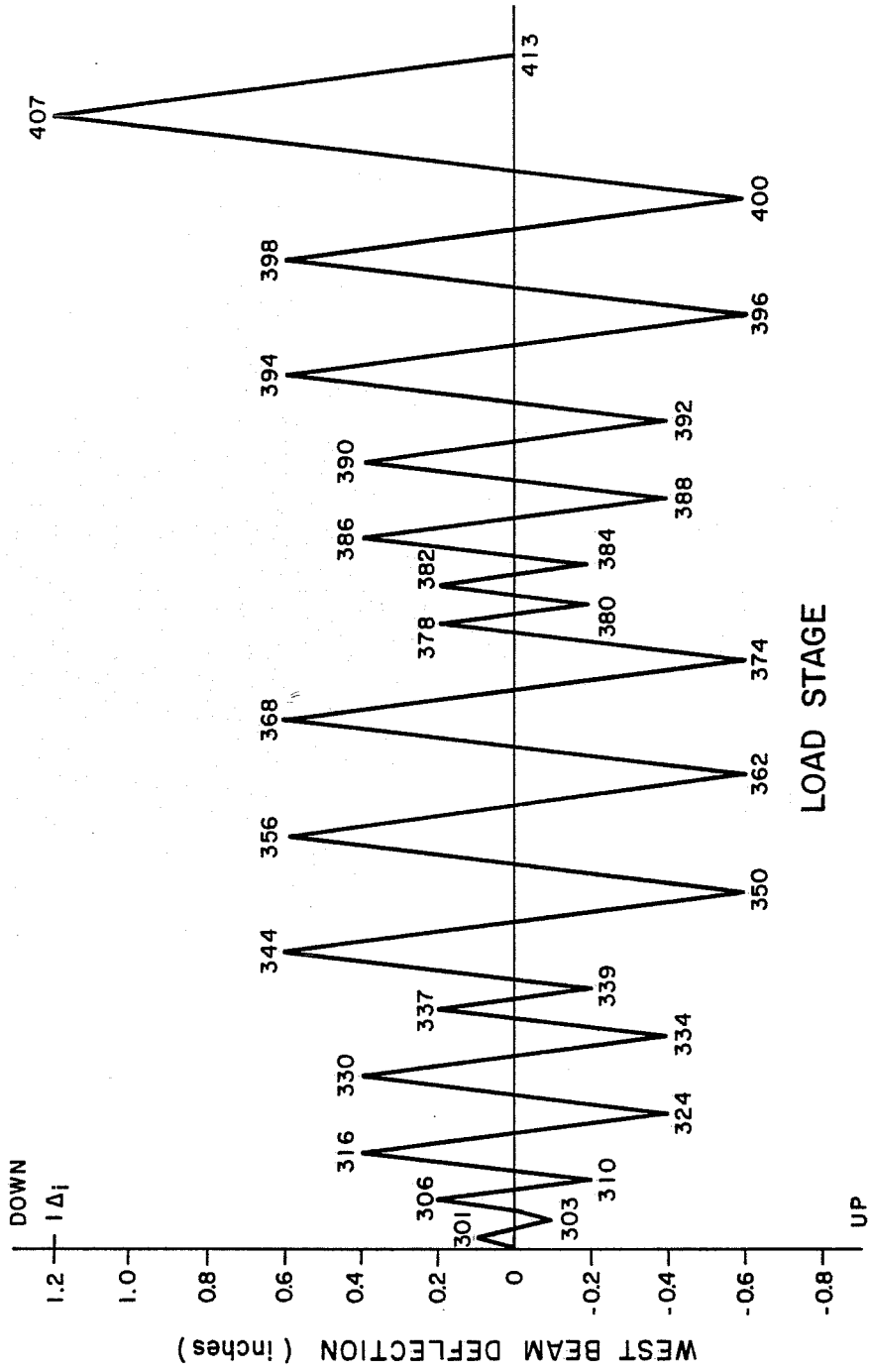
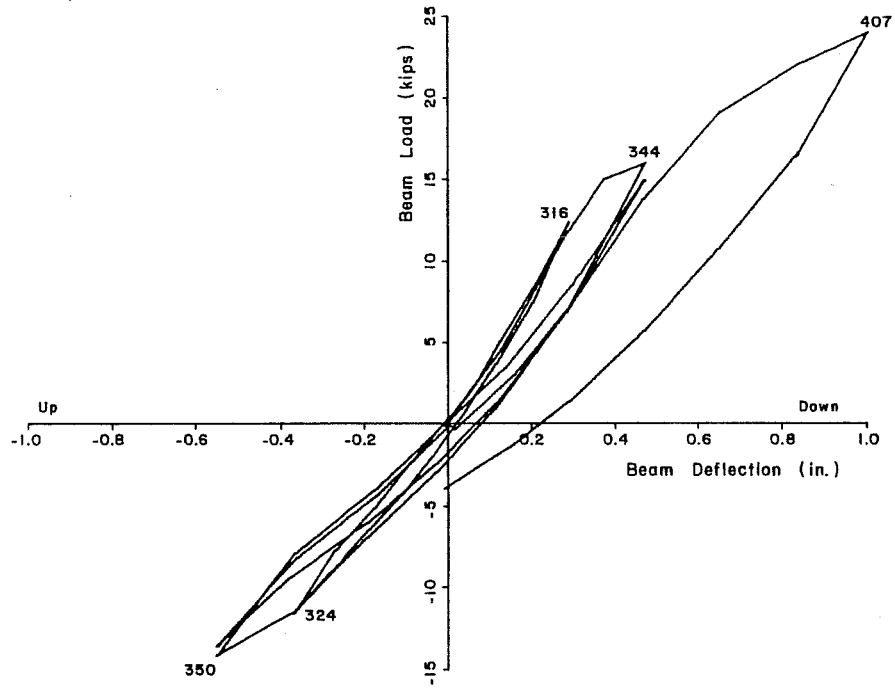
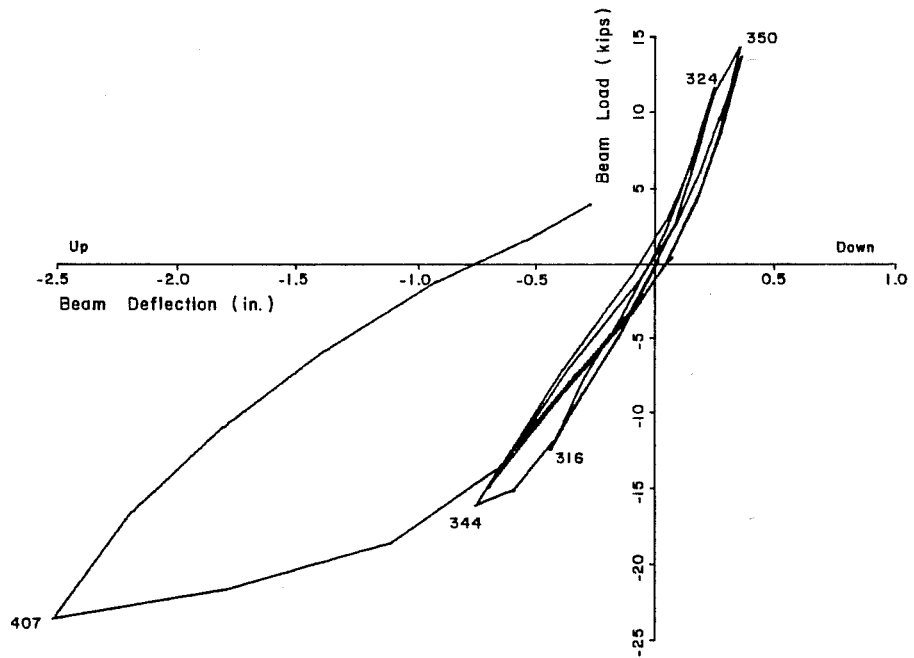


Fig. 4.6 Load history, Test 3



(a) West beam



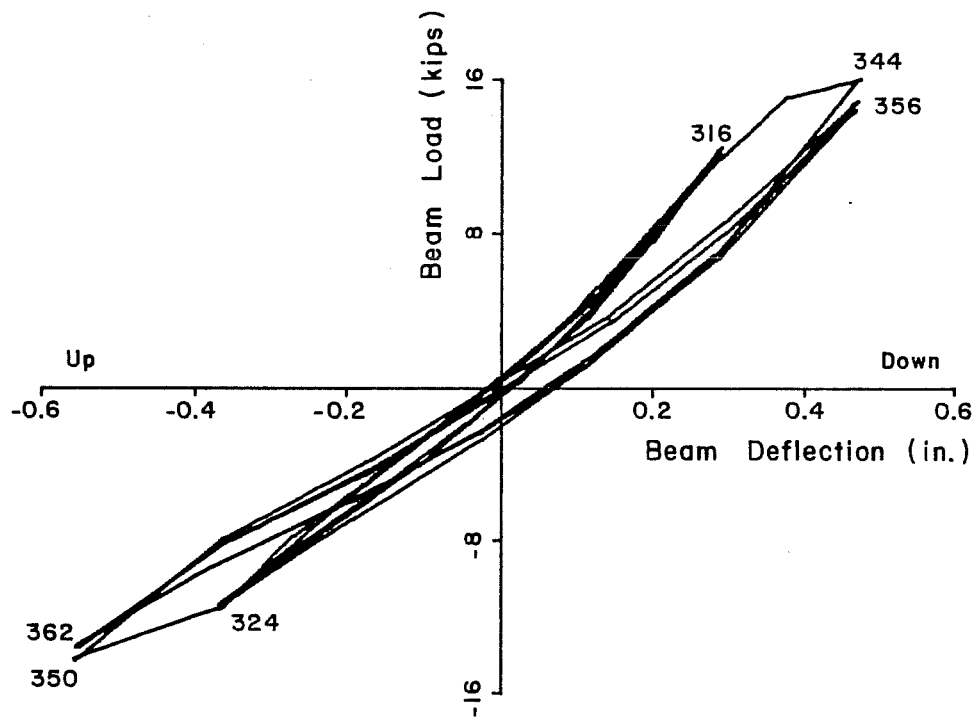
(b) East beam

Fig. 4.7 Load versus deflection behavior, Test 3

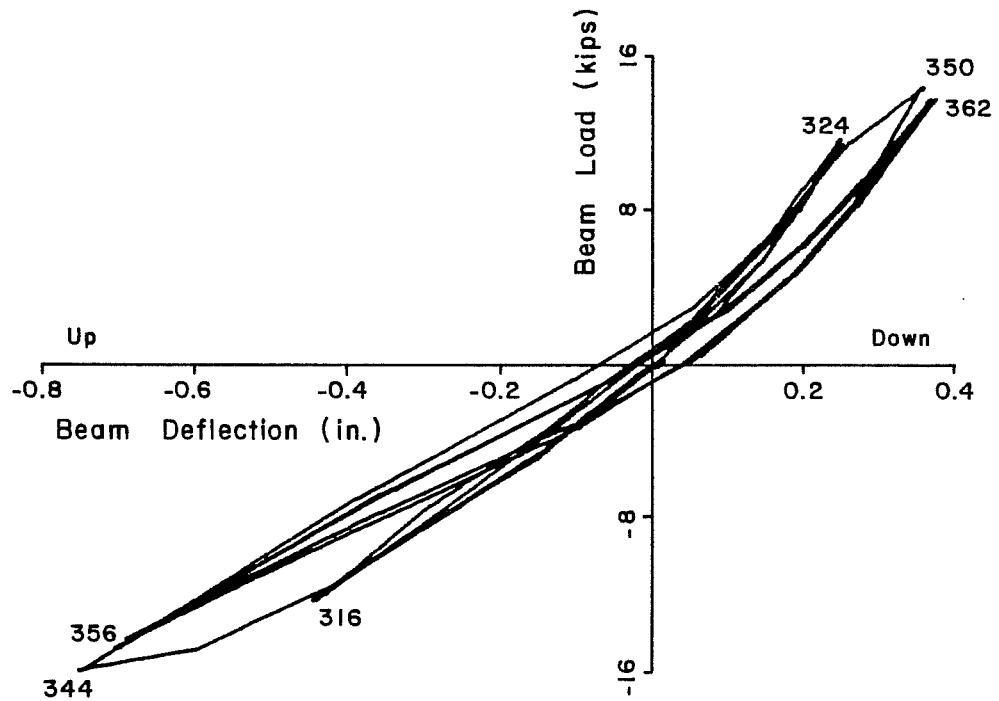
Figure 4.8 shows load-deflection plots for several cycles of loading prior to and including the $\Delta_i/2$ deflection level in Test 3. Some deterioration of the initial beam stiffness due to cracking in the specimen occurred since Test 2 (refer to Fig. 4.3). The stiffness increased, however, as the beam deflections became larger and the cracks closed. Finally, the adverse effect of cyclic loading on stiffness, even at relatively small displacements, is apparent in Fig. 4.8. Note the degradation in stiffness between the first (load stages 344 and 350) and second (load stages 356 and 362) cycles at $\Delta_i/2$.

4.2.3.3 Cracking Patterns. Several new flexural cracks were initiated in the longitudinal beams and column during the first cycle of deflection to $\Delta_i/2$ (see Fig. 4.9). Although the west and east beam deflections differed, the cracking patterns were nearly symmetric about the centerline of the transverse beam. The flexural cracks originating at the bottom of the longitudinal beams extended nearly to the slab. Flexural cracks in the slab propagated in the transverse direction toward the edge of the slab on top and bottom (see Fig. 4.10). Two of these cracks, one on either side of the transverse beam approximately 12 in. from the column face, extended through the slab and into the longitudinal beam. No new cracks and minimal crack propagation, primarily in the slab, were observed as cycling continued at this deflection level.

Torsional cracks on the east face of the transverse beam near the column first appeared at load stage 406 (see Fig. 4.11). The corresponding west and east beam deflections were 0.85 in. and -1.8 in., respectively; and a load of 22 kips was measured on each beam. A wide separation crack between the east beam and the lower east column face developed during load stages 406 to 408, attributed to the large beam displacements. Some new flexural cracking was present in the east beam and the slab, as well as extensions of existing cracks. Finally, note the crack propagating diagonally,



(a) West beam



(b) East beam

Fig. 4.8 Stiffness deterioration, Test 3



Fig. 4.9 Flexural cracking in east beam



Fig. 4.10 Flexural cracking in the slab

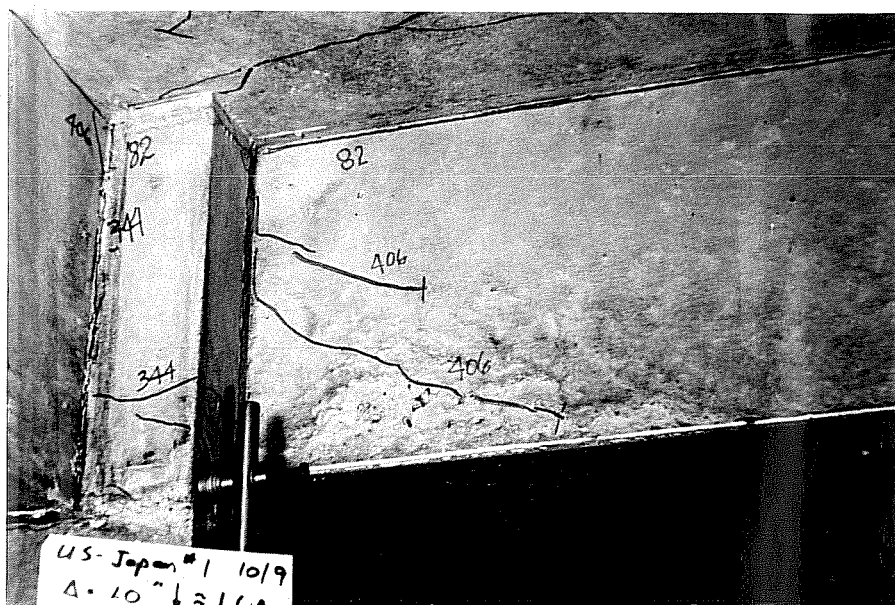


Fig. 4.11 First torsional cracks in transverse beam



Fig. 4.12 Crack propagating diagonally in slab

at approximately 45° , from the southeast column corner in the bottom of the slab (see Fig. 4.12). A similar crack appeared on the opposite side of the east beam, also at load stage 406.

4.2.4 Test 4

4.2.4.1 Load History. The load history for Test 4, shown in Fig. 4.13, included peak deflection cycles of 1.2 in. and 2.4 in. After correcting for slip, the actual peak beam displacements were approximately 1.1 in. and 2.3 in., respectively. As in the previous tests, smaller deflection cycles were repeated before continuing to the new displacements of $1\Delta_i$ and $2\Delta_i$. The hydraulic loading systems worked very well in Test 4 and the west and east beam deflections were virtually identical.

4.2.4.2 Load-Deflection Behavior. The load-deflection plots for the west and east beams (see Figs. 4.14 and 4.15) illustrate the transition from predominantly elastic to inelastic behavior as the deflection level was increased. Figures 4.14 and 4.15 indicate that significant degradation in beam stiffness occurs with cyclic loading at larger deflection levels. Observe that the stiffness of the east beam was less than the west beam in both loading directions, particularly at $1\Delta_i$ and $2\Delta_i$ (see Fig. 4.16). This softness in the east beam was attributed to the damage suffered in Test 3 and the influence of the loading direction. At the $2\Delta_i$ deformation level, pinching of the hysteresis loops in the second and third cycles suggests beginning signs of shear distress in both beams.

The yield point of the beams in the strong direction, positive displacement, is not well defined in Figs. 4.14 and 4.15. However, from measured beam strains, yielding was estimated to occur at a load of 30-32 kips for the west beam and 26-28 kips for the east beam at a deflection of 1.4 in. The west beam load was approximately 25 percent greater than the predicted yield load of 25 kips which was calculated assuming an effective slab width of

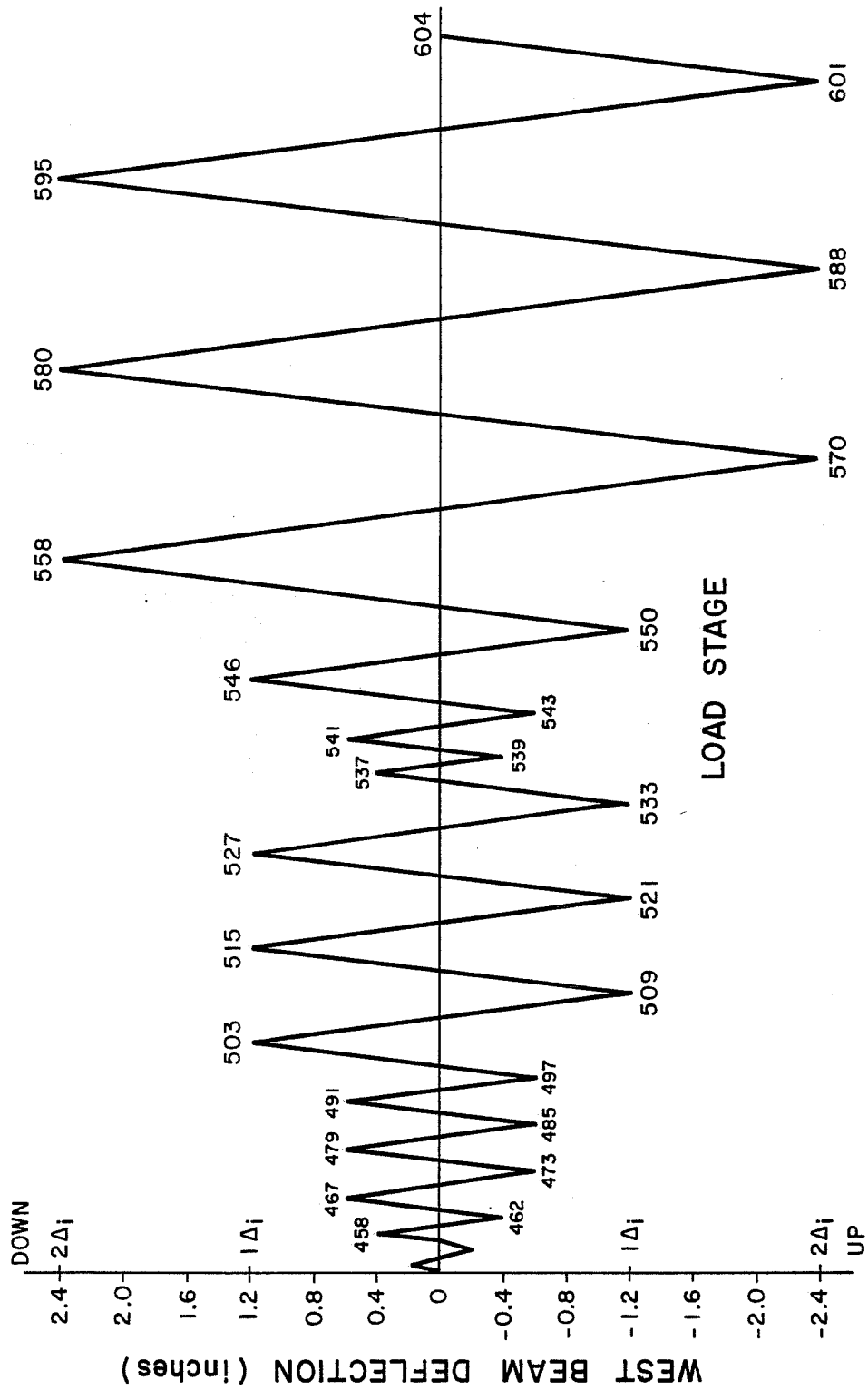


Fig. 4.13 Load history, Test 4

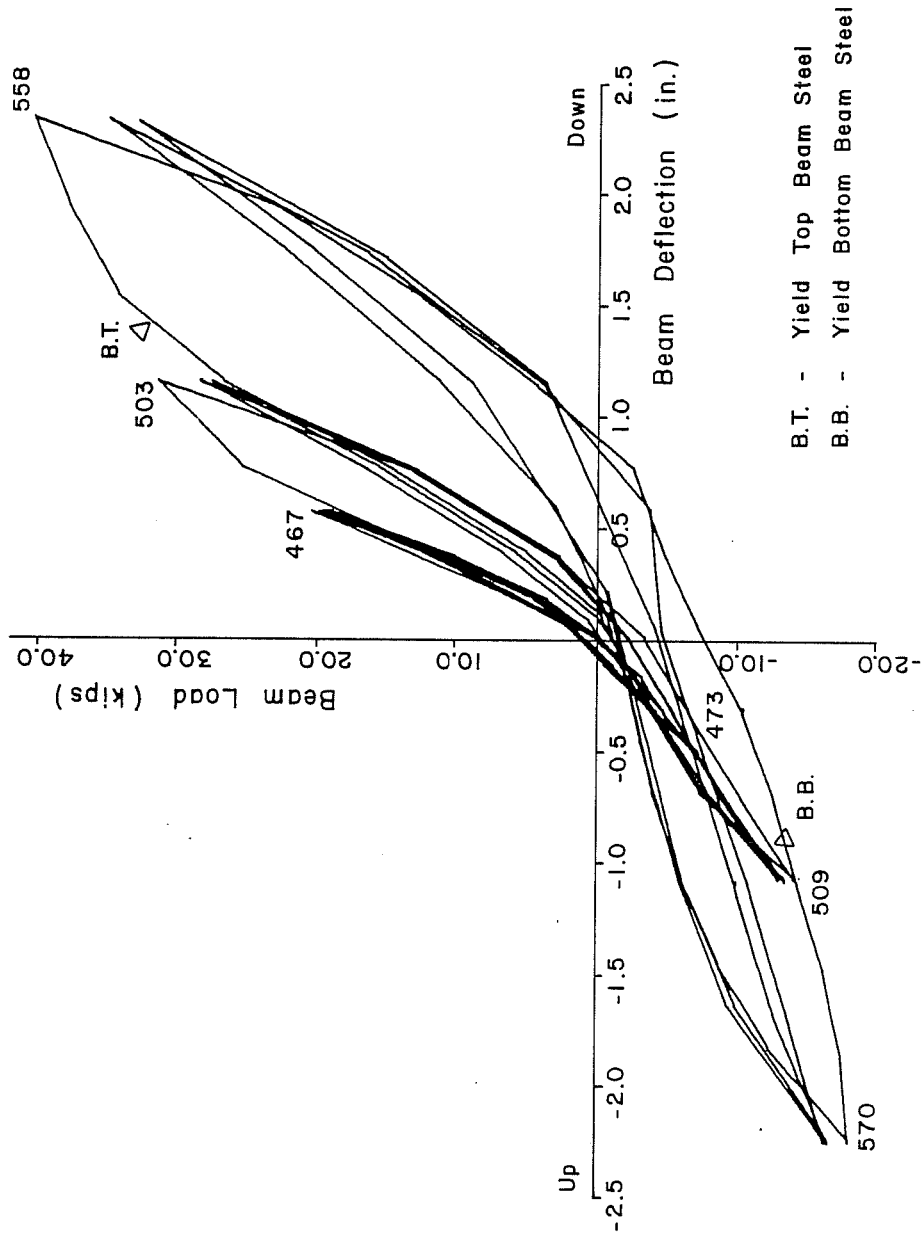


Fig. 4.14 Load versus deflection behavior, west beam (Test 4)

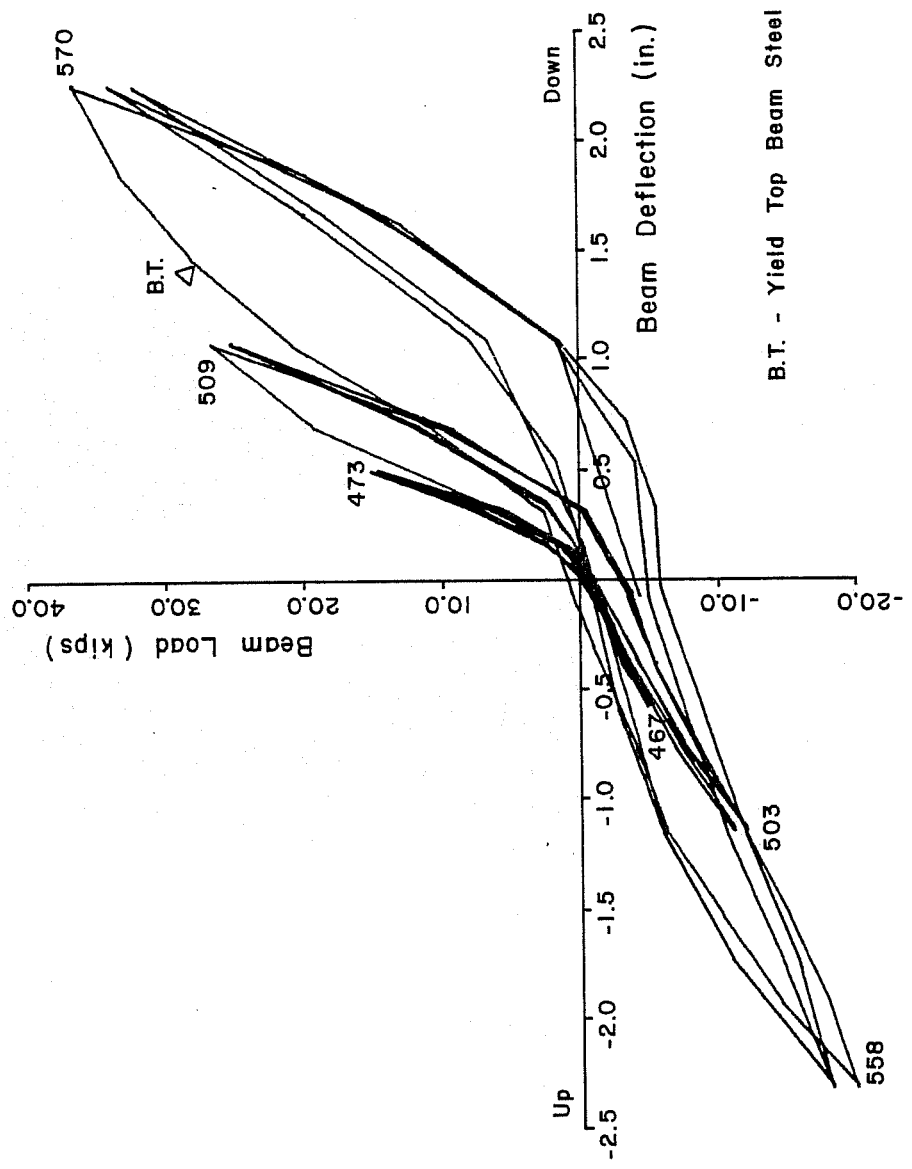


Fig. 4.15 Load versus deflection behavior, east beam (Test 4)

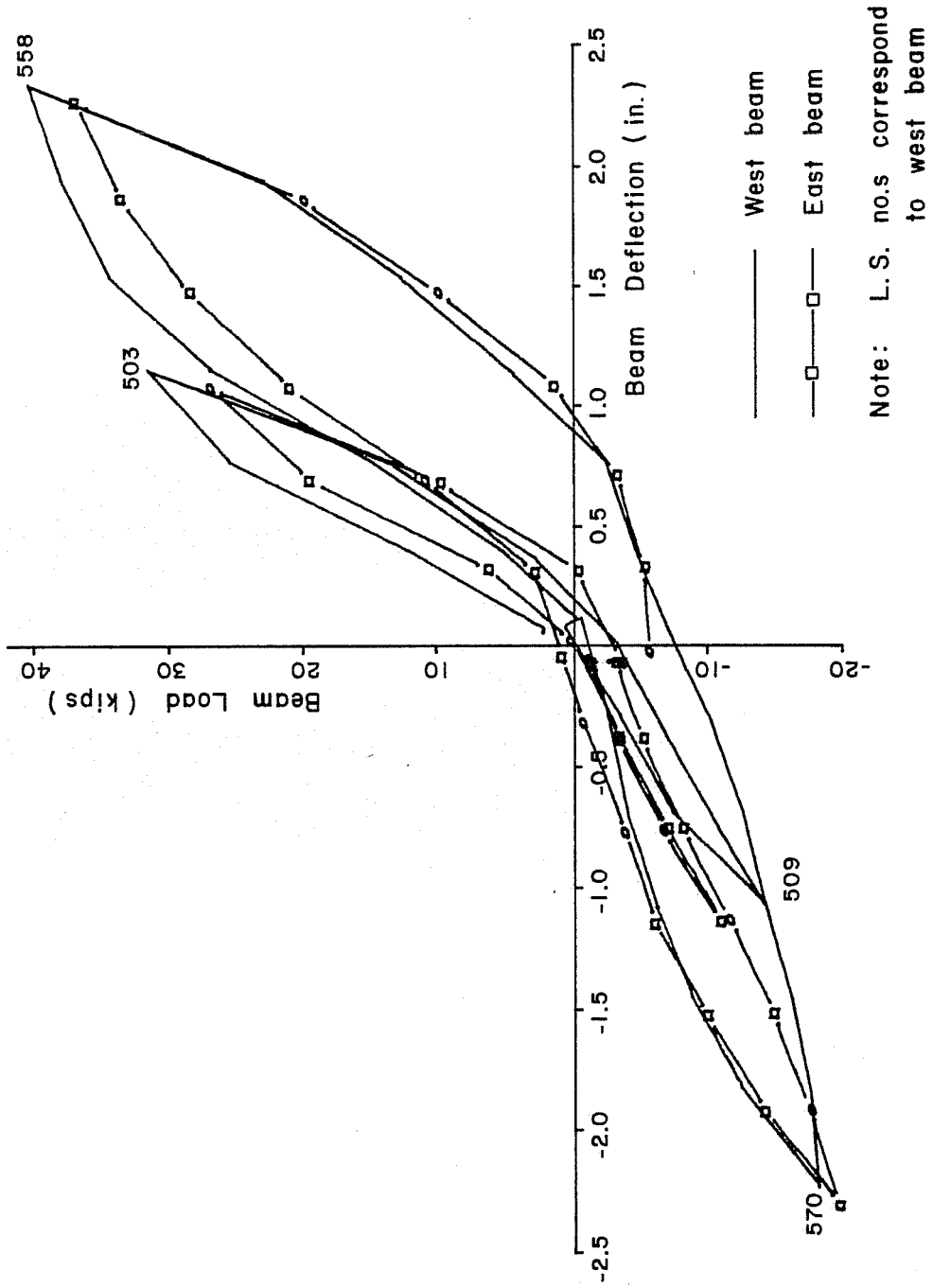


Fig. 4.16 Comparison of west and east beam stiffness, Test 4

59 in. in accordance with ACI design recommendations.³ As loading continued, the beam loads increased implying a greater effective slab width and possibly some strain hardening in the beam steel. During the first cycle at $2\Delta_1$, the west beam reached a maximum load of 40 kips and the east beam 36.5 kips. A moderate reduction in strength (about 15 percent) was observed in the following two cycles for both beams.

4.2.4.3 Cracking Patterns. Extensive cracking in the longitudinal beam, slab, and column was observed at the higher deflection levels of Test 4. The flexural cracks initiated in the slab at $1\Delta_1$, and the existing cracks, propagated diagonally into the west and east beams (see Fig. 4.17). Another set of cracks developed near the longitudinal ends of the slab at load stages 503 and 509, and extended in a semi-circular pattern around the loading points (see Fig. 4.18). Torsional cracking in the west face of the transverse beam and cracks extending diagonally in the slab from the northwest and southwest column corners appeared at load stage 509 (see Fig. 4.19), similar to the crack patterns observed during Test 3 on the east side of the specimen.

As cycling continued to $2\Delta_1$, very few new cracks were initiated, but extensions of existing cracks were observed, particularly in the slab. Splitting cracks along the longitudinal reinforcement of the beams and column appeared at load stages 558 and 570. Figure 4.20 shows the initial development of a longitudinal beam hinge at the column face. Note the wide cracking at the beam-column interface and the concrete that spalled when the loading direction was reversed. There was some evidence of joint shear distress in Test 4 indicated by a few shear cracks located on the column corners in the joint region.

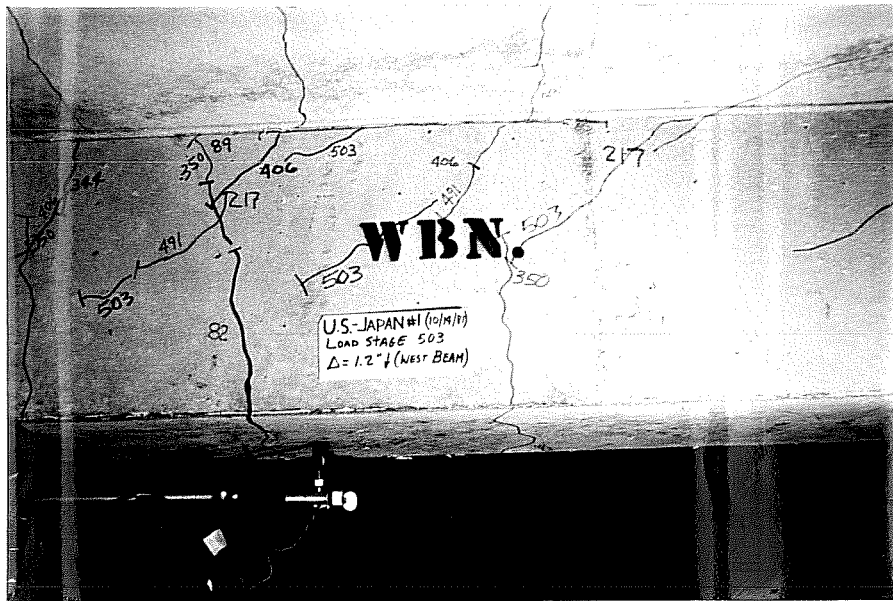


Fig. 4.17 Diagonal cracks in west beam, Test 4



Fig. 4.18 Cracking in slab near loading points



Fig. 4.19 Crack patterns at load stage 509



Fig. 4.20 Deterioration in hinging zones, west beam

4.2.5 Test 5

4.2.5.1 Load History. The load history for Test 5 (see Fig. 4.21) consisted of peak deflection cycles to nearly $4\Delta_i$. To remain consistent with earlier testing, smaller displacement cycles were again repeated before the new deflection levels, $3\Delta_i$ and $3.8\Delta_i$, were applied. The maximum positive west beam displacement was limited to 4.6 in. ($\approx 3.8\Delta_i$). However, a maximum negative displacement of 5.4 in. ($4.5\Delta_i$) was reached during the third cycle.

4.2.5.2 Load-Deflection Behavior. The load-deflection behavior of the specimen in Test 5 is illustrated in Figs. 4.22 and 4.23. The degradation in stiffness observed in Test 4, due to cyclic loading, became more pronounced as the beam deflections increased. At $3\Delta_i$, and particularly $3.8\Delta_i$, large beam displacements were necessary to close cracks before stiffness recovered. A significant decrease in beam strength, in the strong direction, occurred following the initial excursion to the $3\Delta_i$ level. This reduction in strength was probably due to the loss of bond of the tensile reinforcement as cycling continued. The severe pinching of the hysteresis loops, at $3.8\Delta_i$, indicates the presence of shear distress near the joint region. Slip of the beam reinforcement through the joint may also have contributed to this behavior.

Figure 4.24 illustrates the detrimental effect cyclic loading to large displacement levels had on the load-deflection behavior between Tests 2 and 5 at the 0.4 in. deflection level. The degradation in stiffness, indicated in the load-deflection plot, was due to the extensive flexural cracking which occurred in the beams and slab prior to Test 5. Bond deterioration probably contributed to the beam softness as well. A beam load about one-third the initial load in Test 2 was reached at this deflection level in Test 5.

4.2.5.3 Cracking Patterns. The crack patterns of Test 5 were similar to those observed during Test 4, but more extensive. At $3\Delta_i$ and $3.8\Delta_i$, the diagonal shear cracks extended nearly to the

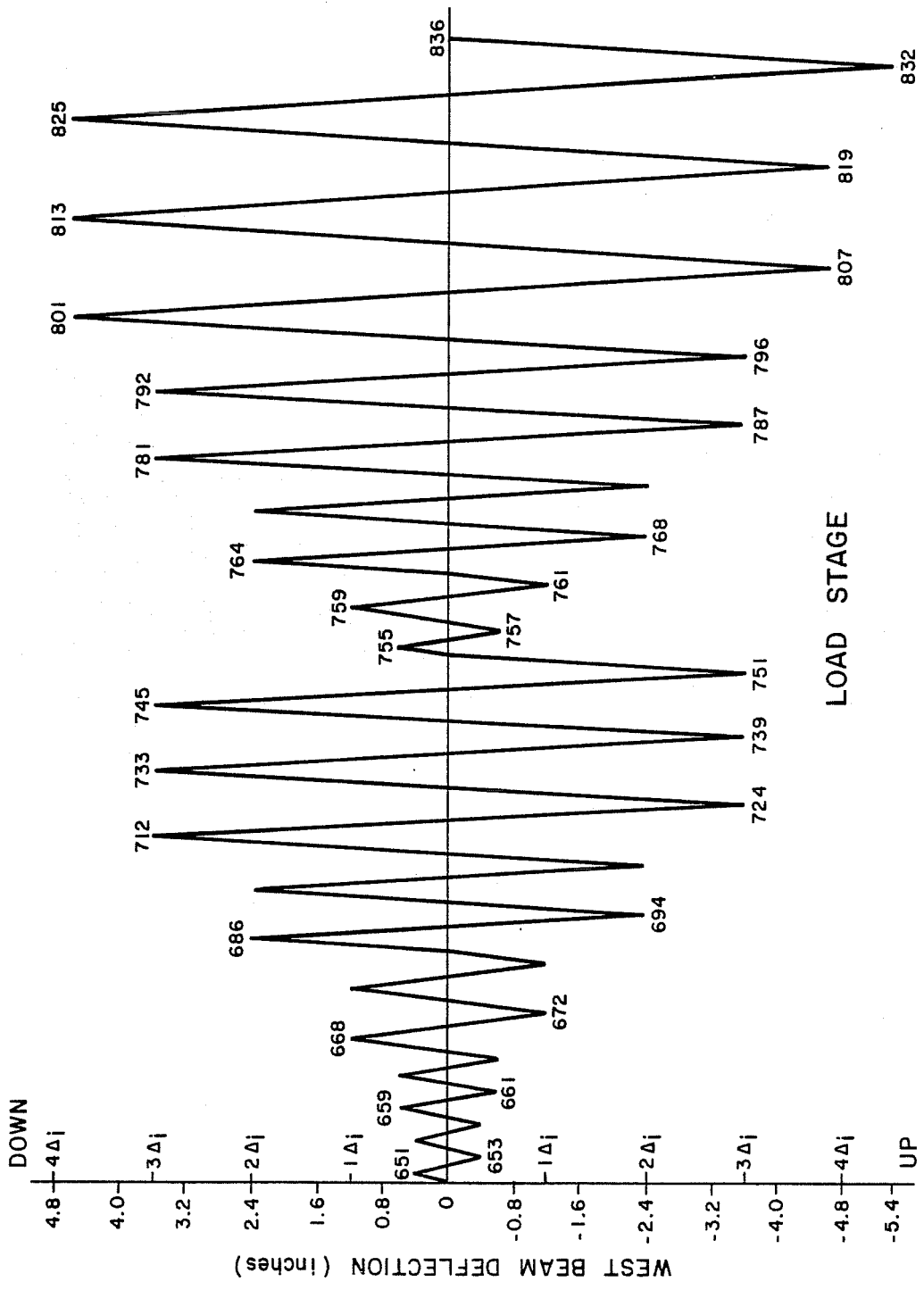


Fig. 4.21 Load history, Test 5

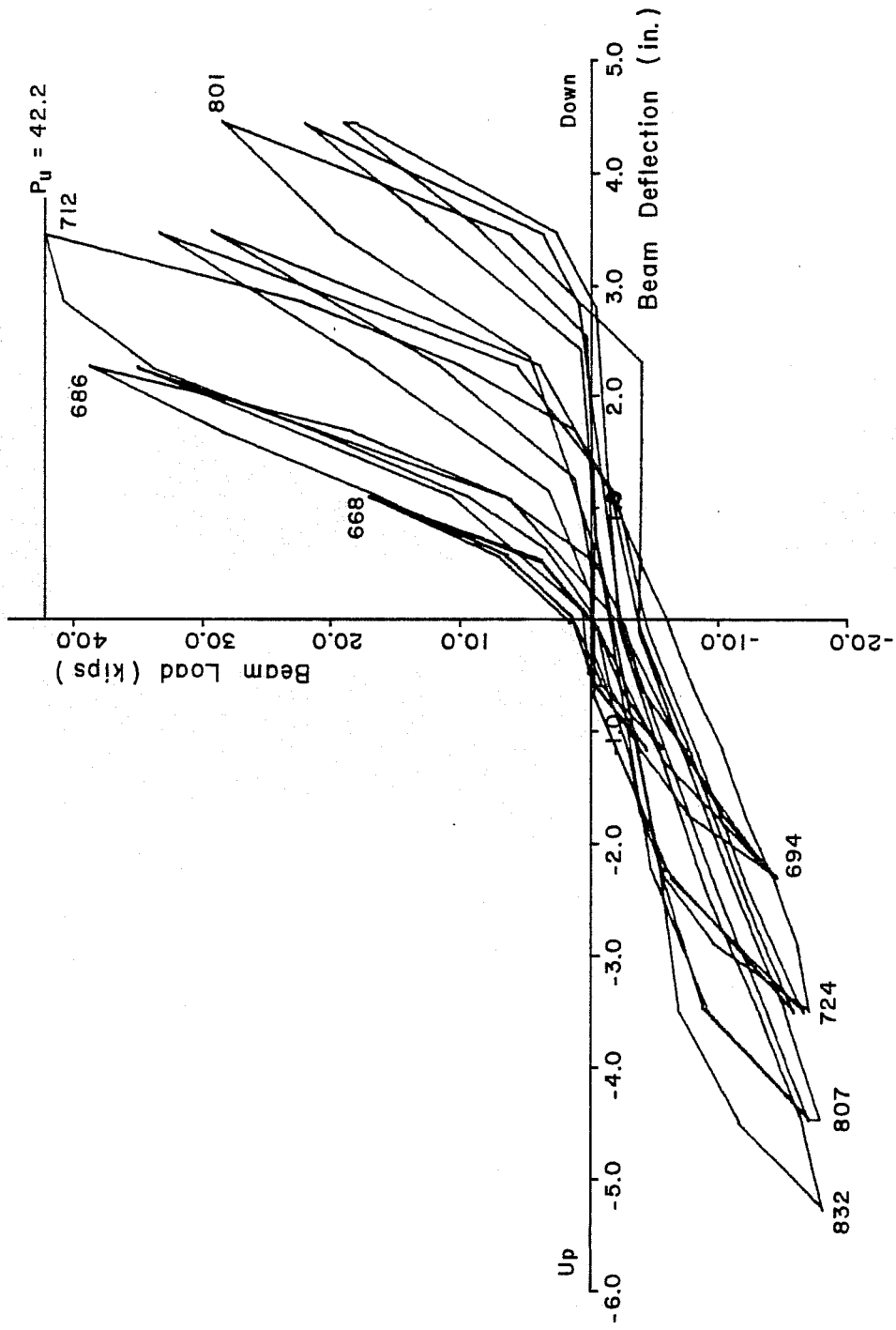


Fig. 4.22 Load versus deflection behavior, west beam (Test 5)

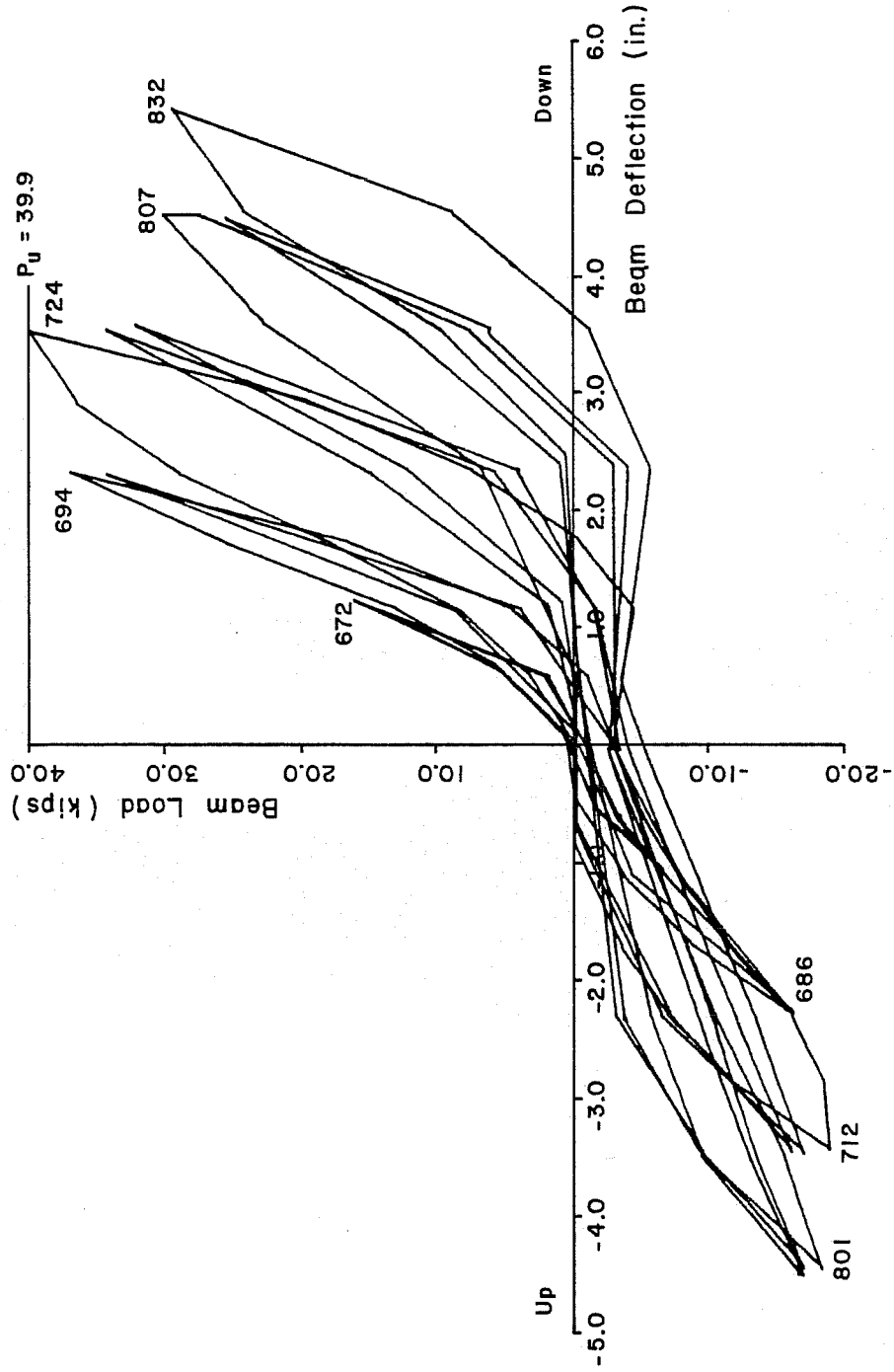


Fig. 4.23 Load versus deflection behavior, east beam (Test 5)

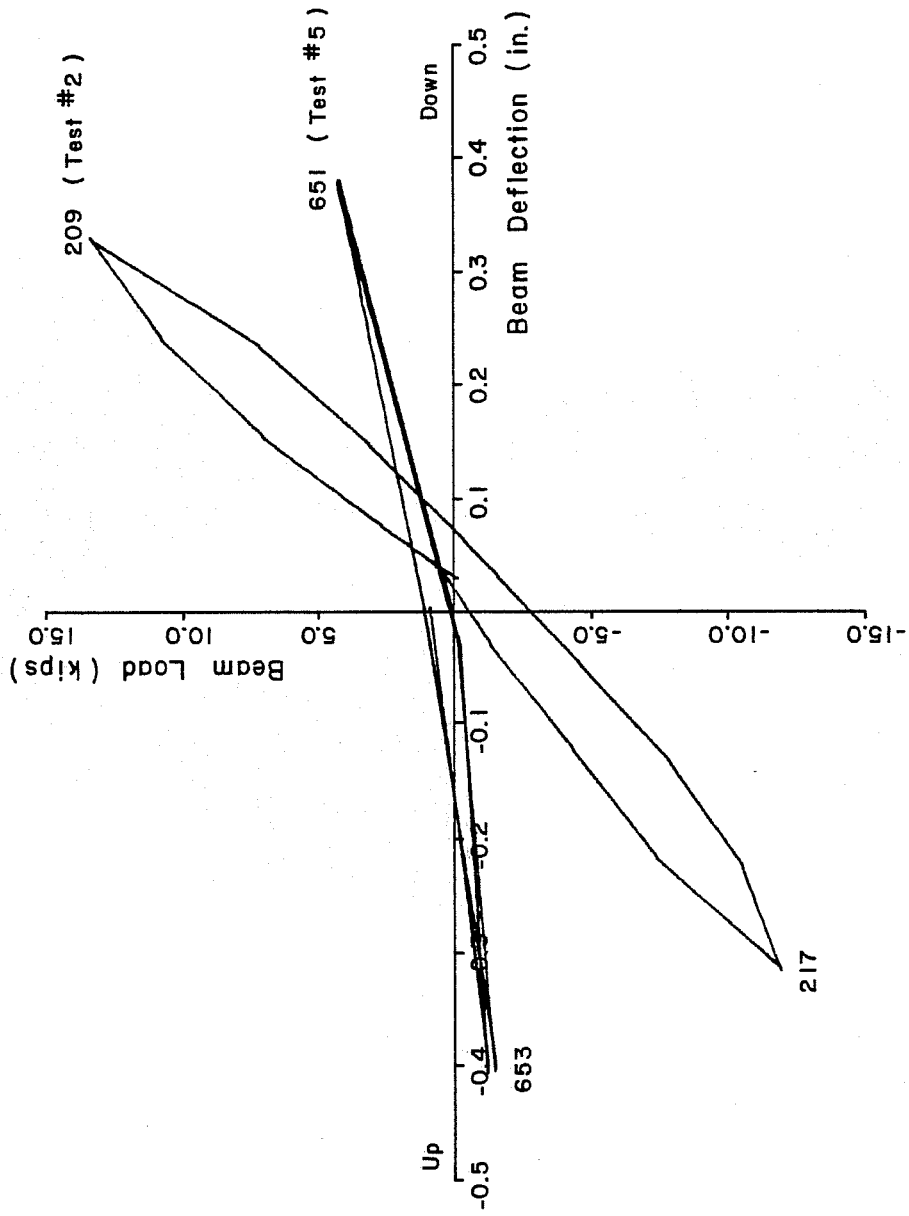


Fig. 4.24 Stiffness degradation with cyclic loading, west beam

bottom of the west and east beams indicating that the compression zones had become smaller and highly stressed. The crushed and spalled concrete observed near the joint was a further indication of the high compressive stresses present in the beams (see Fig. 4.25). As the load was reversed, very wide separation cracks opened between the longitudinal beams and column faces (see Fig. 4.25). Similar cracking, but accompanied by much less spalling, was observed on top at the slab-column interfaces. The spread of torsional cracking was apparent due to the orthogonal crack patterns on the transverse beam faces and the propagation of cracking to the bottom of the beam (see Fig. 4.25). In addition, several joint shear cracks are present in Fig. 4.25 on the northeast-column corner.

At load stages 686 and 801, two cracks, nearly vertical, appeared on the west face of the south beam approximately 24 in. and 36 in. from the column face. Similar cracks on the other three faces of the transverse beam were also observed at the $2\Delta_1$ and $3.8\Delta_1$ deflection levels (see Fig. 4.26). The cracks extended only partially across the bottom of the beam and likely were the result of a combination of bending and torsion in the transverse beam.

The extent of cracking and damage to the specimen, particularly near the joint, after testing was complete and the loose concrete removed is illustrated in Figs. 4.27 and 4.28. Most of the deterioration in the joint region was concentrated below the slab in the beam hinging zones and the column corners.

4.3 Test Results

4.3.1 General Behavior and Observations. The response of the specimen throughout the series of tests was predominantly flexural as indicated by the extent of flexural cracking in the beams, column, and slab. The general mode of failure was characteristic of flexural behavior with the development of longitudinal beam hinges at the west and east column faces. As noted earlier, the inelastic



Fig. 4.25 Cracking near NE corner of joint, Test 5



Fig. 4.26 Vertical cracks in north beam

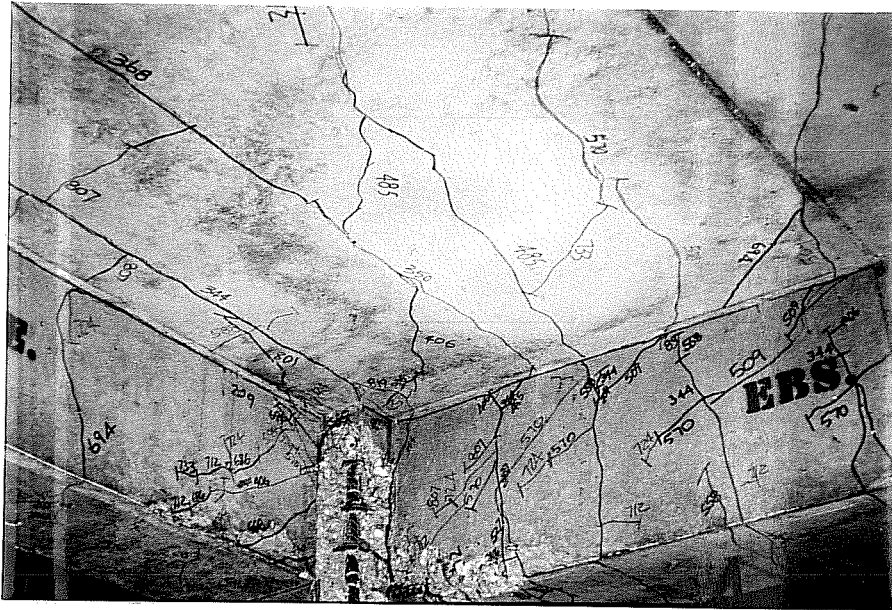


Fig. 4.27 SE quadrant after testing



Fig. 4.28 Deterioration of NW joint region

behavior of the beam hinging regions was advantageous since this provided a mechanism for energy dissipation. Several problems associated with shear degradation in and near the joint appeared as the loading history became more severe, and the load-deflection behavior of the specimen began to deteriorate rapidly. However, the applied beam deflections which initiated this deterioration were very large and corresponded to story drifts of 3-1/2 to 5 percent.

In Table 4.1, the positive and negative yield and ultimate loads measured for each beam are summarized and compared with the predicted yield loads which were calculated using an effective slab width of 59 in. (see Sec. 2.3.2). The ultimate beam loads in both loading directions were significantly higher than the calculated yield loads due to the contribution of the slab bars and to strain hardening of the longitudinal beam and slab bars. The large positive beam loads, at $2\Delta_i$ and $3\Delta_i$, indicated that nearly the entire slab width was effective when in tension. In the negative loading direction, high tensile strains present in the bottom slab bars, because of the shallow compression zone, accounted for the increased beam

TABLE 4.1 MEASURED AND CALCULATED BEAM LOADS

Beam	Loading Direction	Measured		Calculated	$\frac{P_y \text{ meas.}}{P_y \text{ calc.}}$	$\frac{P_u \text{ meas.}}{P_y \text{ calc.}}$
		P_y^*	P_u^*	$P_y^* \text{ (ACI)}$		
West	down(+)	32.0	42.2	25.0	1.28	1.69
	up(-)	13.4	18.3	11.6	1.16	1.58
East	down(+)	--	39.9	25.0	--	1.60
	up(-)	15.8 ¹	24.0 ²	11.6	1.36	2.07

* Units in kips

¹ Measured during Test 3

² Measured during Test 3, l.s. 407

loads beyond initial yielding of the bottom beam bars. Note, however, that the negative, ultimate beam load was considerably larger for the east beam. This load was measured during Test 3 when the applied east beam deflection was slightly greater than $2\Delta_1$. As a result, the yield and ultimate beam loads recorded in Tests 4 and 5 were likely affected, particularly the negative loads for the west beam since yielding of the bottom bars spread into the joint during Test 3.

As the resistance provided by the slab increased, the positive beam loads became larger and diagonal cracks propagated from the slab and into the longitudinal beams. In the other direction, beam loads were not large enough to initiate diagonal cracking. However, the combination of high positive beam shear and the cyclic load history resulted in deterioration of the beam shear capacity in the hinging zones. The decay in beam strength and the severe pinching of the hysteresis loops observed in Test 5 were characteristic of shear degradation (refer to Figs. 4.22 and 4.23).

Column and Joint Behavior. The column and the joint sustained increasing levels of damage as the slab became more effective and higher shears were transferred through the joint region. The #7 column bars yielded near the peak of the $2\Delta_1$ deflection level in Test 4 which indicated the initial formation of column hinges. However, signs of inelastic behavior; i.e., wide flexural cracks and spalled concrete, at the column and joint boundaries were minimal as testing continued. Most of the inelastic behavior was concentrated in the beam hinging zones.

The shear distortion of the joint clearly increased as the shears imposed on the joint region from the beams and slab became larger. The maximum shear strains measured, however, were only on the order of 0.02 rad. (1.2°) in Test 5. Furthermore, yielding of the joint hoops did not occur prior to the $2\Delta_1$ displacement level.

Bond Deterioration. In the early stages of Test 3, bond deterioration of the beam and column bars in the joint became apparent. This deteriorating bond condition in the joint was a result of the increasing number of reversed load cycles and the larger deformation levels applied, which required larger bar forces to be developed through the joint. In a recent study by Viwathanatepa, Popov, and Bertero⁶ the detrimental effects of cyclic loading on the bond of bars anchored in concrete blocks, simulating an interior joint of a frame structure, were clearly shown. Results from this study indicated that the extent of bond degradation depended on the severity and the number of load cycles applied. Cracking and spalling of the joint concrete cover, particularly near the hinging zones, probably contributed to the bond deterioration observed in USJ-1, as well. The bottom beam bars were not instrumented to measure slip, but after the cover concrete spalled, movement of the bars relative to the west and east column faces was observed during testing. This indicated a very unfavorable bond condition for the bottom beam bars in the joint.

Finally, note that the beam bars of the interior joint specimen did not satisfy the recommendations of the New Zealand Code. To prevent or delay bond deterioration in the joints of seismic-resistant structures, a maximum beam bar diameter of $1/35$ the column width is recommended. In this case, for USJ-1, the maximum bar size permitted in the beams would be a #5 bar. However, with such small bar sizes, joints would be very congested and difficult to fabricate. To avoid these construction problems, larger column and beam cross sections would be necessary.

4.3.2 Drift Angle Index (R). The test measurements; strains, beam rotations, and joint shear strain, were plotted versus a non-dimensionalized parameter referred to as the drift angle index, R. The drift angle index was used as the reference parameter to compare test results from the component specimens and the full-scale structure.

To calculate the drift angle for the full-scale interior joint specimen, the total relative beam deflection of the west and east beams was divided by the length between the loading points (see Fig. 4.29). A positive drift angle corresponded to a positive (down) west beam displacement and a negative (up) east beam displacement.

The drift angles calculated for Tests 2 and 3 were average values since the west and east beam deflections differed. However, for the last load cycle of Test 3 where an extreme difference in beam displacements existed, a separate drift angle was calculated for each beam.

4.3.3 Bar and Hoop Strains. The steel strains considered in the following sections include strains for the longitudinal beam bars, column bars, joint hoops, and the longitudinal slab bars in the west half of the specimen. The locations of these gages were

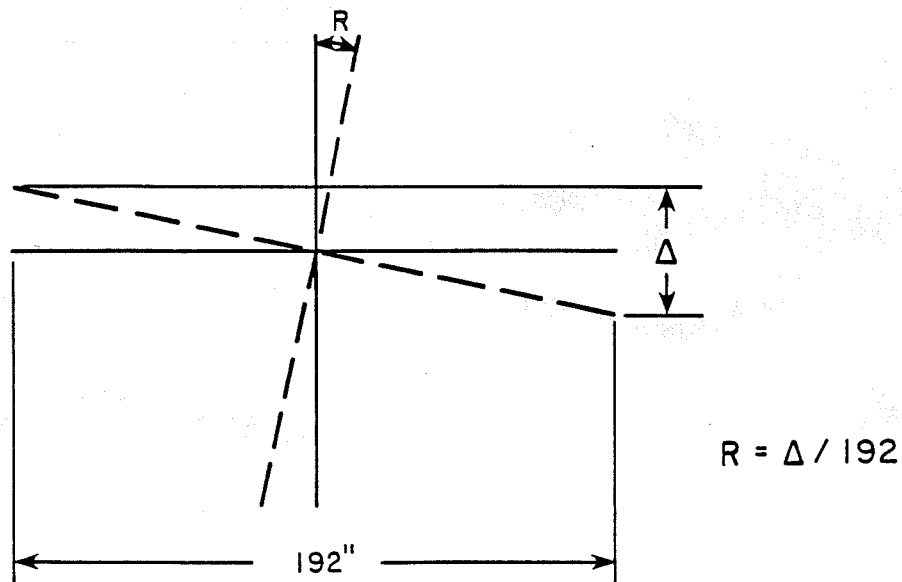
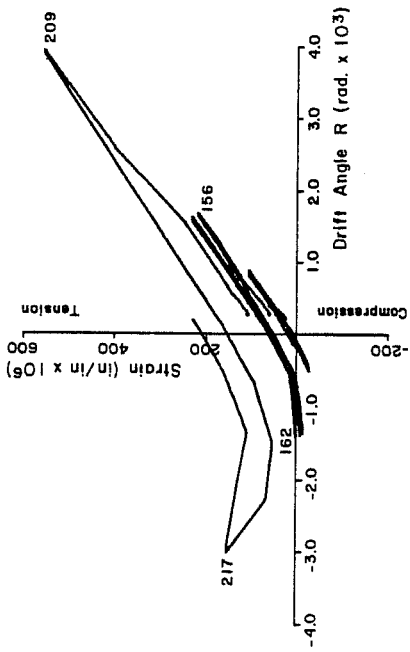


Fig. 4.29 Drift-angle calculation

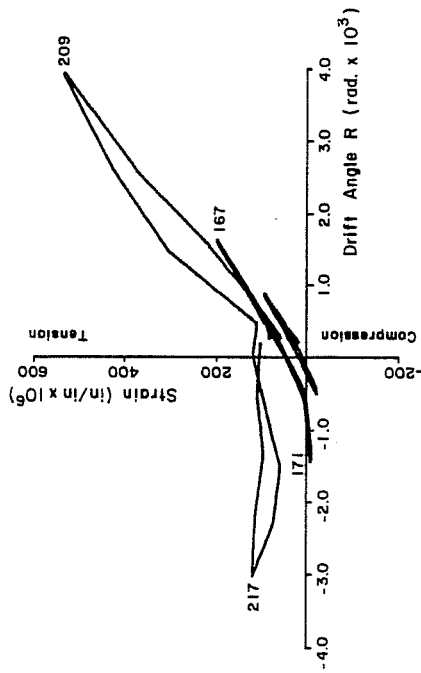
given in Chapter 3 (see Figs. 3.13, 3.14, and 3.15). Strains rather than stresses in the reinforcement will be presented since the former were measured directly and because steel strains from the other tests were available for comparisons. A strain of 2000μ was assumed to be the yield strain for all of the reinforcement except the column bars. The column bar yield strain was in the range of $2600-2800\mu$.

Longitudinal Beam Bar Strains. Strains measured for two top beam bars at the west column face (gages W1T and W3T) during Test 2 are shown in Figs. 4.30(a) and (b). The plots are very similar and illustrate a relatively uniform strain distribution near the top of the beam at any calculated drift angle. Note that tensile strains were always present in the top bars during the last cycle of loading. This indicated that the neutral axis for the T-section had moved into the flange above these bars as the loading intensity increased. In Fig. 4.30(c), the strain versus drift-angle plot for a bottom bar in the west beam (gage W1B) shows a rapid increase in tensile strain as larger negative drift angles were applied. The propagation of flexural cracking in the bottom of the longitudinal beam coincided with the higher tensile strains. In the opposite loading direction, relatively small compressive strains were generated in the bottom of the beam (see Fig. 4.30(c)).

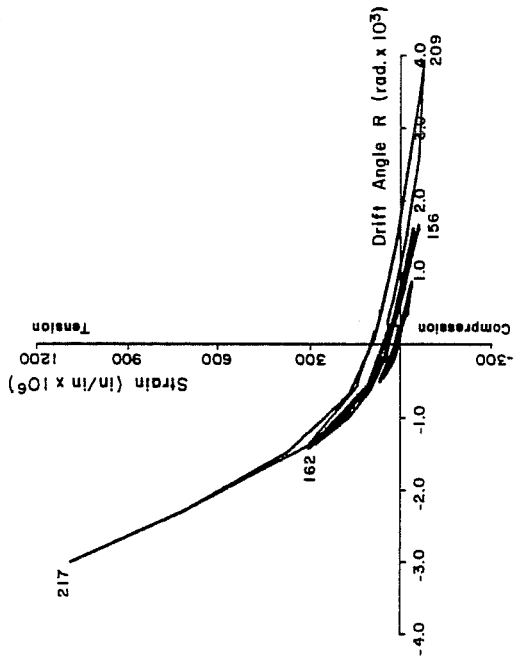
In general, the strain versus drift-angle relationships of the longitudinal beam bars in Tests 3 and 4 were similar to those in Fig. 4.30, but higher strains were measured. Note that tensile strains were present in the bottom of the west beam as the deformation level was increased beyond a positive angle of 4.0 in Test 3 (see Fig. 4.31(a)). Normally, compressive strains in these bars would be expected, but due to bond deterioration of the bars in the joint from several cycles of loading which were relatively small in magnitude, tensile strains had spread through the joint panel. Strains measured for a longitudinal beam bar at the center of the joint (gage EW3B) further indicated this spread of tension in the



(a) Top bar (W1T)

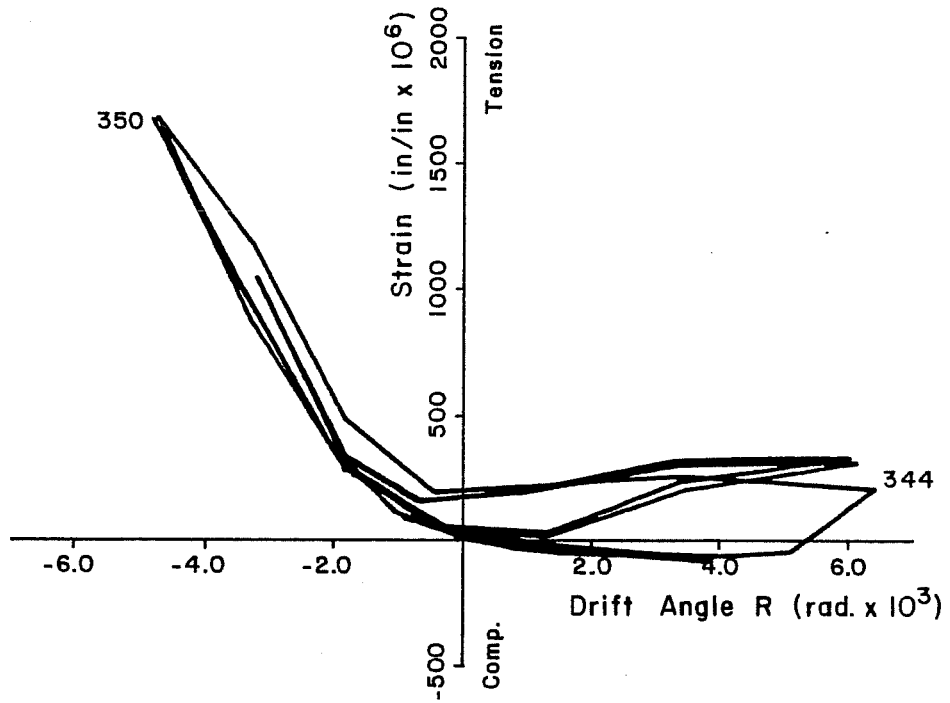


(b) Top bar (W3T)

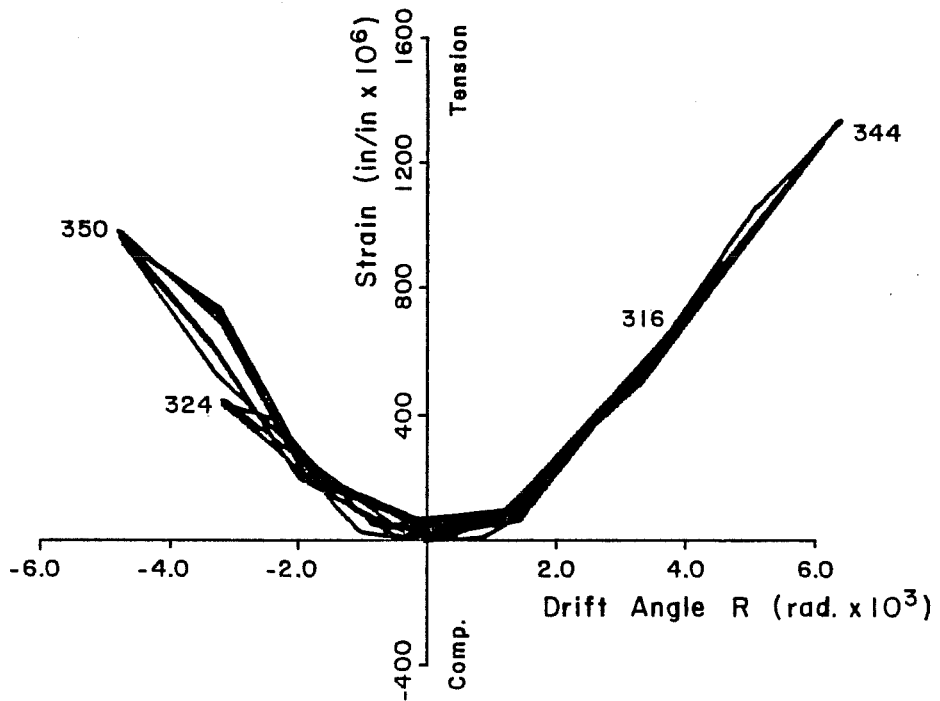


(c) Bottom bar (W1B)

Fig. 4.30 Strain versus drift angle, west beam bars (Test 2)



(a) Bottom of west beam (W1B)



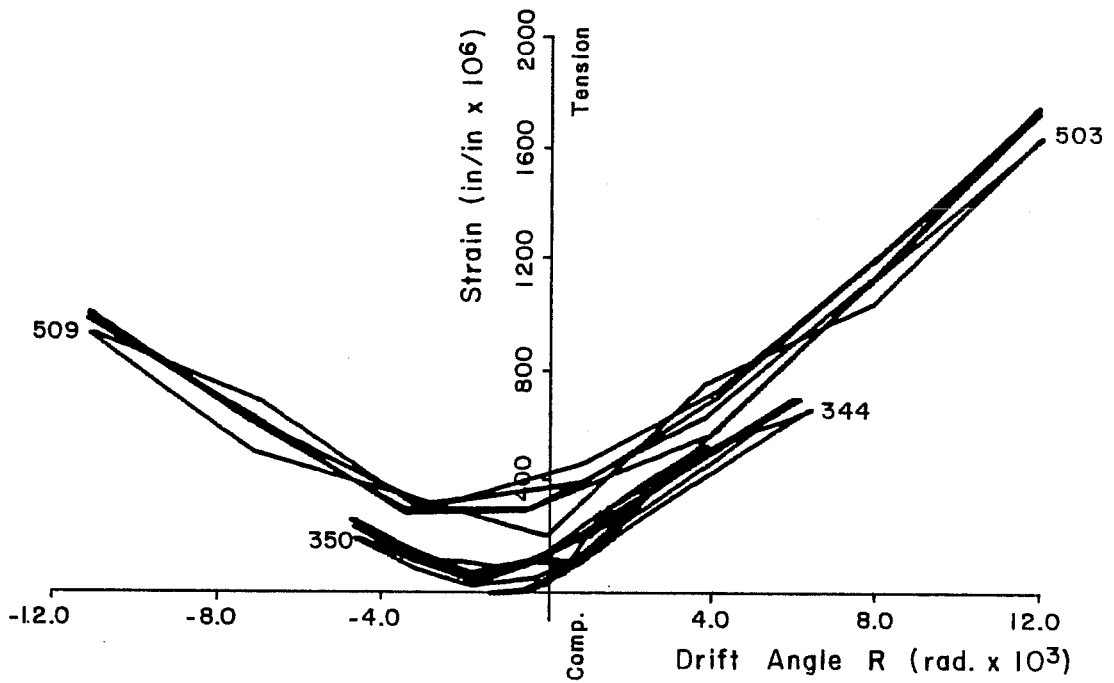
(b) Center of joint (EW3B)

Fig. 4.31 Strain versus drift angle, longitudinal beam bars (Test 3)

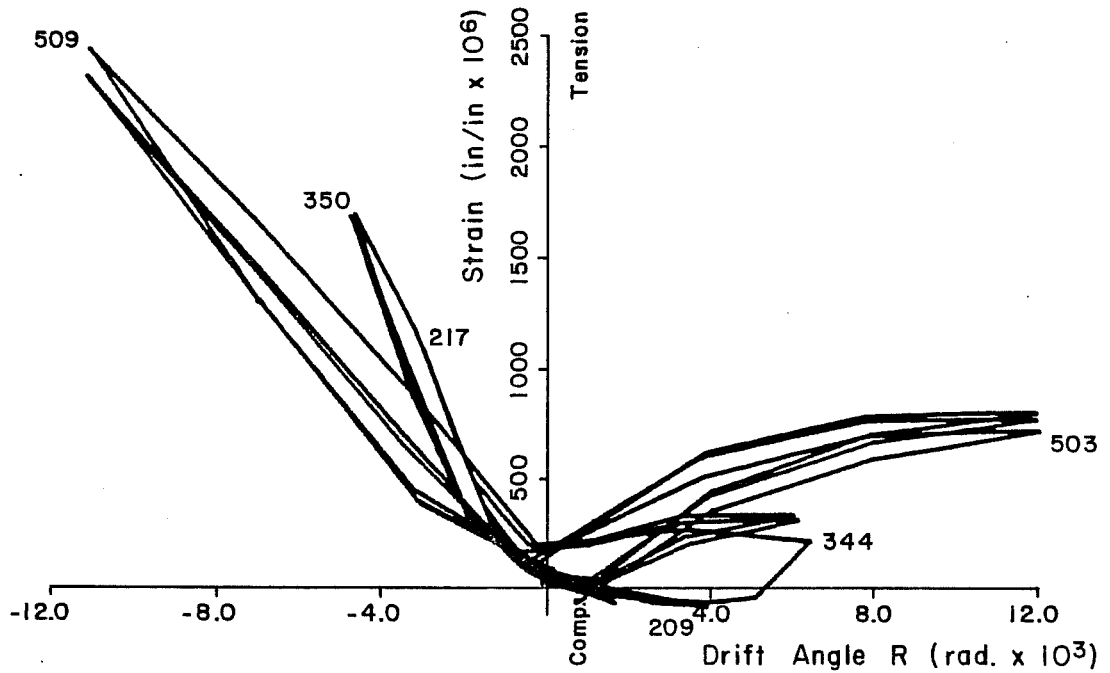
bottom beam bars (see Fig. 4.31(b)). Note the magnitude of tensile strain at load stage 344 in the center of the joint, nearly 1400μ .

The strains measured for a top and bottom bar in the west beam (gages W3T and W1B) for Tests 2 through 4 are shown in Fig. 4.32. The relationship between strain and applied positive drift angles for the top beam bars was more or less linear up to the point of yielding. The top steel in the west beam yielded at a drift angle of 0.014, which corresponded to a positive (down) west beam deflection of nearly 1.4 in. (see Fig. 4.14). At load stage 509, the rather high tensile strains in the top bars of the west beam indicated that a steep strain gradient existed in the slab (the top of the slab was in compression). Some bond deterioration of the top bars may have developed in the joint as well.

In Fig. 4.32(b), note the decreasing slope, or deterioration, of the strain-drift angle relationship as larger negative drift angles were applied in Tests 3 and 4. Yield strains in the bottom bars of the west beam were reached during Test 4 at a drift angle of approximately -0.0095 , or a negative (up) west beam deflection of 0.9 in. However, if the smaller cycles in Test 2 (load stage 217) had been increased to yield and the linear strain relationship maintained, the corresponding beam deflection would have been 0.5 in.; much closer to the calculated yield deflection in the weak loading direction. Bond deterioration and subsequent slip of the bars through the joint, and an increasing softness of the specimen with testing contributed to the declining slope of the strain relationship. Furthermore, strains measured at the center of the joint indicated a worse bond condition for the bottom beam bars than the top beam bars. Better confinement of the top beam bars due to the slab, and yielding of the bottom beam bars which spread into the joint near the end of Test 3 probably accounted for this variation of bond deterioration in the joint.



(a) Top bar (W3T)



(b) Bottom bar (W1B)

Fig. 4.32 Strain versus drift angle, west beam bars (Tests 2 through 4)

Longitudinal Slab Bar Strains. Strains measured for a top and bottom longitudinal slab bar during Test 4 are shown in Figs. 4.33 and 4.34. The bars were located 30 cm from the centerline of the longitudinal beam in the south-west quadrant of the specimen. In Fig. 4.33, the strain versus drift angle plot for a bottom bar at the west face of the transverse beam (gage 5CB) illustrates a relationship similar to those of the top bars in the west beam. This was consistent since the bottom slab bars were located just below the top beam bars in the T-section (see Fig. 2.3(a)). Figure 4.34 indicates that both high tensile and compressive strains were measured in a top slab bar at approximately 50 cm from the west face of the transverse beam (gage 5DT). Note that tensile yielding occurred in the top bar over a rather large distance from the critical section, near the slab and transverse beam interface.

Strain distributions for top and bottom longitudinal slab bars at the critical section, over the west face of the transverse beam, are shown in Figs. 4.35 and 4.36. The distributions were reasonably symmetric about the centerline of the west beam. The distributions labeled A in Figs. 4.35 and 4.36 corresponded to initial yielding of the top beam bars at a west beam deflection of 1.4 in. In Fig. 4.35, the strains for the top beam bars were included since they were located at a similar depth as the bottom slab bars. The effective width of the slab at $2\Delta_1$, which appeared to be nearly the entire width (see Fig. 4.36), was clearly much larger than generally considered in design calculations. Finally, as mentioned earlier, the large negative beam displacements in Test 5 produced high tensile strains in the bottom bars across most of the slab width, substantially increasing the negative beam loads.

Column Bar Strains. Nearly all of the strain gages on the column bars were damaged during casting or ceased to function in the early stages of testing. However, strain measurements for a bar in the east column face at the top of the joint (gage 1T_j) were salvaged

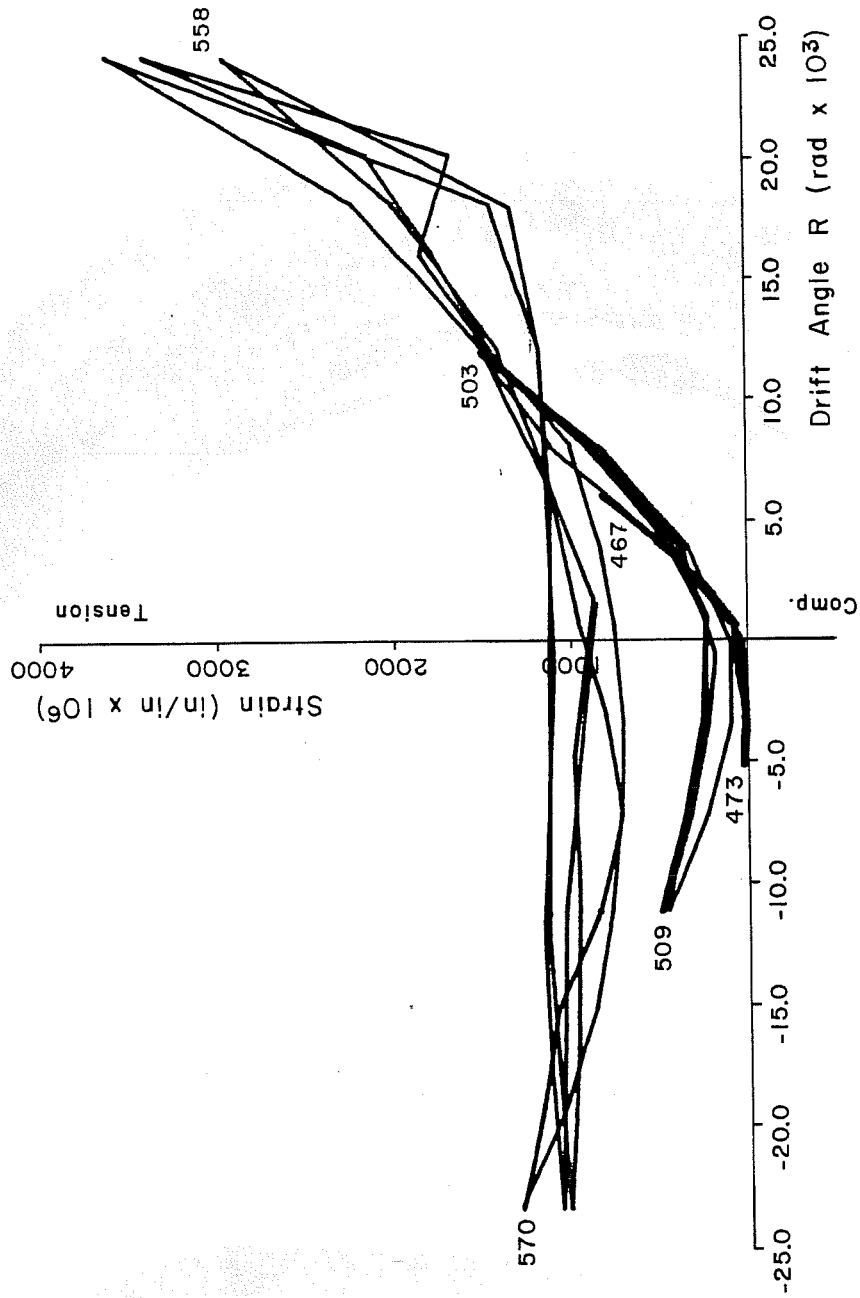


Fig. 4.33 Strain versus drift angle, longitudinal slab bar (5CB), Test 4

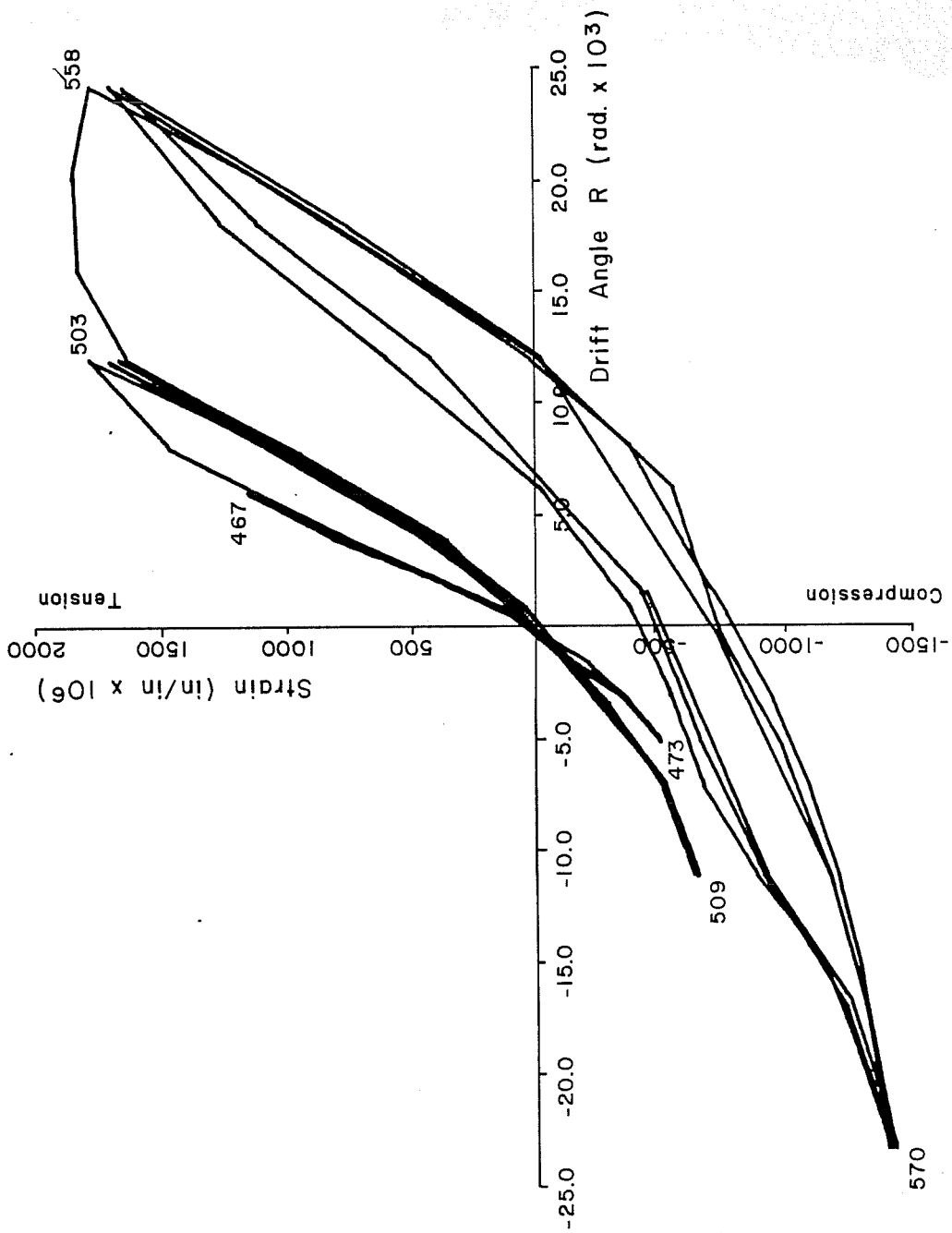
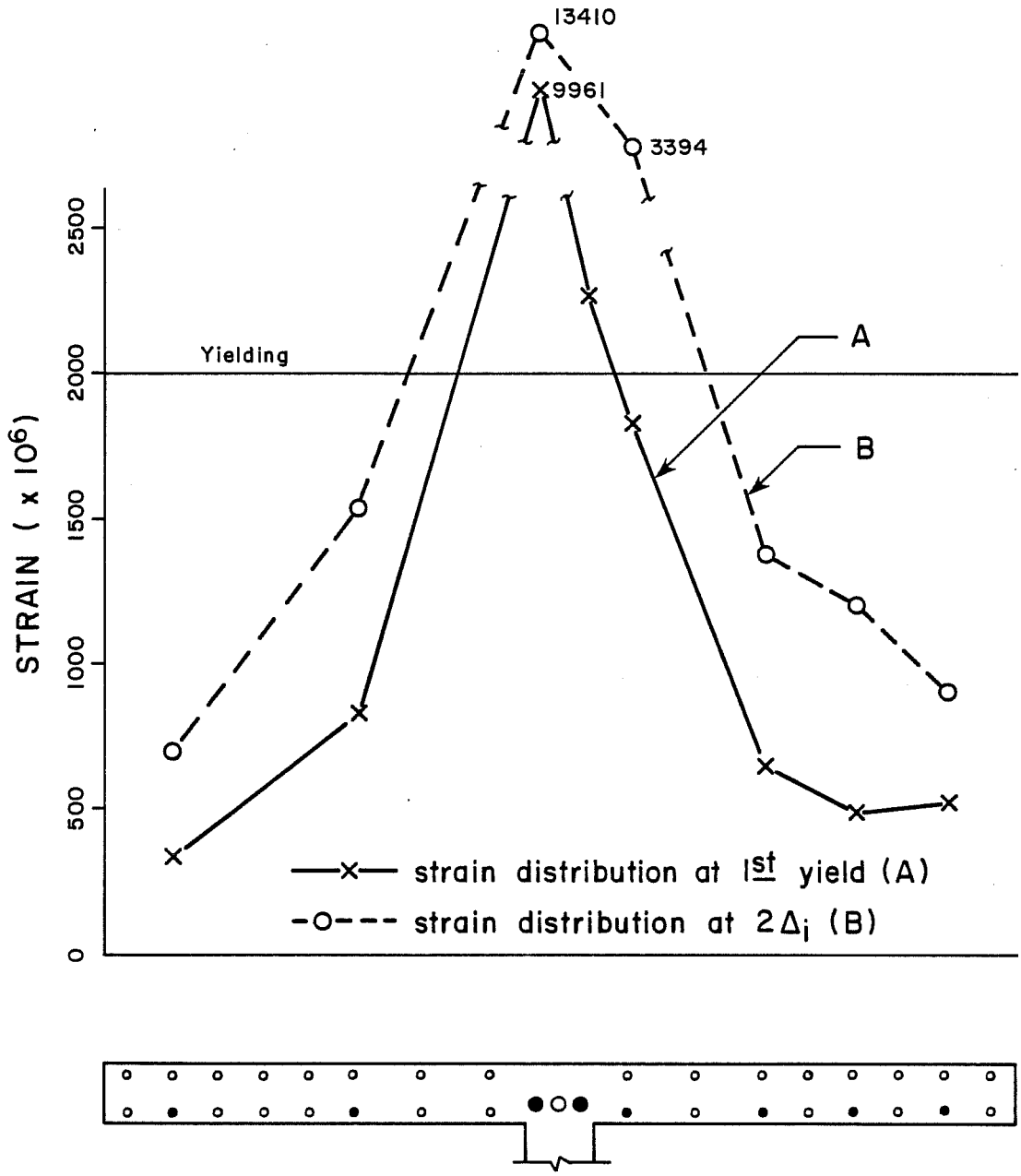


Fig. 4.34 Strain versus drift angle, longitudinal slab bar (5DT), Test 4



• Strains plotted for these bars

Fig. 4.35 Strain distribution of bottom slab bars (Test 4)

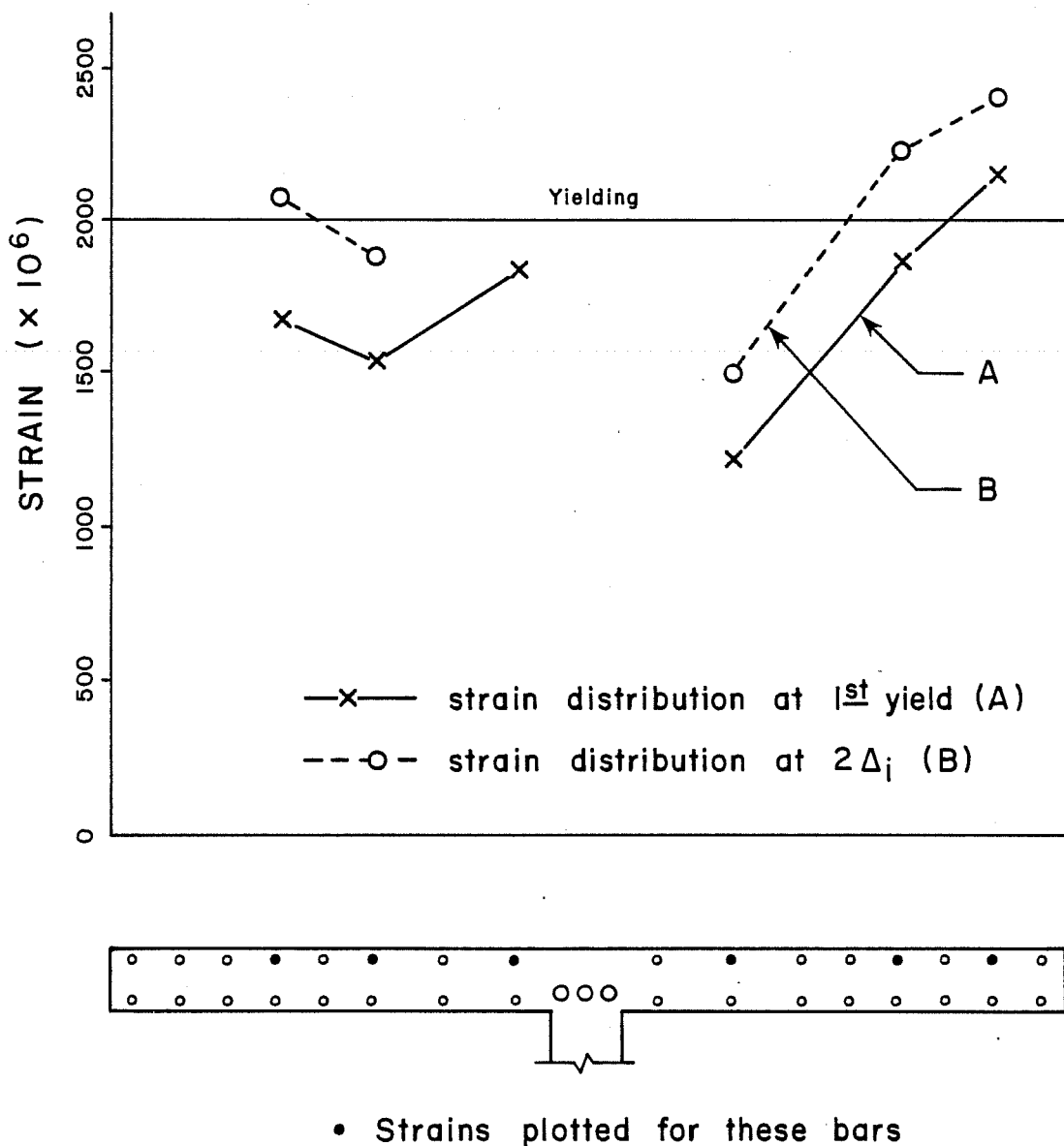
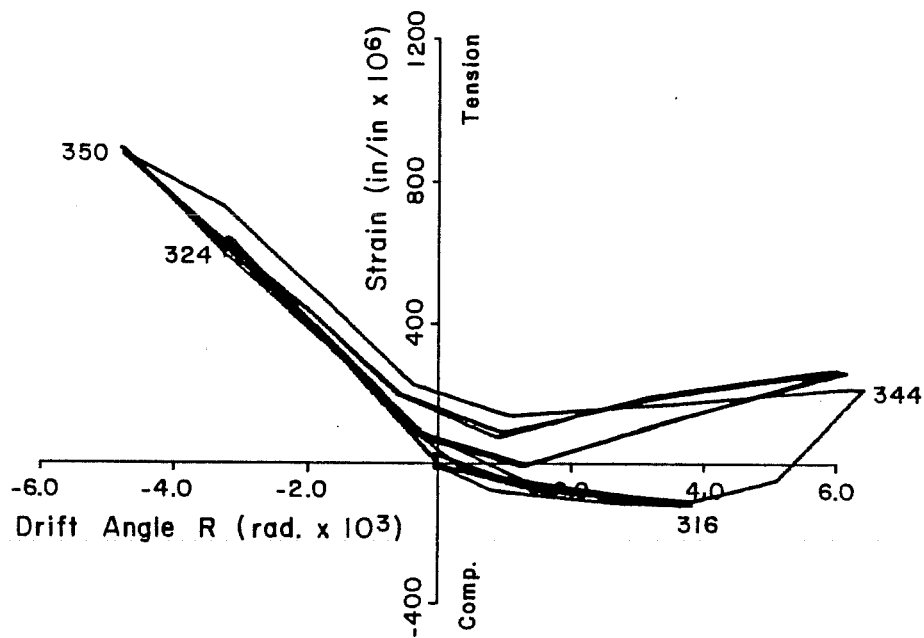


Fig. 4.36 Strain distribution of top slab bars (Test 4)

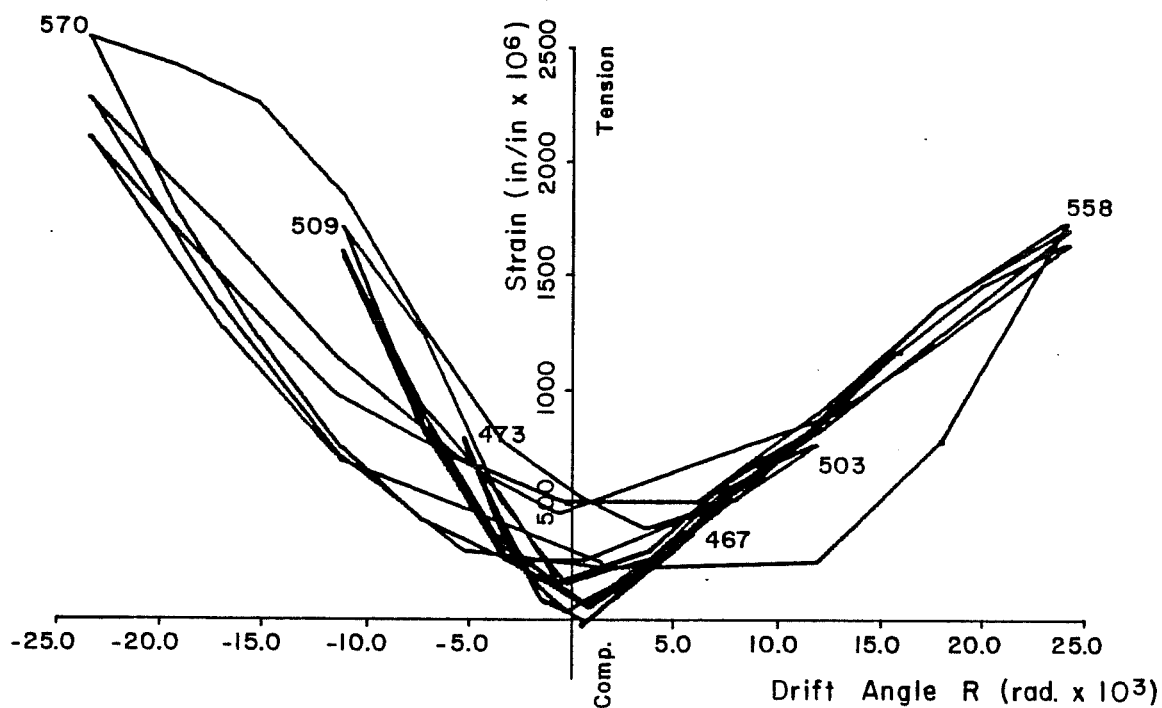
(see Fig. 4.37). The strain versus drift-angle plots for the column bar had a very similar appearance to those of the bottom beam bars. In Fig. 4.37(a) compressive strains were measured in the bar for small positive drift angles, but as the angle increased, the strains changed sign and indicated tensile forces. The presence of tensile strains in both loading directions indicated, as for the beam bars, that bond deterioration of the #7 column bars penetrated through the joint. At the peak of the $2\Delta_i$ deflection level in Test 4, initial yielding in the column bars was observed (see Fig. 4.37(b)).

Joint Hoop Strains. The joint hoop strains measured for beam displacements up to $1\Delta_i$, primarily Tests 2 and 3, were relatively small, less than 1000μ . Shear distress in the joint hoops was not expected to be serious at these load levels, however, because of the considerable shear capacity provided by the concrete due to the size of the joint. As the shears transferred to the joint increased with the higher deformation levels, $2\Delta_i$ and $3\Delta_i$, yield strains were measured initially in the center two hoops, and then in all four of the joint hoops.

4.3.4 Longitudinal Beam Rotations. In general, the beam rotations measured 6 in. from the column face increased linearly with the drift angle in Test 2 (see Fig. 4.38). The linear relationship was reasonable since the joint rotations and shear distortions were insignificant at these load levels. Comparisons of measured west and east beam rotations in Tests 3 through 5 are illustrated in Fig. 4.39. Deterioration of the relationship between beam rotation and the drift angle as testing continued was indicated by the steeper slopes, particularly in Test 5. The larger beam rotations reflected the increasing influence of joint rotations and shear distortions, and inelastic rotations of the beams in the hinging zones, as well. Inelastic deformations, including the measured beam rotations, accounted for greater percentages of the beam deflection as the loading intensity increased.

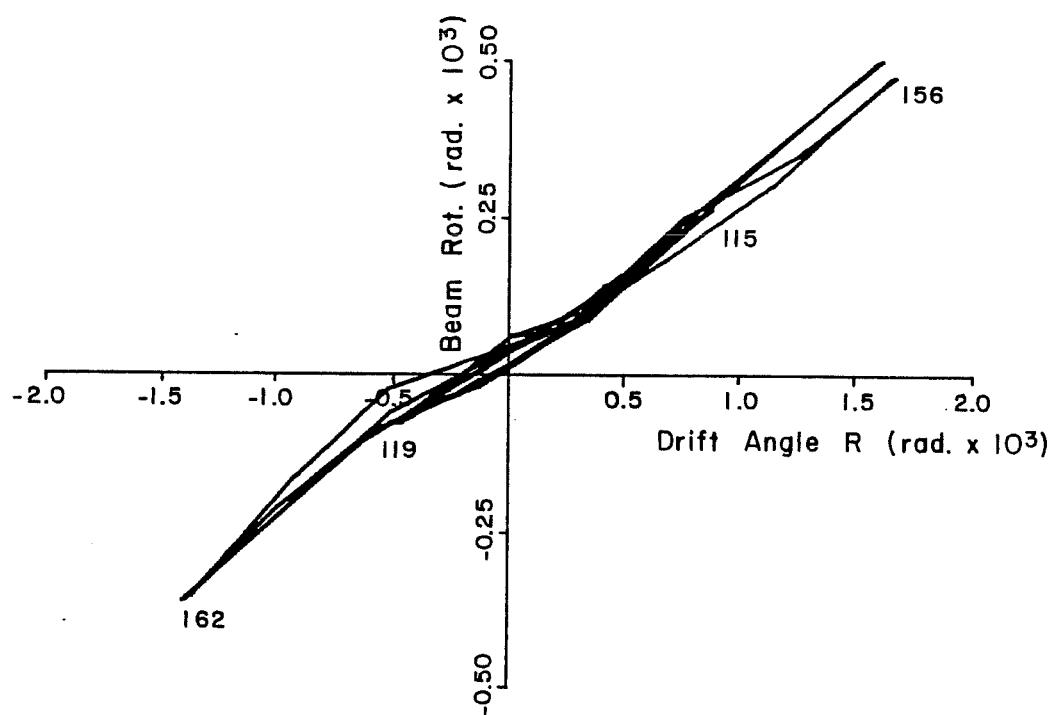


(a) Gage 1T_j, Test 3

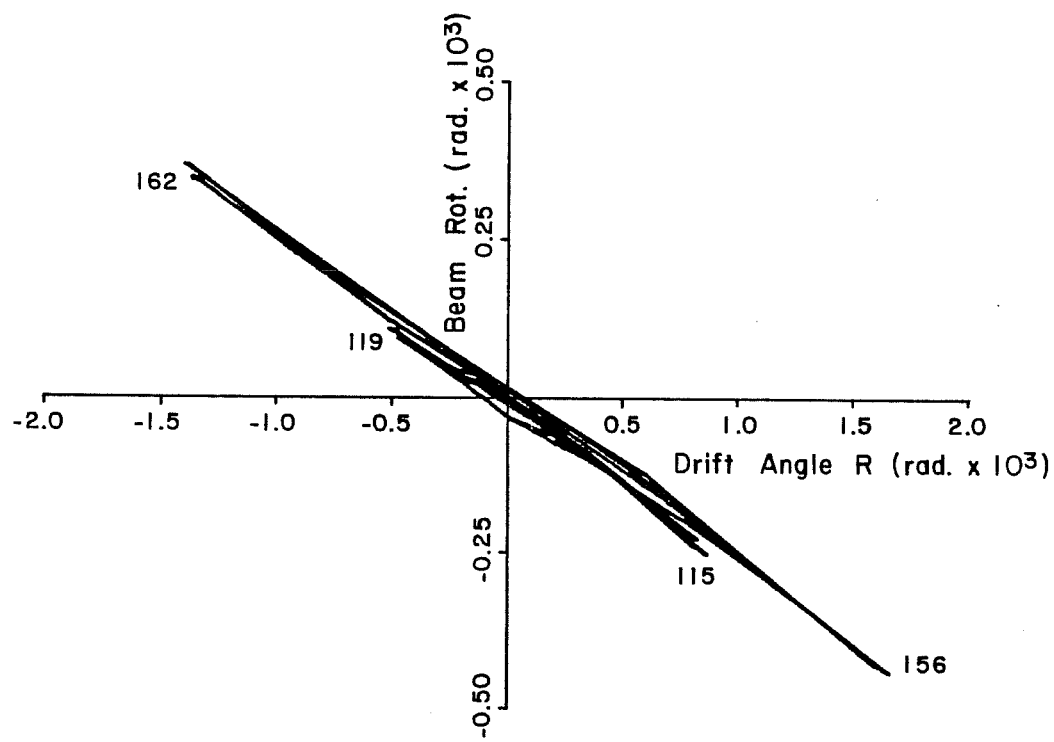


(b) Gage 1T_j, Test 4

Fig. 4.37 Strain versus drift angle, east column face bar

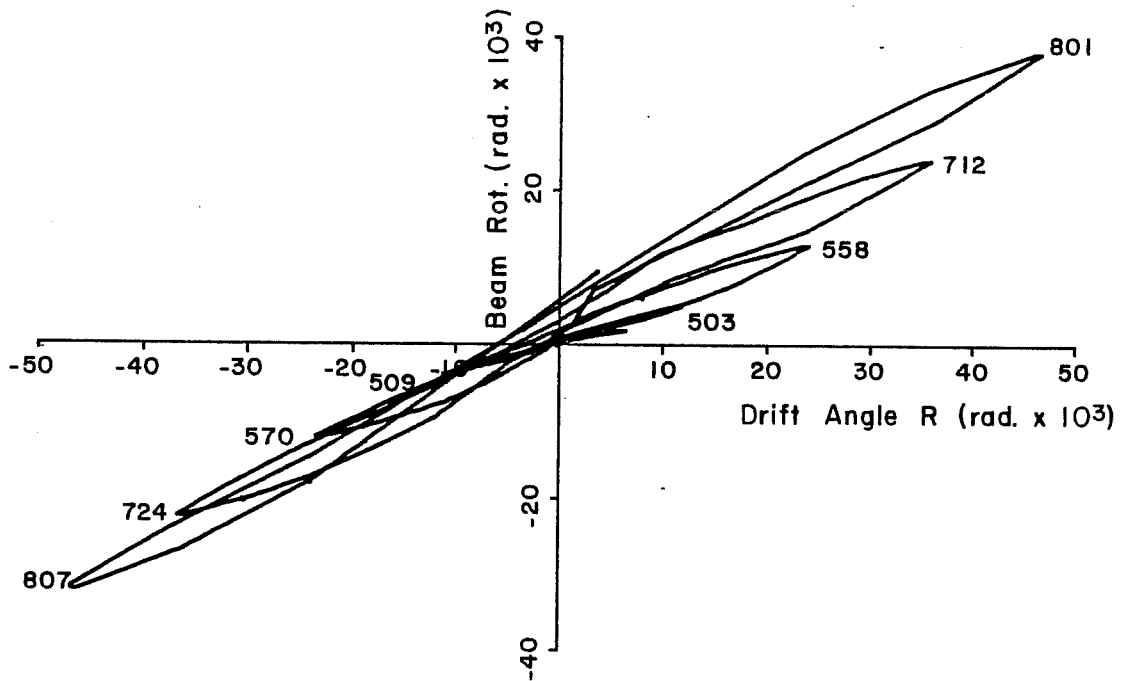


(a) West beam

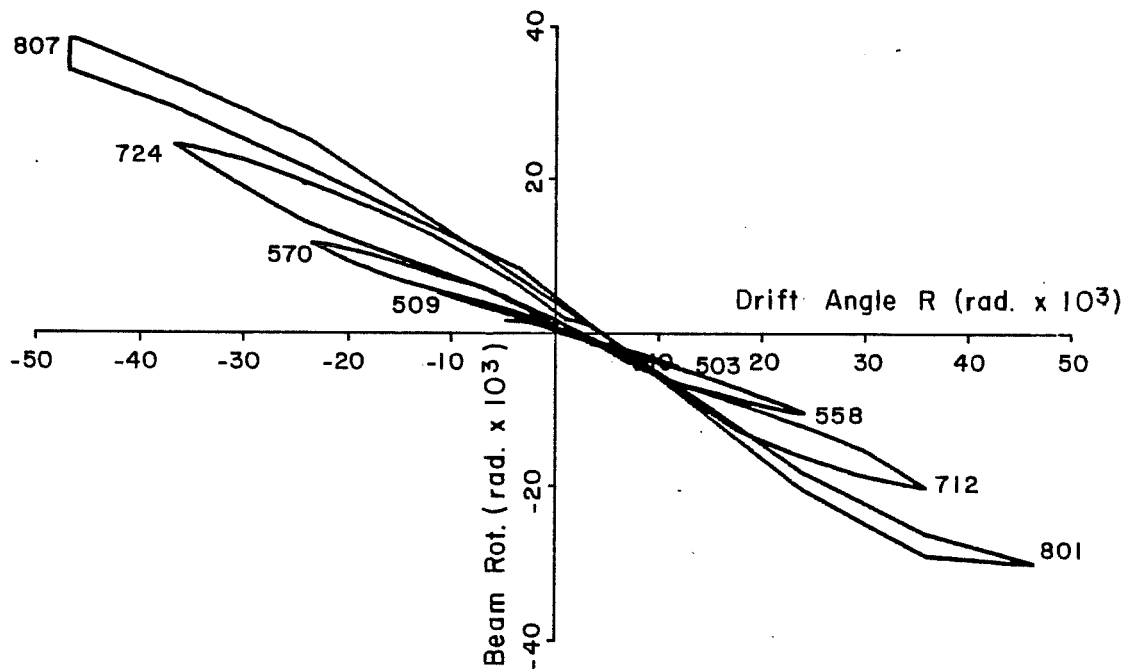


(b) East beam

Fig. 4.38 Beam rotation versus drift angle, Test 2



(a) West beam



(b) East beam

Fig. 4.39 Beam rotation-drift angle relationships, Tests 3 through 5

4.3.5 Joint Shear Strain. In general, the joint shear strain versus drift-angle relationships were linear for Tests 3 through 5 (see Fig. 4.40). Note, however, that the curves were displaced from the origin, up the y-axis, as the load levels increased in Tests 4 and 5. The steady increase in positive shear strain and decrease in negative shear strain was likely an indication of the deterioration which occurred in the joint due to the cyclic load history and to the high shears transferred to the joint as the resistance of the slab increased. The initial direction of loading and the orientation of the shear strain instrumentation (see Sec. 3.3.5) may have accounted for this difference in positive and negative shear strain magnitude, as well. Another indication of the inelastic behavior of the joint was the ratio of beam deflection due to shear distortion of the joint, which increased from a range of 20 to 25 percent to 30 to 33 percent in the latter stages of testing.

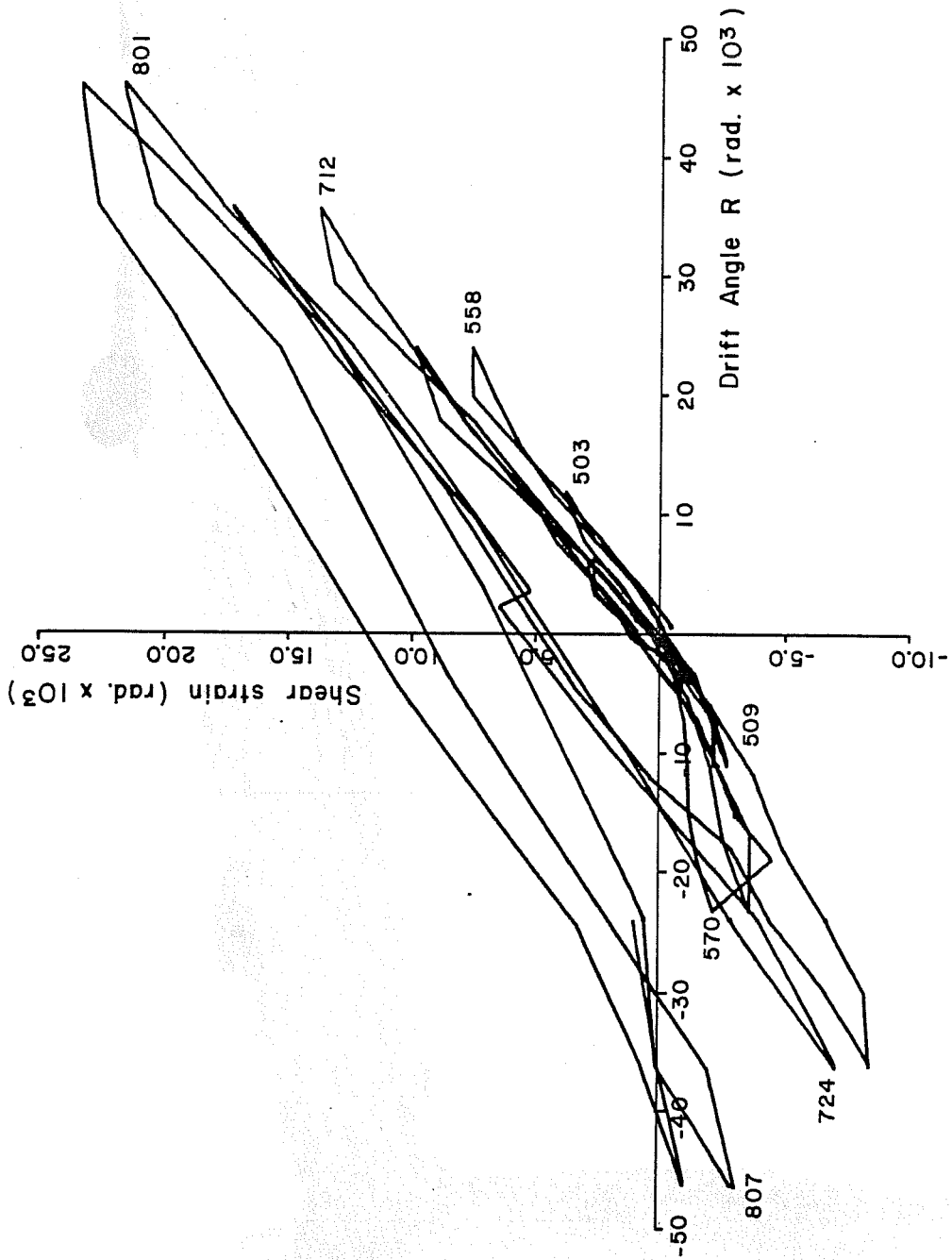


Fig. 4.40 Joint shear strain-drift angle relationships, Tests 3 through 5

CHAPTER 5

COMPARISONS OF TEST RESULTS

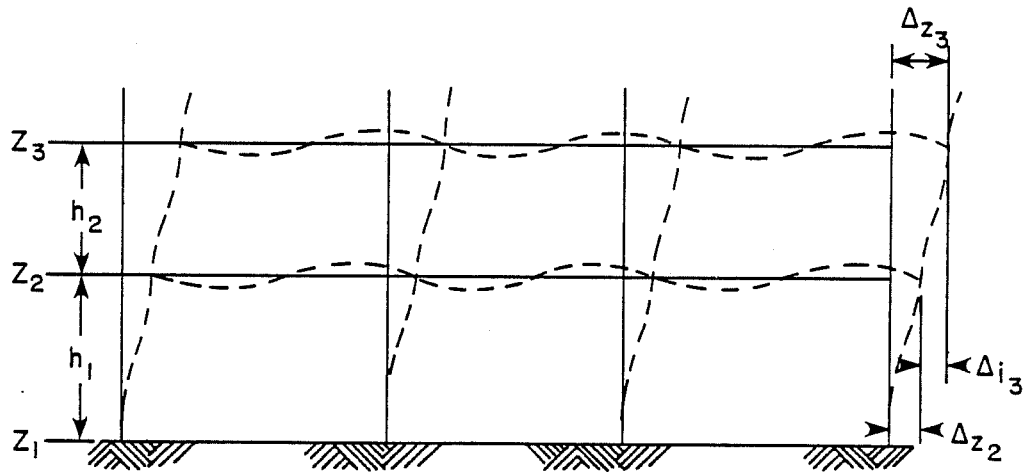
5.1 Introduction

In this chapter the test results from the full-scale interior joint specimen, USJ-1, were compared with the half-scale component and the full-scale structure test results. The comparisons included cracking patterns, longitudinal beam and column bar strains, longitudinal beam rotations, and for the component assemblies non-dimensionalized hysteresis relationships. It should be mentioned that the test data obtained from the half-scale tests and the full-scale structure tests were limited and in some cases difficult to interpret. Comparisons of similar test measurements; e.g., strains, rotations, etc., between the three test programs were not possible.

The drift-angle index, R , defined in Chapter 4, was used as a reference parameter to compare the test results and behavior of each specimen. This parameter was calculated in an identical manner for the full-scale and half-scale joint specimens. For the full-scale structure, the relative lateral drifts of the second and third levels were used to calculate drift angles for the first and second stories of the structure (see Fig. 5.1). An approximate drift angle, R , for a joint at the second level was calculated by averaging the drift angles of the first and second stories, both of which contributed to the rotation of the joint.

5.2 Comparisons with Half-Scale Tests

5.2.1 Description of Tests. Two half-scale beam-column joint specimens (I-1 and I-2), with slabs, were fabricated to model an interior joint at the second level of the full-scale structure. The



Δ_{z_2} = total horizontal displacement at level z_2 , cm.

Δ_{z_3} = total horizontal displacement at level z_3 , cm.

Δ_{i_3} = interstory drift between levels z_2 and z_3 , cm.

h_1 = first story height, cm.

h_2 = second story height, cm.

R = drift-angle index for joint at z_2 , rad.

R_1 = drift-angle index for first story, rad.

R_2 = drift-angle index for second story, rad.

$$R_1 = \frac{\Delta_{z_2}}{h_1}$$

$$R_2 = \frac{\Delta_{i_3}}{h_2}$$

$$R = \frac{R_1 + R_2}{2}$$

For $h_1 = 375$ cm. and $h_2 = 300$ cm.

$$R = \frac{\Delta_{z_2} + 1.25\Delta_{i_3}}{750}$$

Fig. 5.1 Drift-angle index, full-scale structure

longitudinal beams and the columns were dimensioned assuming inflection points at the mid-span of the beams and at the mid-story height of the columns. The width of the specimens was controlled by the effective width of the slab which was calculated to be 75 cm according to both the AIJ Standard⁸ and ACI 318-77.³ Beam and column reinforcement ratios were identical in both specimens, but were not scaled precisely due to the available bar sizes. The slab reinforcement ratio was similar to the prototype structure, but the steel was placed in a single layer. The difference between the two half-scale assemblies was the amount and arrangement of lateral reinforcement in the beams and columns. Specimen I-1 was detailed according to Japanese practice and specimen I-2 according to U.S. practice; neither of which compared closely with the full-scale structure. However, the performance of the two half-scale joints was similar and not significantly affected by the amount of transverse reinforcement. The test results of specimen I-2 were used in the following comparisons with the full-scale interior joint.

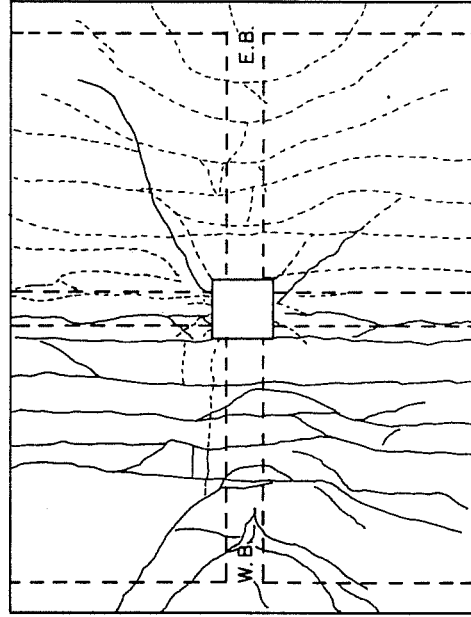
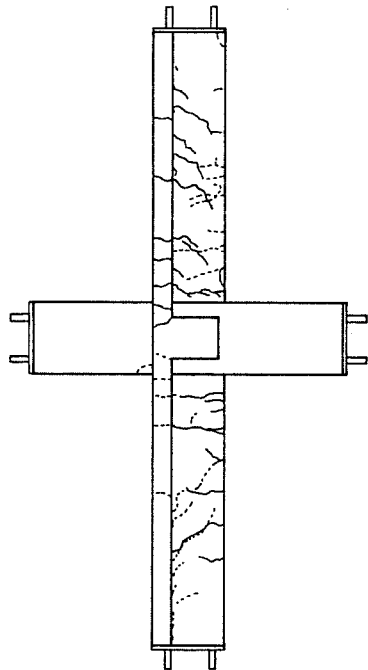
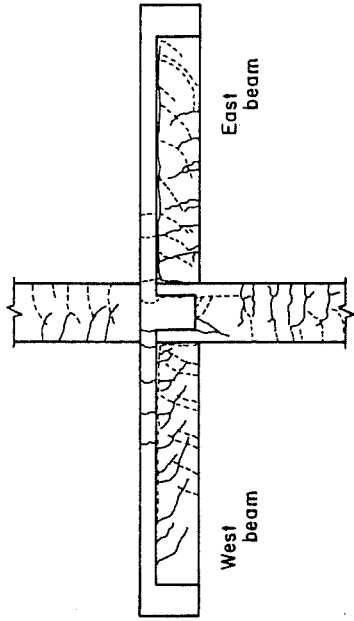
The half-scale specimens were subjected to a reversed, cyclic load history with increasing levels of deformation. Loads were applied at the longitudinal beam-ends by controlling beam displacement in a manner similar to the loading system for USJ-1. The top of the column was supported by a vertical roller and the bottom of the column was pin-connected to the loading frame. An axial load was applied to the column to simulate the gravity load conditions in the prototype structure.

The subsequent comparisons between the half-scale and full-scale joint tests were rather general because of limited information available from the half-scale tests, geometric differences, and dissimilar load histories applied to the two specimens. The extent of the test results obtained from the half-scale tests included cracking patterns and hysteresis relationships. The slab width of the half-scale joint assemblies was, by comparison, much smaller than the slab width of the full-scale interior joint. Therefore,

it was likely that a greater resistance provided by the slab would be observed in the full-scale joint tests. Furthermore, the single layer of slab steel in the half-scale specimens was not consistent with the two mats of slab steel in USJ-1. Finally, the load histories applied in the two test programs were substantially different. The full-scale interior joint was subjected to several, pre-yield cycles of deformation. Conversely, in the half-scale specimens the bottom beam steel yielded during the first or second cycle of loading.

5.2.2 Cracking Patterns. The crack patterns of the half-scale specimens were primarily flexural and resembled the cracking observed in the full-scale interior joint. Figure 5.2 illustrates the cracking which appeared in specimen I-2 and USJ-1 at drift angles of 0.005 (1/200) and 0.00625 (1/160), respectively. The extent of flexural cracking in the longitudinal beams and slab of each specimen was comparable. Diagonal shear cracks which extended into the beams from the slab first appeared at this load level in both specimens. The larger shear forces produced when the slab was in tension caused the shear cracks to develop in the beams of the component assemblies.

The after-test crack patterns of specimen I-2 and the documented crack patterns of USJ-1 at the completion of Test 4 are shown in Fig. 5.3. The maximum level of deformation applied in each test corresponded to a drift angle of approximately 0.025 (1/40), excluding the last load cycle in the half-scale tests. Flexural cracking was extensive in both joint specimens. Several diagonal shear cracks appeared in the longitudinal beams and propagated into the lower portion of the beams, indicating the presence of high beam shears. In the negative (up) loading direction, beam shears were not large enough to initiate diagonal cracks at the bottom of the beams in either specimen. Wide flexural cracks opened in the longitudinal beams near the lower column faces in the half-scale and full-scale joint specimens. No concrete crushing or spalling was observed in specimen I-2; however, after three cycles at the

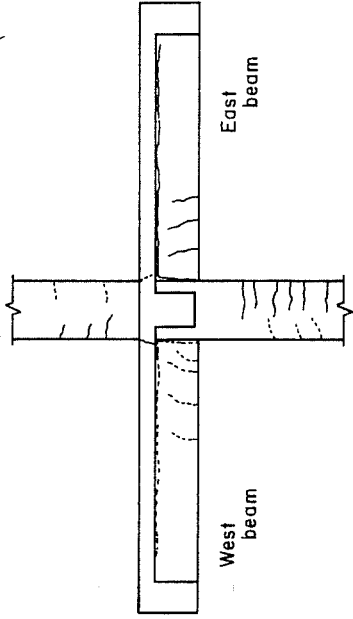


(a) Specimen I-2 (after test)⁹

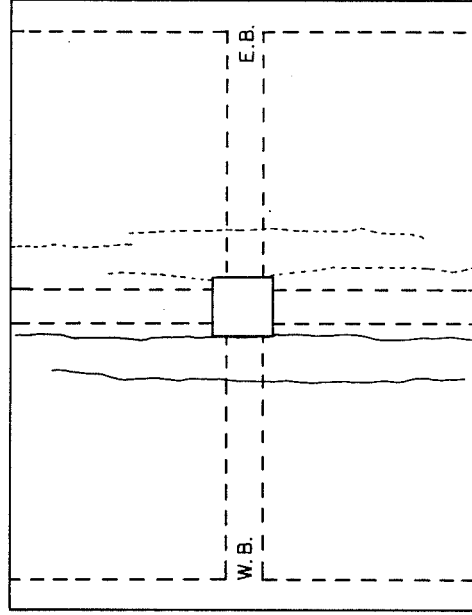
2) Plan view

(b) Specimen USJ-1 (after Test 4)

Fig. 5.3 Cracking patterns for half-scale and full-scale joint specimens

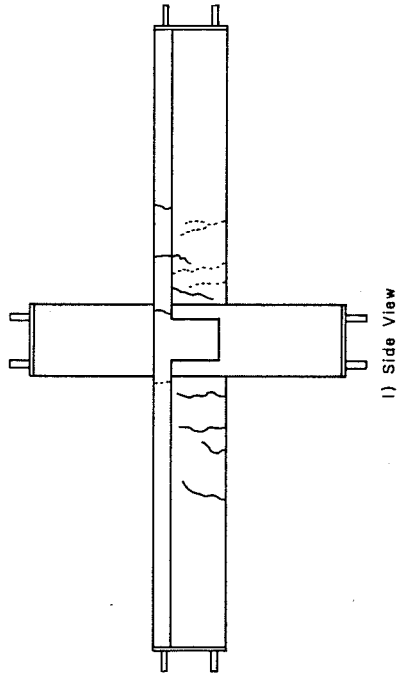


1) Side view

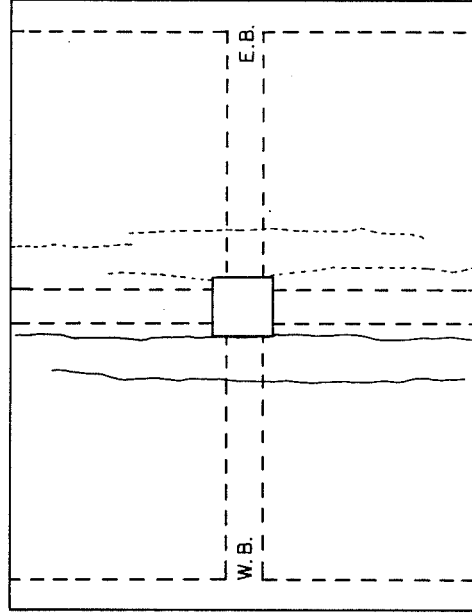


2) Plan view

(a) Specimen I-2 (R = 1/200)⁹



1) Side view



2) Plan view

(b) Specimen USJ-1 (R = 1/160)

Fig. 5.2 Cracking patterns for half-scale and full-scale joint specimens

peak deformation level ($R \approx 1/40$) some crushing and spalling occurred near the joint in USJ-1. In the slab, similar radial cracking patterns developed about the loading points in both specimens. Substantially less flexural cracking occurred in the column of the half-scale component joint due to the applied axial load.

5.2.3 Hysteresis Relationships. The story shear versus story displacement relationships for specimen I-1 and I-2 indicated that the behavior of the two specimens was very similar (see Figs. 5.4 and 5.5).⁹ The fat and stable hysteresis loops for drift angles less than 0.0133 (1/75) were characteristic of good hysteretic response. In general, the points at which yielding of the beam reinforcement and slab reinforcement occurred in both specimens were consistent. Stiffness and strength deterioration were apparent in the response of the two half-scale joint assemblies during the fifth cycle of loading ($R \approx 1/40$). Slip of the beam reinforcement through the joint and shear degradation in the beam hinging zones were probably responsible for the pinching of the hysteresis loops observed during this cycle of loading.

In Fig. 5.6 nondimensionalized hysteresis relationships for the half-scale and full-scale joint specimens are presented from which comparisons of the behavior of the specimens were made. The drift angle, R , was plotted on the x-axis and a ratio defined as the story shear (Q) divided by the yield story shear (Q_y), which corresponded to yielding of the lower beam steel, was plotted on the y-axis. Since the negative yield loads (bottom steel in tension) of the beams were essentially independent of the slab width, it was reasonable to use this story shear to nondimensionalize the vertical axis.

The hysteretic behavior of I-2 and USJ-1 compared well considering the geometric and scaling differences. In the initial cycles of loading, beam displacements applied to the half-scale specimen were large enough to produce yielding in the bottom beam

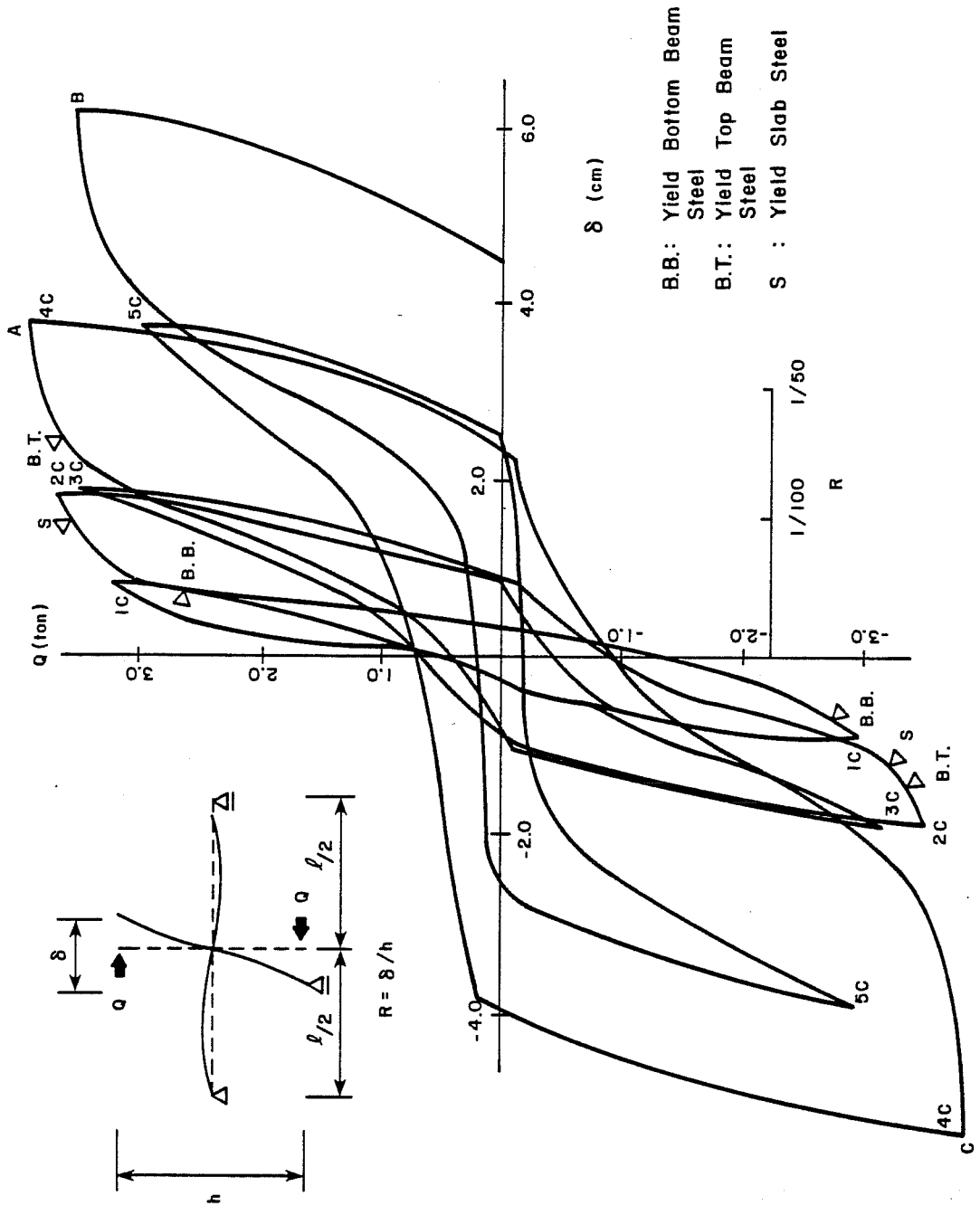


Fig. 5.4 Story shear versus story displacement relationship (Specimen I-1)

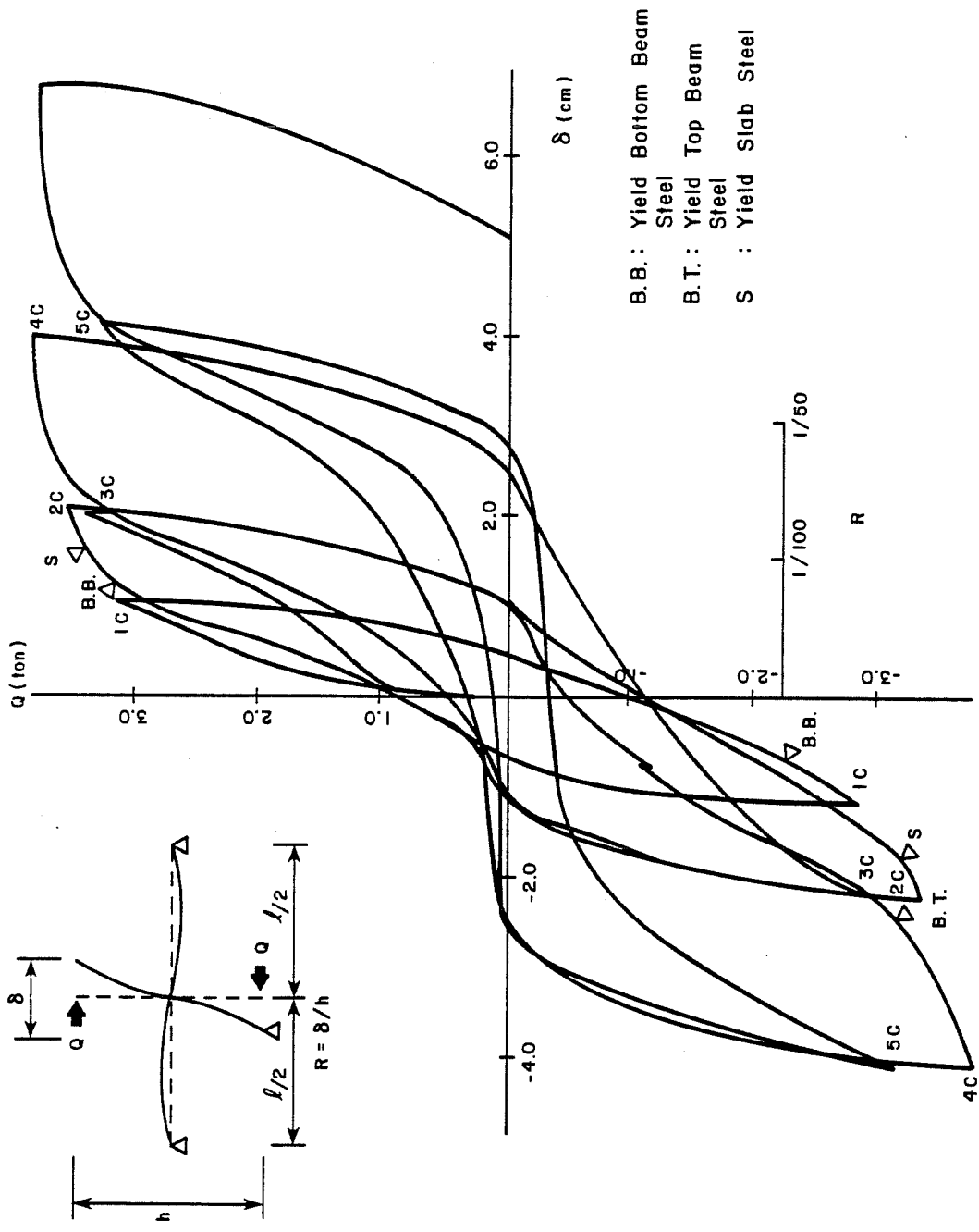
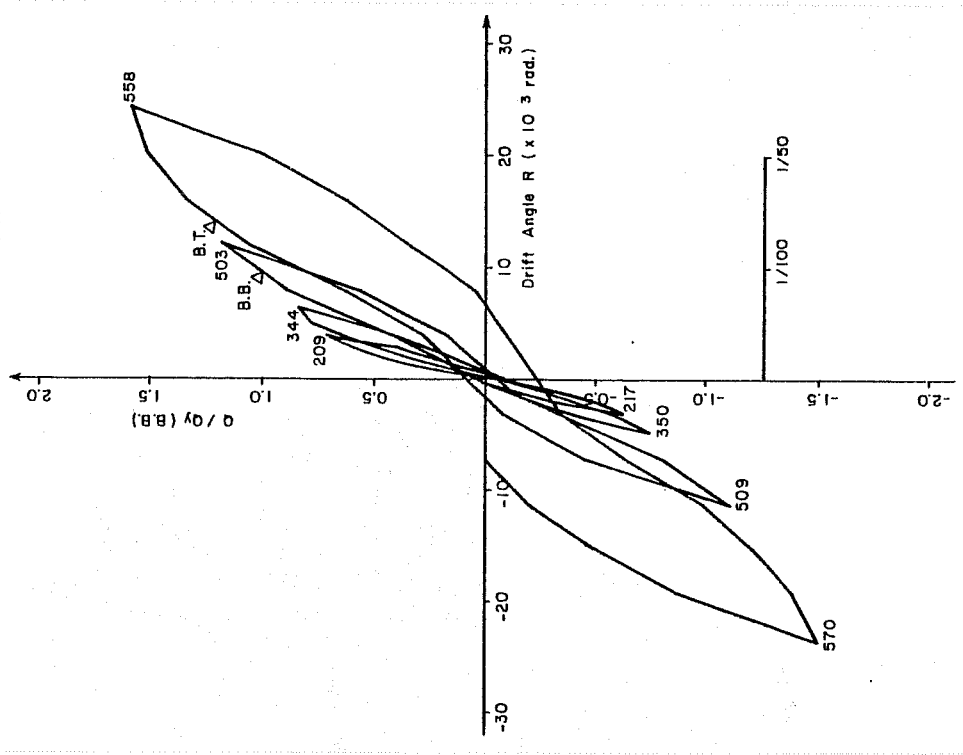
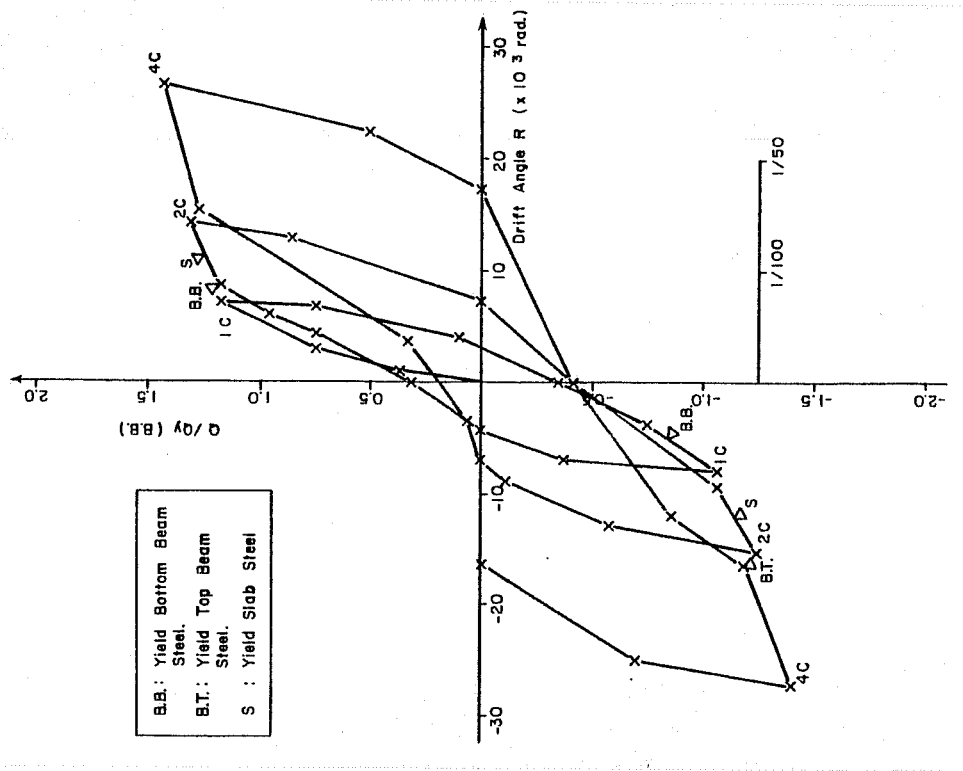


Fig. 5.5 Story shear versus story displacement relationship (Specimen I-2)



(a) Half-scale joint specimen I-2



(b) Full-scale joint specimen

Fig. 5.6 Nondimensionalized hysteresis relationships

bars. Note that a Q/Q_y ratio of 1.0 was exceeded in all three cycles of deformation in Fig. 5.6(a). By comparison, the first two cycles of deformation shown for the full-scale specimen (see Fig. 5.6(b)) were relatively small and nearly elastic. The initial stiffness for the half-scale specimen was slightly larger than for the full-scale specimen. However, the stiffness of the full-scale component assembly may have deteriorated slightly due to several small cycles of loading applied in a previous test (Test 1).

In the half-scale specimens, the slab steel and the top beam steel yielded at nearly the same Q/Q_y ratio (see Figs. 5.4, 5.5 and 5.6(a)). The response of the half-scale joint assemblies was primarily inelastic as indicated by the flat slope of the hysteresis curves beyond these points and the wide hysteresis loops. However, for similar deformation levels inelastic behavior was not as predominant in the full-scale specimen. Note that the width of the hysteresis loops for the third and fourth loading cycles shown in Fig. 5.6(b) was much smaller compared to the hysteresis loops for I-2. The slope of the hysteresis curves for the full-scale joint were much steeper beyond the yield points of the slab steel and the top-beam steel. The maximum Q/Q_y ratio of about 1.6 was reached at a drift angle of 0.024 (1/41) in the full-scale joint tests compared to 1.43 in the half-scale tests. The higher ultimate strength of USJ-1 was attributed to the comparatively larger slab width which was effective at deformation levels in the range of 0.02 ($R = 1/50$). For the half-scale specimen, the effective slab width was limited to 75 cm., or the width used in design calculations.

The points at which the top beam steel yielded in each specimen compared favorably. The corresponding drift angles for I-2 and USJ-1 were approximately 1/60 and 1/70, respectively. In general, the story shear ratios were slightly higher in the half-scale tests. Yielding of the bottom beam bars did not compare as well. The drift angle required to yield the bottom beam steel in the half-scale specimens was about half of the drift angle for the

full-scale joint, $1/200$ compared to $1/110$. However, the larger angles or beam deflections required to yield the bottom bars in USJ-1 were due to bond deterioration and slip of the bars, and a general softening of the specimen with testing (refer to Sec. 4.3.3). It was mentioned that with more favorable bond conditions and less specimen deterioration the beam deflection at yield may have been much closer to a drift angle of $1/200$.

5.3 Comparisons with the Full-Scale Seven-Story Structure

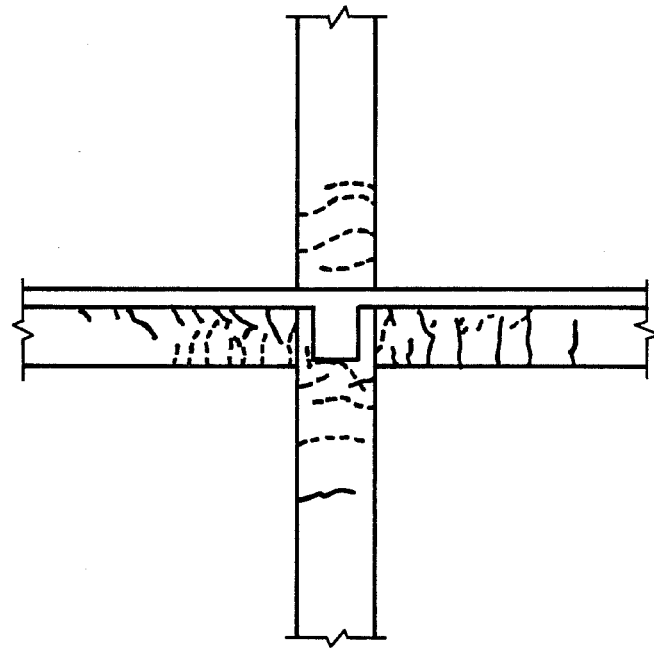
5.3.1 Introduction. Cracking patterns, column and longitudinal beam bar strains, and longitudinal beam rotations for a typical interior joint at the second level of the full-scale structure were considered in the following comparisons with the full-scale interior joint specimen, USJ-1. The relevant test data and results were obtained from the third and fourth tests in the initial series of tests conducted on the prototype structure. In the third test yielding occurred in the beams and columns, and during the fourth test the response of the full-scale structure was primarily inelastic. The maximum drift angles (as calculated in Sec. 5.1) imposed at the second level of the prototype specimen were 0.0054 ($1/185$) and 0.0075 ($1/133$) in the third and fourth tests, respectively. Deformations of this magnitude corresponded to beam deflections of 0.52 in. and 0.72 in. for the full-scale joint specimen. Beam displacements in this range were applied in Tests 2 and 3, and in the early stages of Test 4.

It should be mentioned that the two specimens were not subjected to equal load intensities prior to the tests considered above for comparisons. The maximum drift angle imposed at the second level of the full-scale structure was 0.000173 ($1/5800$) prior to the third test. By comparison, the maximum drift angle applied to USJ-1 prior to Test 2 was much larger, 0.002 ($1/500$). However, note that the prototype structure was very stiff at the lower story

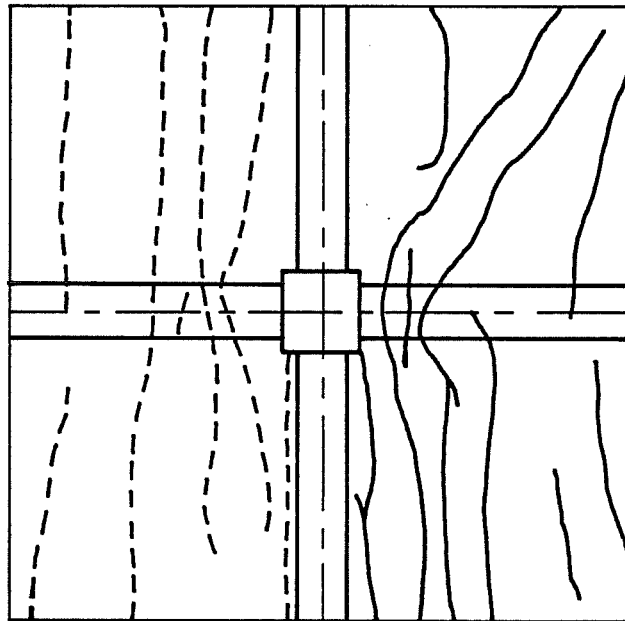
levels because of the shear wall. The drift angle for the structure using the applied lateral displacement at the roof level and assuming a linear relationship along the height of the structure was 0.0015 (1/660). Furthermore, similar cracking, although minimal, was observed in both specimens at these load levels.

5.3.2 Cracking Patterns. The cracking patterns for an interior joint, frame A and frame 2, of the full-scale structure (see Fig. 1.2) at completion of the fourth test are shown in Fig. 5.7.¹⁰ In general, the cracking observed in the prototype structure was similar to the crack patterns of USJ-1 at load stages 344 and 350 (see Figs. 4.9 and 4.10). The maximum drift angles at this point for the full-scale structure and the component specimen were 0.0075 (1/133) and 0.0064 (1/156), respectively. Several flexural cracks were present in the longitudinal beams, column, and slab of each specimen, but diagonal shear cracking was not as extensive in the interior joint specimen. At load stages 503 and 509 diagonal cracking comparable to the cracking in the prototype structure appeared in the west and east beams of USJ-1 (see Figs. 4.17 and 4.19). However, the corresponding deformations applied to the interior joint specimen were slightly larger ($R \sim 1/90$).

The interior columns in frames A and C of the full-scale structure were cracked in only one loading direction because of shear-wall deformations which lifted one end of the structure. This uplifting reduced or possibly eliminated the compressive forces due to gravity loads which inhibited flexural cracking in the columns. When the loading direction was reversed, compressive forces were present in the columns and cracking did not occur. In addition, the uplift of the center frame B, which contained the shear wall, was greater relative to frames A and C, and therefore bending moments were introduced into the transverse beams and flexural cracking was observed.



1) Side view



2) Plan view

Fig. 5.7 Cracking patterns of the full-scale structure

5.3.3 Reinforcement Strains. The strain gage locations for column and longitudinal beam bars at an interior joint at the second level of the full-scale structure (frame A) are shown in Fig. 5.8.¹⁰ Strains for top and bottom longitudinal beam bars at the critical section were plotted versus the drift angle for the prototype structure and the interior joint specimen, USJ-1 (see Figs. 5.9 and 5.10). The strains given in Figs. 5.9 and 5.10 were representative of strains measured for top and bottom beam bars in both specimens. Note that during the fourth test of the full-scale structure, many of the strain gages were not functional and very little valid data were obtained.

For a given drift angle, the top beam bar strains in the full-scale structure were approximately twice the measured strains in the joint specimen (see Fig. 5.9). However, some characteristics of the strain versus drift-angle relationship for each specimen were similar. Both of the plots in Fig. 5.9 have a general saddle shape and both plots show that no significant compressive strains occurred in the top bars, giving an indication as to the shallow depth of the compression zone. A maximum strain of nearly 1200μ , less than yield strain, was measured in the top beam bars of the prototype structure during the third test.

Figure 5.10 indicates a generally poor correlation for the strains measured in the bottom beam bars of the full-scale structure and the joint specimen. In the negative loading direction, the slope of the strain-drift angle relationship was much steeper for the prototype structure. The bottom beam bars yielded at a drift angle of approximately 0.0027 (1/370) compared to 0.0095 (1/105) for USJ-1. However, at this point, twice as many load cycles had been applied to the interior joint specimen as had been applied to the full-scale structure. Bond deterioration of the bottom beam bars developed in the joint of USJ-1 as a result of the large number of applied load cycles. The unfavorable bond condition of the bottom bars and the reduced stiffness of the component specimen with testing, probably

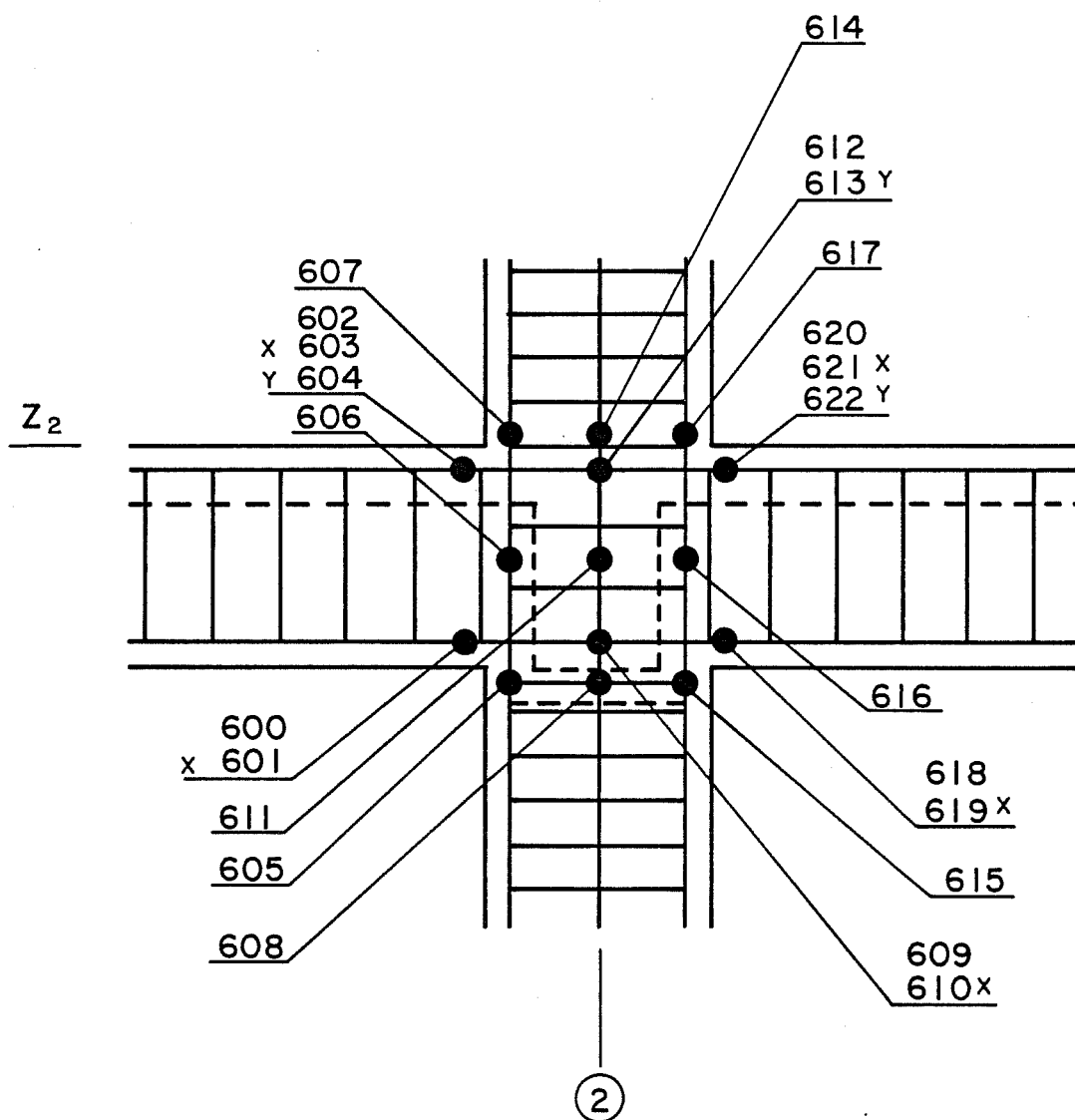


Fig. 5.8 Strain gage locations for joint in full-scale structure

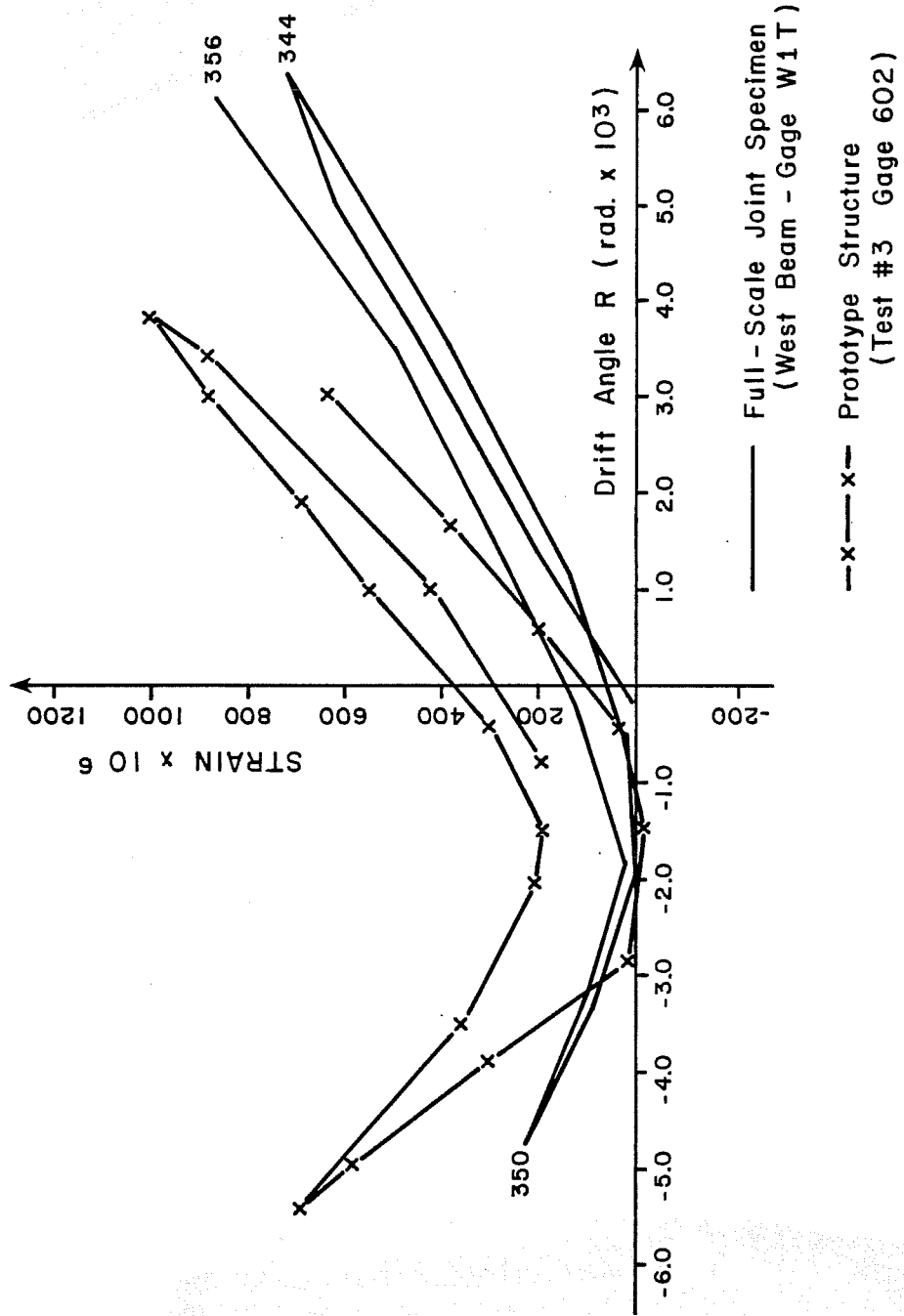


Fig. 5.9 Strain versus drift-angle relationships, top beam bars

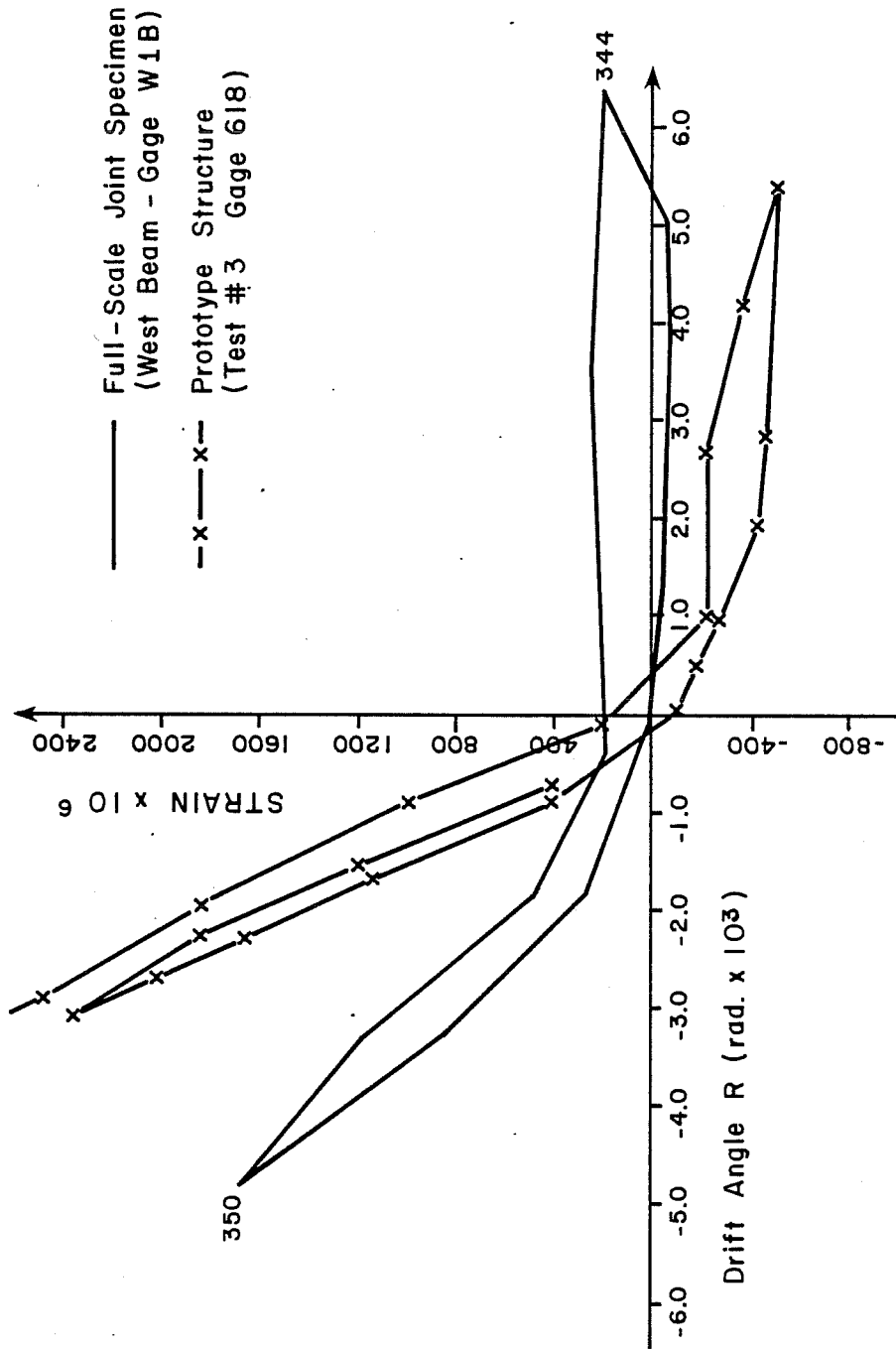


Fig. 5.10 Strain versus drift-angle relationships, bottom beam bars

increased the negative yield drift angle (refer to Sec. 4.3.3). In the full-scale structure, bond deterioration of the bottom beam bars was apparently not a problem. Note that appreciable compressive strains were produced in the bottom bars of the prototype structure in the positive loading direction, but not in the component specimen. Bond deterioration probably contributed to this difference, as well.

Strains measured for an upper column bar at the critical section show a relatively good correlation between the prototype structure and the joint specimen (see Fig. 5.11). Maximum tensile strains, about half of yield, were measured at nearly the same drift angle ($R \approx 1/200$) in both tests. Note, as the positive deformation levels applied to each specimen increased, the measured strains changed sign and indicated tensile forces. It appears that bond deterioration of the column bars may have occurred in the full-scale structure as well.

5.3.4 Longitudinal Beam Rotations. The measured longitudinal beam rotations of the interior joint specimen did not compare favorably with the beam rotations measured in the full-scale structure (see Fig. 5.12). Beam rotations were defined as positive when the beam-end displacement was positive (downward) or when the top of the beam was in tension. In general, the positive and negative beam rotations in the prototype structure were, respectively, about 2 and 2-1/2 to 3 times larger than the positive and negative beam rotations of USJ-1. Slightly larger beam rotations were expected in the full-scale structure tests since the rotations were measured over a larger gage length (refer to Sec. 3.3.2). However, once beam hinges begin to form, the beam rotation would be approximately linear (rigid body rotation) and the point at which they are measured would make little difference. Therefore, this discrepancy between the measured rotations was probably due to the method of load application and the boundary conditions, both of which were substantially different for the two specimens. The locations of the inflection points of the

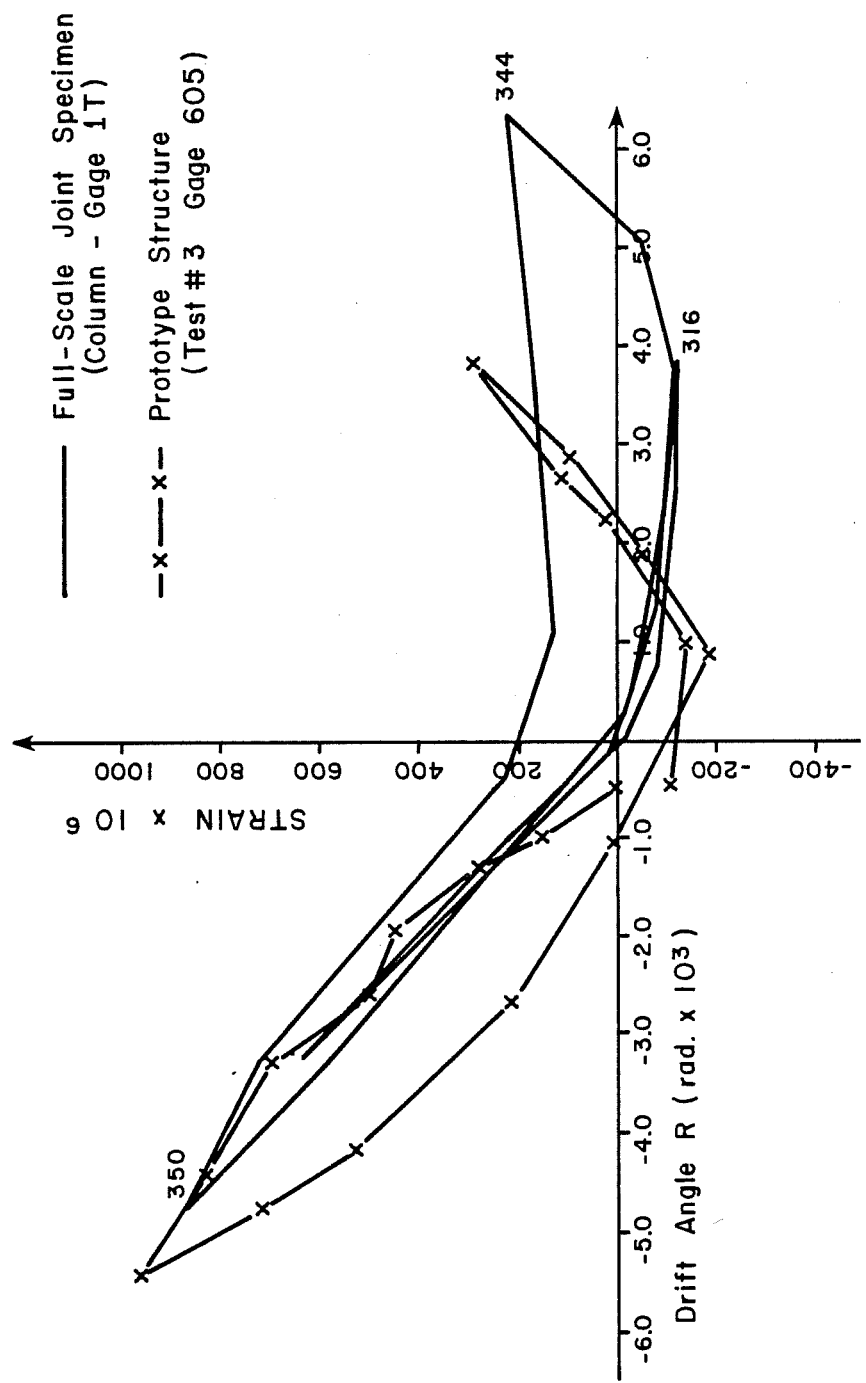


Fig. 5.11 Strain versus drift-angle relationships, upper column bars

longitudinal beams in the full-scale structure changed during testing, and the beams were free to rotate without restrictions from the loading apparatus. However, for the interior joint specimen, loads were applied at the assumed inflection points (mid-span) and the beam rotations depended, primarily, on the applied beam-end deflections.

In Fig. 5.12 the measured beam rotations of the interior joint specimen are linear with respect to the drift angle. Since the beam-end deflections were controlled during testing, and the inelastic behavior of the joint and column prior to the $2\Delta_i$ displacement level was insignificant, the linear relationship was not unreasonable. In the prototype structure the negative beam rotations were consistently larger than the positive rotations. This may have been due to slightly larger beam curvatures when bending in the weak direction.

5.4 Suggestions for Future Testing

To compare the test measurements and response of the three specimens, it was necessary to establish a reference index or parameter upon which the comparisons were based. The parameter selected in this study was the drift angle or story drift. Whether the angles calculated for the full-scale structure were accurate measures of the actual beam and column deformations is questionable. However, much of this uncertainty could be eliminated by simply providing some additional instrumentation on a selected joint in the prototype structure. If, for instance, the deflected shape of a beam in the full-scale structure was known, it could be duplicated in the component testing. The deflected shape of the beams framing into the joint of the prototype structure could be obtained by using displacement transducers attached to a reference bracket (frame A) fixed to the column just above the slab (see Fig. 5.13). Several transducers could be used along the length of the beam out to mid-span on either side of the column. Having several displacements along the beam

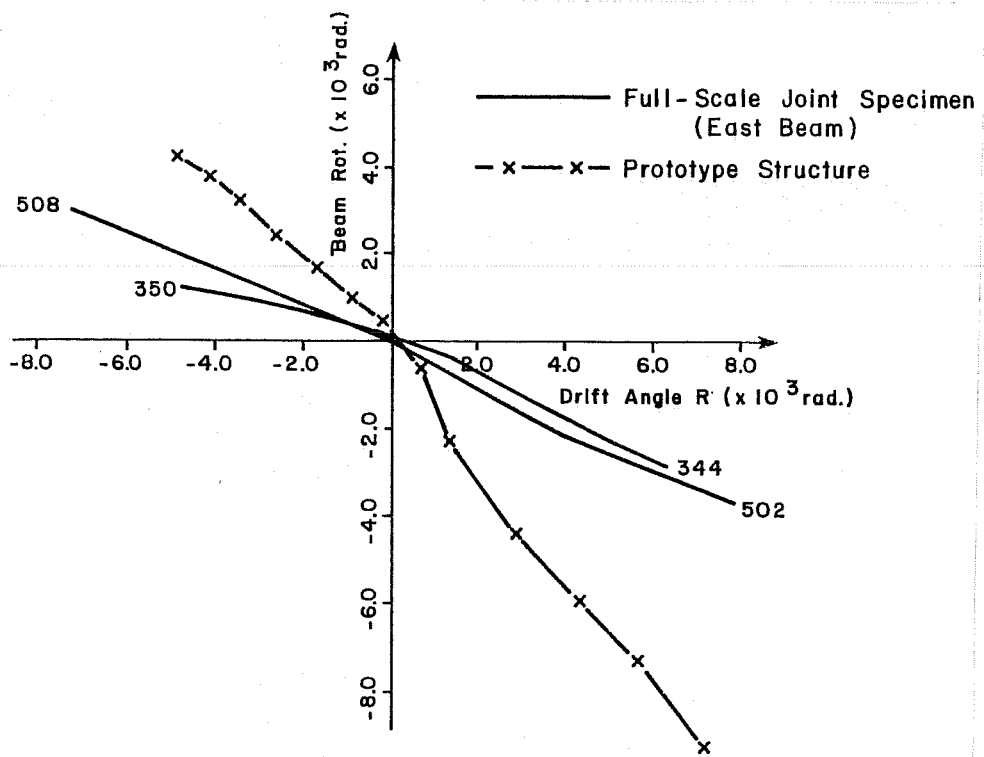
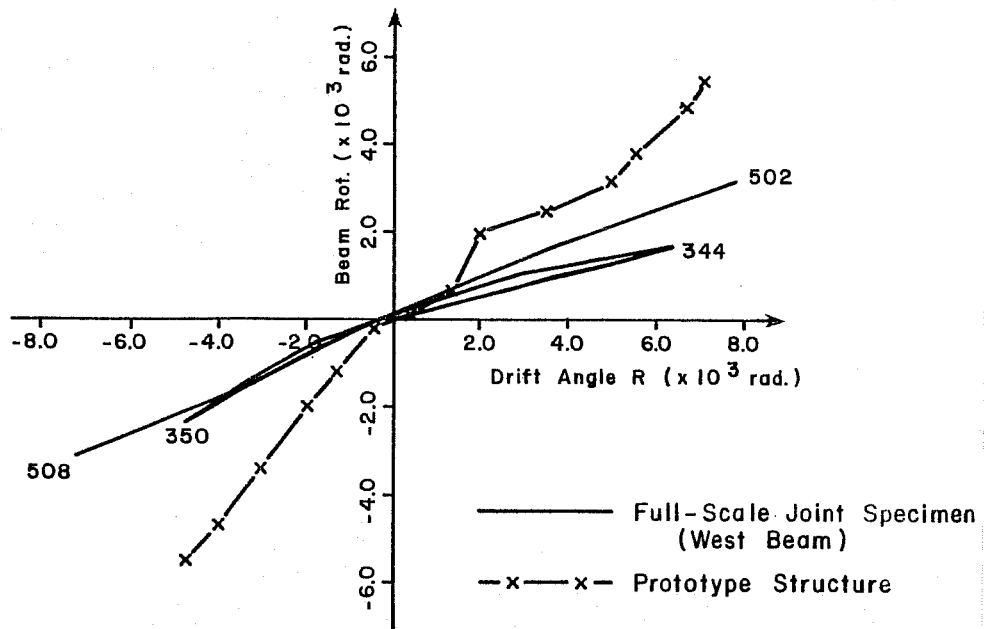


Fig. 5.12 Beam rotation versus drift-angle relationships

length would provide a very good approximation to the deflected shape of the beam, and the locations of the inflection points could be determined. Using the deflected beam shapes in component testing would provide a good reference index to base comparisons, and likely more realistic test results and comparisons of those results would be obtained.

To go one step further, the deflected shape of the column could be obtained in a similar manner using an additional bracket (frame B) as shown in Fig. 5.13. Note that it would be necessary to measure the relative displacements of the two instrumentation frames to obtain the correct deflected shape of the column. Possibly, this could be done by using two displacement transducers to measure the displacement of frame B relative to the beams since the deflected shape of the beams would be known (see Fig. 5.13).

A further useful measurement would be the joint rotations measured relative to a fixed reference frame free from the structure. Displacement transducers attached to the fixed reference frame would measure horizontal displacements relative to the column face at points just above and below the longitudinal beams, in much the same way beam rotations were measured in the joint specimen USJ-1, and the full-scale structure. The absolute joint rotations would give a good indication as to the extent of joint deformation occurring, and could be compared in a straightforward manner with the component joint deformations.

Furthermore, it is recommended that a joint located near the top of the structure, say the fifth or sixth level, be fully instrumented, identically to the joint at the second level. Since the lateral drifts along the height of the structure increased nonlinearly, due to the influence of the wall deformations, larger element (beam, column, etc.) deformations were imposed near the roof level. If test measurements; strains, rotations, etc., would have been available from a joint near the roof level, it is quite possible that a much

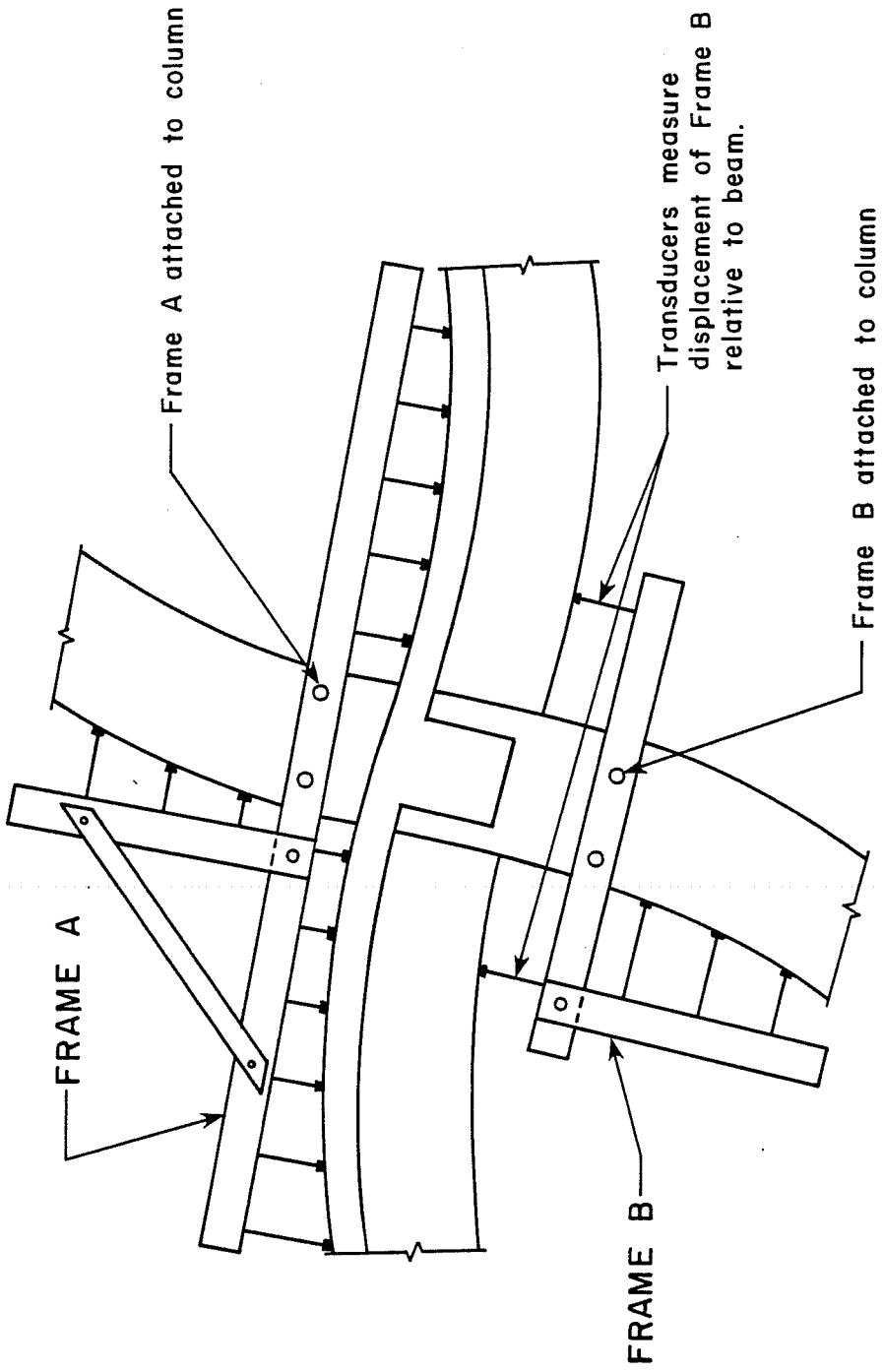


Fig. 5.13 Schematic of suggested instrumentation

better correlation would have been obtained with the test results of USJ-1. The intent of these suggestions for further instrumentation is to provide researchers with a better understanding of the actual deformations that beam, column, and joint elements sustain in the response of a "real" structure to lateral loads, and hopefully to improve the results obtained from component testing.

Finally, some comments should be made concerning the load histories used in the three test programs. In the full-scale structure tests, the load histories were based on ground motion, but idealized to obtain a first mode response of the structure. An inverted triangular load distribution was applied along the height of the structure which was controlled by the lateral forces required to impose the predetermined displacements at the roof level. The load histories used in the full-scale joint tests consisted of selected peak cycles of beam displacement. Initially, the load cycles applied to USJ-1 were very small, but they gradually increased in amplitude as the testing continued. In the half-scale component tests, the applied load cycles were relatively large in amplitude, but few in number (refer to Sec. 5.2.3). Since the load histories applied to the three test specimens were substantially different, it was difficult to compare the test results. Therefore, for future full-scale testing, a simplified cyclic load history with selected peak deformation levels would be more reasonable and easier to duplicate in component testing. Furthermore, several problems including variations in the number of load cycles and the magnitude of deformations applied would be avoided.

CHAPTER 6

SUMMARY AND CONCLUSIONS

6.1 Summary

The purpose of this experimental study was to compare the observed behavior and test results of a full-scale beam-column joint specimen, USJ-1, subjected to reversed, cyclic loads with the response of a full-scale seven-story structure to simulated seismic excitations. The full-scale structure was fabricated and tested in the Large Size Structures Laboratory, Tsukuba, Japan. Half-scale component joint assemblies were tested in Japan as well, and comparisons with the full-scale joint assembly were based on the hysteretic behavior (load-deflection relationships) and the cracking patterns of the two specimens. This project was part of a research program in which a primary objective was to compare and correlate the results of component testing with the response of a full-scale structure under controlled test conditions.

The full-scale joint specimen, USJ-1, was fabricated with reinforcing details and geometry identical to those of an interior beam-column joint at the second level of the prototype structure. The joint specimen was tested under unidirectional loads applied cyclically by controlling the displacements of the longitudinal beam ends. A series of five tests with increasing peak beam displacements were conducted on the interior joint specimen. The performance of USJ-1 was satisfactory to maximum deformation levels corresponding to story drifts of 2-1/2 percent. For design purposes, a practical limit of 2 to 2-1/2 percent is typically recommended as the largest allowable story drift of a structure under the maximum probable earthquake.¹¹ The failure characteristics of the joint

specimen were primarily flexural with the formation of beam hinges at the column faces. Shear degradation was observed in the beam hinging zones due to the high beam shears produced when the slab was in tension and to the cyclic load history. However, this shear degradation occurred at relatively large story drifts, 3-1/2 to 4 percent.

Test results compared in Chapter 5 included cracking patterns, hysteretic response of the component assemblies, reinforcement strains, and beam rotations. The test results of the component specimens and the full-scale structure were correlated using the reference parameter, R, the drift-angle index, established for each specimen. For the component joint specimens, the drift angle was calculated using the beam displacements and the specimen geometry. However, for the full-scale structure it was more difficult to obtain an accurate measure of the drift angle which reflected the actual deformation of a joint at the second level of the structure. An approximate angle was calculated using the lateral drifts measured at the second and third levels of the building. The stiffness of the shear wall clearly affected the deformation of the structure, but it was impossible to determine to what extent. The drift angle or story drift increased along the height of the structure, but due to the influence of the wall, the calculated drifts at the second level were very small.

A second factor which had a direct influence on the outcome of the test comparisons was the refinement or sensitivity of the test measurements and observations. Relatively good test result correlations were obtained when more general measures of specimen performance, such as hysteretic response and cracking patterns, were compared. Furthermore, for such comparisons an approximate reference angle (R) was sufficient. On the other hand, reinforcement strains measured in the full-scale joint specimen and the prototype structure did not compare as well. However, strains are measures of very localized behavior and may be affected by several factors including the method

of load application, material properties, crack locations, bond characteristics, locations of strain gages, etc. Furthermore, the strain comparisons were likely influenced by the reference parameter, R , since the accuracy of this parameter calculated for the full-scale structure was questionable. Therefore, the apparent discrepancies between the strain measurements of the two specimens were not entirely unreasonable.

6.2 Conclusions from Full-Scale Joint Tests

- (1) The response of the interior joint specimen to cyclic loads was satisfactory to story drifts of 2-1/2 percent. Stiffness deterioration was observed due to the cyclic load history, but the strength of the specimen was still increasing and the behavior was predominantly flexural.
- (2) The resistance contributed by the slab was substantially greater than what is generally considered in design calculations according to existing Code recommendations. Due to the conservative nature of Code provisions, the maximum effective slab width used in this case was 59 in. However, at a story drift of 2-1/2 percent, nearly the entire slab width (4 m) of the specimen was effective, as determined from the measured strains of the slab reinforcement. This potentially large effective slab width should be considered in the design of seismic-resistant structures since column hinging may develop due to the higher moments transferred by the slab-beam floor system.
- (3) Bond deterioration and subsequent slip of the column and beam bars through the joint may be difficult to prevent in reinforced concrete structures subjected to lateral loads. After several relatively small cycles of loading, the bond of the bottom beam bars deteriorated in the joint of USJ-1. Note that for a joint of this size detailed with #6 and #7 bars, small by U.S. standards, a bond problem would probably not be anticipated.

6.3 Conclusions from Test Comparisons

The following conclusions are based on the comparisons of test results from the component tests and the full-scale structure tests. This study and other associated experimental programs will

help to identify and understand the relationships between component and full-scale testing, but much more research work is needed in this area.

- (1) The response of the half-scale and full-scale component specimens and the full-scale structure was satisfactory for maximum expected deformations due to seismic forces. The behavior of the three test specimens was primarily flexural and the crack patterns were very similar.
- (2) The hysteretic response (load-deflection relationships) of the full-scale and half-scale joint specimens compared reasonably well. The inconsistencies apparent were primarily due to geometric and scaling differences between the slabs of the two specimens.
- (3) Reinforcement strains and beam rotations measured in the full-scale structure and the interior joint specimen, USJ-1, did not compare well in some cases. However, due to the nature of such measurements which are representative of very localized behavior, this was not entirely unreasonable. Material properties, crack locations, bond characteristics, etc., probably contributed to the unfavorable strain and rotation comparisons as well.
- (4) The general lack of correlation with the test results from the full-scale structure was apparent for several reasons:
 - (a) Method of load application--in the full-scale tests lateral forces were applied along the height of the structure. However, the forces resisted by individual elements (beams, columns, etc.) cannot be determined. In the full-scale joint tests, shears were applied directly to the beams, and therefore the forces resisted by the beam and column elements of the joint specimen were known precisely.
 - (b) Geometric and boundary constraints--the dimensions of the joint specimen were selected by assuming inflection points at the mid-span and the mid-story height, but the actual locations of the inflection points in the structure may have varied considerably. The boundary conditions around the perimeter of the slab were much different in the full-scale structure, as well. Finally, the shear wall of the prototype specimen contributed significantly to the stiffness of the structure, but the effect of the wall on the

stiffness of a typical joint in the structure was not known. Since a load-deformation relationship cannot be measured for a beam-column assemblage in the full-scale structure, stiffness comparisons could not be made with USJ-1.

- (c) Drift angle index (R)--since this nondimensionalized parameter was used to compare the test results, it may have had the greatest influence on the outcome of the comparisons. The drift angles calculated for the full-scale structure were approximate and the drift increased along the height of the structure. Note, if an average drift angle was defined as the total lateral displacement of the roof level divided by the building height, the corresponding drift angles would be approximately twice those calculated at the second level of the structure. The correlation between tests would have been improved if this average drift angle had been used, however, in using an average drift, the actual deformations at the second level would be neglected. It is apparent that improvements are needed in the definition of this reference index used to compare test results.
- (5) Additional instrumentation to obtain more accurate beam, column, and joint deformation relationships is needed in future programs in which component-prototype test comparisons are to be undertaken.

B I B L I O G R A P H Y

1. Nielsen, N. N., and Nakagawa, K., "The Tokachi-Oki Earthquake, Japan, May 16, 1968: A Preliminary Report on Damage to Structures," International Institute of Seismology and Earthquake Engineering, Report No. 2, Tokyo, Japan, June 1968.
2. U.S.-Japan Planning Group, "Recommendations for a U.S.-Japan Cooperative Research Program Utilizing Large-Scale Testing Facilities," Report No. EERC-79/26, Earthquake Engineering Research Center, University of California, Berkeley, September 1979.
3. ACI Committee 318, Building Code Requirements for Reinforced Concrete (ACI 318-77), American Concrete Institute, Detroit, 1977.
4. ACI-ASCE Joint Committee 352, "Recommendations for Design of Beam-Column Joints in Monolithic Reinforced Concrete Structures," Journal of the American Concrete Institute, Proc. V. 73, No. 7, July 1976.
5. Longwell, J. E., "A Comparative Study of Biaxially Loaded Reinforced Concrete Beam-Column Joints," unpublished Master's thesis, The University of Texas at Austin, May 1980.
6. Viwathanatepa, S., Popov, E. P., Bertero, V. V., "Effects of Generalized Loadings on Bond of Reinforcing Bars Embedded in Confined Concrete Blocks," Report No. EERC-79/22, Earthquake Engineering Research Center, University of California, Berkeley, August 1979.
7. Concrete Design Committee (31/12), Draft New Zealand Standard: Code of Practice for the Design of Concrete Structures, Standards Association of New Zealand, Wellington, 1978.
8. Structural Standards Committee, AIJ Standard for Structural Calculation of Reinforced Concrete Structures, Architectural Institute of Japan, Tokyo, 1979.
9. Nakata, S., Otani, S., Kabeyazawa, T., Kai, Y., and Kimura, S., "Tests of Reinforced Concrete Beam-Column Assemblages--U.S.-Japan Cooperative Research Program," Department of Structural Engineering, Building Research Institute, Tsukuba, Japan, October 1980.

10. U.S.-Japan Cooperative Research Program Utilizing Large-Scale Testing Facilities, The Second Joint Technical Coordinating Committee Meeting, Building Research Institute, Tsukuba, Japan, July 1981.
11. "Recommended Lateral Force Requirements and Commentary," Seismology Committee, Structural Engineers Association of California, San Francisco, California, 1975.
12. U.S.-Japan Cooperative Research Program Utilizing Large-Scale Testing Facilities, The First Joint Technical Coordinating Committee Meeting, Building Research Institute, Tsukuba, Japan, January 1981.

V I T A

Paul Alex Murray was born in Bad Axe, Michigan, on June 29, 1958, the son of Patricia Anne Murray and Alex Paul Murray. After completing his work at Western High School, Auburn, Michigan, in 1976, he entered Michigan State University in East Lansing, Michigan. He received the degree of Bachelor of Science in Civil Engineering from Michigan State University in June of 1980. In September 1980, he entered The Graduate School of The University of Texas at Austin.

Permanent address: 1826 Midland Rd.
Bay City, Michigan 48706

This thesis was typed by Tina Robinson.